ACUSTICA

Vol. 8 1958 No. 3

GÉNÉRATEURS PNEUMATIQUES D'ULTRA-SONS INTENSES*

par V. Gavreau

Centre de Recherches Sci., Ind. et Mar., Marseille

Sommaire

Sifflets toroïdaux dérivant du sifflet de police. Fonctionnement à basse pression: oscillation du jet produite par le son lui-même; conditions pour obtenir un bon rendement (30%) ; son pur, dépourvu d'harmoniques. Fonctionnement à haute pression: oscillations entretenues par le jet d'air revenant frapper à sa base; «son de couteau» se superposant aux autres composantes du son très complexe émis; composantes ultra-sonores de fréquence très élevée; mais rendement moins bon. Equation des sifflets et calcul du rendement théorique. Formules des sifflets toroïdaux. Rôle du pavillon: transformation du jet d'air simplement interrompu en ondes sonores et ultra-sonores. Cavité auxiliaire permettant l'adaptation de pavillons aux sifflets. Contradiction entre la théorie et l'expérience dans le cas des pavillons exponentiels: pas de fréquence de coupure; les pavillons largement ouverts ne conviennent pas pour les ultra-sons. Calcul pratique des pavillons exponentiels annulaires pour l'émission d'ondes planes. Batteries de sifflets («panneaux sifflants»). Nécessité de synchronisation. Couplage direct; couplage par tubes résonnants. Synchronisation par buse auxiliaire («la triode acoustique»). Sifflet Levavasseur à buse auxiliaire pour les panneuax sifflants ultra-sonores. Synchronisation par sifflets, par sirènes, par haut-parleurs. Avantages et inconvenients des sifflets et des sirènes (tournantes) ultra-sonores. Applications.

Zusammenfassung

Die Arbeitsweise von kreisringförmigen Ultraschallpfeifen wird beschrieben; bei niederem Druck: Selbsterregung des Luftstrahls, Angabe der Bedingungen für guten Wirkungsgrad (30%) und Erzeugung reiner Töne; bei hohem Druck: Schwingungserregung des Luftstrahls durch Reflexion an der Basis, einem sehr komplexen Tongemisch überlagerter Schneidenton, Ultraschallkomponenten sehr hoher Frequenz, aber verschlechterter Wirkungsgrad. Berechnung der Pfeife. Über Druckkammer angekoppelter Trichter nicht zu großer Öffnung.

Strahlergruppen aus Pfeifen. Notwendigkeit der Synchronisation: Direkte Kopplung oder solche über Resonanzrohr. Synchronisation mit zusätzlichem Hohlraum („akustische Triode"), angewandt bei Pfeifen nach Levavasseur. Synchronisation mit Pfeifen, Sirenen und Lautsprechern. Vor- und Nachteile gegenüber Ultraschallsirenen.

Summary

Toroidal whistles derived from the police whistle are described. Their operation at low pressure—oscillation of the air jet produced by the emitted sound, conditions to obtain high efficiency (30%) and pure sinusoidal tone without harmonics is discussed. Their operation at high pressure—oscillations produced by the air jet returning to strike at its base, edge sound superposed on the other components of the emitted complex sound. The equation of whistles and calculation of their theoretical efficiency are given. Contradiction between the theory of horns and the experimental results: no cut off frequency. Practical calculation of annular exponential horns for emission of plane waves. Advantages and disadvantages of whistles and of ultrasonic sirens. Applications are described.

Introduction

Les sons aigus, à partir d'environ 2 kHz, et les ultra-sons émis dans l'air, provoquent une coagulation rapide et la précipitation de brouillards, fumées, poussières, — lorsque leur intensité dépasse 150 dB (soit 0,1 W/cm^2).

Une autre application très importante des sons et des ultra-sons dans l'air et dans les gaz, est l'accélération considérable de certaines réactions chimiques, telles que la combustion[1] et la catalyse [1], [2], [3], [4].

---

* Communication au 2^{me} Congrès International d'Acoustique à Cambridge, Mass., États-Unis, 17 au 23 Juin 1956.

[1] Essais faits au «Laboratoire National d'Essais des Arts et Métiers», par M. Charpennet, sous la direction du Prof. Veron, pour la société des Chaudières Babkock et Pillard.

De tels sons sont produits par des sirènes tournant à grande vitesse ou, beaucoup plus facilement et plus économiquement, par des sifflets toroïdaux. Dans les sifflets industriels de grande puissance, on utilise le même principe que dans un sifflet de police.

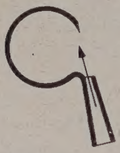

Fig. 1. Sifflet de police.

Rappelons qu'un sifflet de police (Fig. 1) est constitué par une cavité fonctionnant comme un résonateur de Helmholtz. Un jet d'air oscillant, émis par une buse, est dirigé vers le bord bien aiguisé de la cavité resonnante [5]. L'expérience montre qu'il existe trois modes de fonctionnement possibles d'un tel sifflet, ces modes de fonctionnement pouvant d'ailleurs coexister:

1. *Le fonctionnement «normal», à basse pression [6], Fig. 2*

Un sifflet de police ordinaire, alimenté sous sa pression normale de 40 gr/cm² émet *un son très pur, dépourvu d'harmoniques*, et son *rendement est très bon:* de l'ordre de 30%. On croyait autrefois que la forme du couteau était sans importance; en réalité, elle n'influe pas sur la fréquence, mais influe beaucoup sur la puissance et le rendement: le couteau doit être aussi mince et aussi bien aiguisé que possible. La puissance acoustique d'un tel sifflet ordinaire est relativement faible (1,15 W environ pour une puissance pneumatique de 4 W environ fournie par l'agent de police).

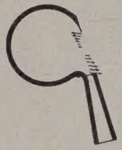

Fig. 2. Fonctionnement à basse pression.

2. *Le fonctionnement «en sirène statique», à haute pression, Fig. 3* (cas d'un compresseur fournissant une pression de plusieurs kg/cm²)

Le jet d'air à vitesse supersonique, contourne intérieurement la cavité resonnante et revient frapper à sa base, ce qui provoque périodiquement une très brusque déviation du jet. Le jet d'air est ainsi périodiquement interrompu au bord de la cavité résonnante. Ceci rappelle le fonctionnement d'une sirène ordinaire dans laquelle le jet d'air est périodiquement interrompu par un disque ou un tambour perforé tournant. Mais ici, c'est le jet qui se déplace par rapport à l'obstacle.

Le son émis n'est pas pur, mais riche en harmoniques (ce qui est favorable pour les applications industrielles).

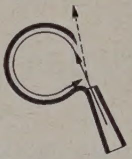

Fig. 3. Fonctionnement à haute pression.

3. *«Son de couteau»*

Ce son est produit par une oscillation très rapide du jet d'air sous l'effet des tourbillons qui l'accompagnent. Ce phénomène n'existe pas dans le sifflets à très basse pression; il apparait cependant, bien avant que la vitesse du jet devienne supersonique.

Le son de couteau donne naissance aux *composantes ultra-sonores intenses de fréquences très élevées.* Les fréquences de ces composantes sont pratiquement indépendantes de la fréquence «fondamentale» du sifflet (ce ne sont pas des harmoniques).

1. Adaptation d'un pavillon exponentiel à un sifflet

Sur un sifflet ordinaire il est impossible d'adapter un pavillon: sa présence arrête instantanément le fonctionnement du sifflet[2]. Or, un pavillon est nécessaire pour obtenir des ondes planes (directivité, et meilleure résonance dans le cas des traitements industriels). Et, contrairement aux simples réflecteurs (miroirs) permettant tout au plus d'obtenir une directivité accrue, les pavillons améliorent considérablement le rendement.

Dans notre Laboratoire, au Centre de Recherches Scientifiques Industrielles et Maritimes de Marseille, M. R. Levavasseur[3] a réussi à tourner cette difficulté. Il utilise une *cavité resonnante auxiliaire*, sensiblement de mêmes dimensions, mais un peu plus ouverte que la cavité «sifflante», Fig. 4. Sur cette figure S est la cavité sifflante et A la cavité auxiliaire. Il devient ainsi possible de munir les sifflets d'un pavillon, par exemple, d'un pavillon exponentiel.

Récemment, R. Levavasseur[3] a apporté un autre perfectionnement très important aux sifflets: il a supprimé le jet d'air qui accompagne le son émis par le sifflet. Ce jet d'air était très nuisible car il diluait la fumée à coaguler et il la refroidissait, ce qui diminuait le tirage des cheminées.

---

[2] Un sifflet de Galton ordinaire, un sifflet de Locomotive, un sifflet de Hartmann peuvent être munis d'un réflecteur (miroir) parabolique, mais pas d'un pavillon (tel qu'un pavillon exponentiel).

[3] Brevets du Centre National de la Recherche Scientifique.

Dans un modèle récent du sifflet Levavasseur, le jet d'air dès qu'il a dépassé le couteau, est capté, comme le montre la Fig. 5, par une fente dans la paroi du pavillon. Ainsi l'air est séparé du son et renvoyé vers l'arrière par une canalisation spéciale.

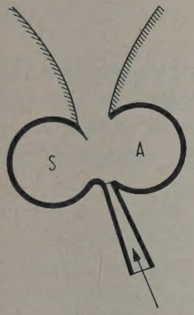

Fig. 4. Sifflet à cavité auxiliaire.

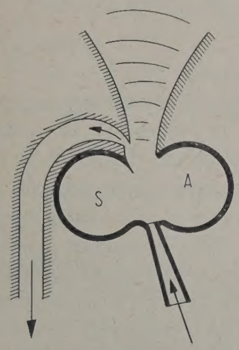

Fig. 5. Sifflet avec séparation du jet d'air.

2. Sifflets toroidaux

Les sifflets industriels de grande puissance sont des sifflets toroïdaux Fig. 6. Leur cavité sifflante et leur cavité auxiliaire sont toutes les deux toroïdales, tandis que le jet d'air est annulaire. Leur pavillon exponentiel est annulaire, semblable à celui des sirènes industrielles. Sur la Fig. 7 on voit le plus grand et le plus petit sifflets réalisés dans notre Laboratoire. Le plus grand («sifflet No. 5») est un sifflet à basse pression, débitant environ 200 litres d'air par seconde, — mais cet air est séparé du son et renvoyé en arrière. Il émet un son de 2,5 kHz (c'est la fréquence d'un sifflet de police ordinaire[4]; accompagné d'un ultra-son beaucoup moins intense de 28 kHz environ. Sa puissance acoustique est de 1 kW environ. Ce sifflet coagule bien la poussière humide des usines de ciment, mais reste sans effet lorsque cette poussière est sèche. Le diamètre de l'ouverture du pavillon est de 60 cm.

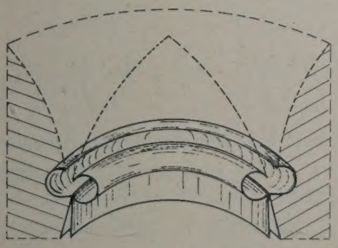

Fig. 6. Principe du sifflet toroïdal.

Le petit sifflet qu'on voit sur la Fig. 7 est un sifflet ultra-sonore de laboratoire il émet un mélange de deux sons tous les deux très intenses: un son de 22 kHz et un son de 460 kHz. Sa puissance est de quelques watts acoustiques seulement, ce qui suffit d'ailleurs pour les essais de laboratoire et pour la signalisation[5].

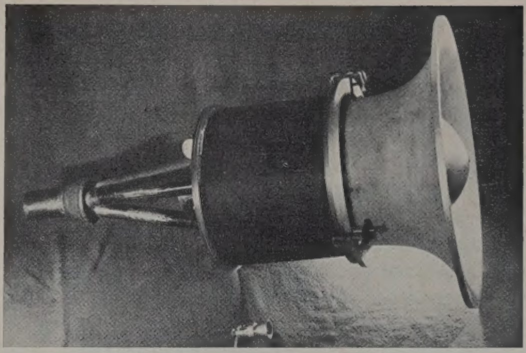

Fig. 7. Grand sifflet industriel et petit sifflet de laboratoire.

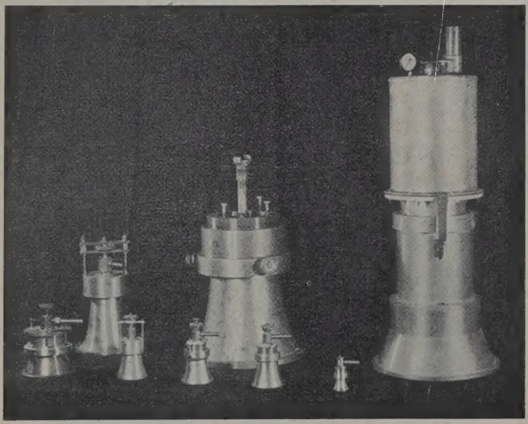

Fig. 8. Différents types de sifflets toroïdaux.

Sur la Fig. 8 on voit toute une gamme de sifflets toroïdaux de différentes dimensions et de différents types, réalisés dans notre Laboratoire. Le plus grand, à droite est le sifflet industriel No. 4 à basse pression, avec séparation complète du son et du jet d'air. Il émet un son riche en composantes ultra sonores, convenant bien pour le dépoussièrage et la précipitation de fumées (fumée de tabac précipitée en 2 secondes) les fréquences des composantes les plus intenses sont: 2,72 kHz et 38 kHz. Sa puissance acoustique est de 262 W environ. Il consomme 108 litre par seconde; la pression d'alimentation est de 400 gr/cm^2. Ce sifflet est utilisé dans la première installation industrielle, dans une usine de blancs de zinc.

---

[4] Mais beaucoup plus efficace ... pour disperser une foule par exemple.

[5] Les sifflets de commerce, dits «ultrasonores» («pour le dressage de chiens») émettent un son parfaitement audible dont la fréquence ne dépasse jamais 14 kHz.

Sur la même Fig. 8, à l'extrême gauche, on voit le «sifflet en bronze» émettant un son de 9,4 kHz + 150 kHz avec une puissance acoustique de 60 W environ. C'est un sifflet à haute pression: 2,3 kg/cm²; il ne consomme que 7 litres par seconde environ (tous les débits sont indiqués, ramenés à la pression atmosphérique). Des sifflets de ce type, un peu modifiés, à trou central, sont utilisés dans des bruleurs industriels de charbon pulérisé et de mazout.

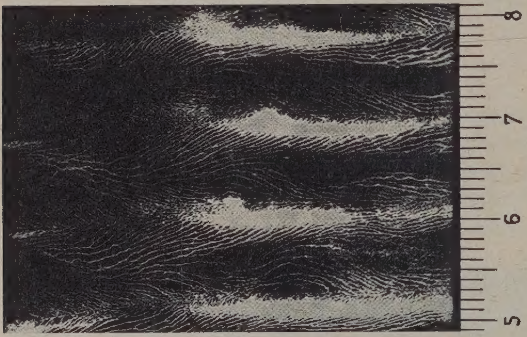

Fig. 9. Rides de sable produites par le petit sifflet de laboratoire (la graduation à droite est en centimètres).

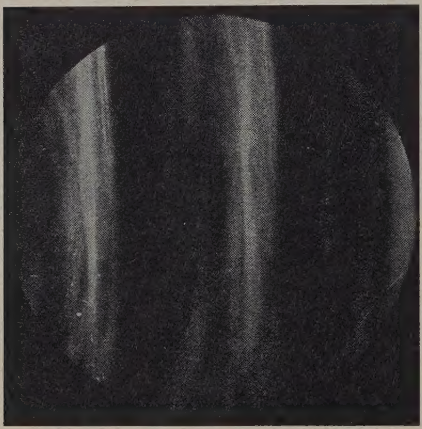

Fig. 10. Visualisation strioscopique du son émis par un grand sifflet.

Le plus petit des sifflets de cette figure est le même que sur la Fig. 7. Sur la Fig. 9 on voit les rides de sable produites par ce petit sifflet. Tandis que sur la Fig. 10 on voit l'image strioscopique (donnée par un miroir parabolique de 30 cm de diamètre) des ondes sonores planes émises par le grand sifflet à haute pression (Fig. 8 au centre), dans le voisinage immédiat de son pavillon également de 30 cm de diamètre.

3. Calcul des sifflets toroïdaux

Le fonctionnement des sifflets toroïdaux est tout à fait analogue à celui d'un sifflet de police. La fréquence d'un sifflet de police est donnée par la même formule que celle d'un résonateur de Helmholtz

$$f = \frac{c}{2\pi}\sqrt{\frac{\gamma}{V}} \qquad (1)$$

Où c est la vitesse de propagation du son dans l'air, V le volume de la cavité resonnante et γ un coefficient qui dépent de la forme et des dimensions de l'ouverture par laquelle la cavité résonnante communique avec l'extérieur.

Or, l'expérience montre que, dans le cas des sifflets cylindriques (sifflets de police), la fréquence ne dépend pas de la longueur L de la cavité résonnante cylindrique. Son volume V étant proportionnel à cette longueur L, le coefficient γ doit également être proportionnel à L

$$\gamma = k\,L\,. \qquad (2)$$

Donc

$$f = \frac{c}{2\pi}\sqrt{\frac{k\,L}{V}} = k'\sqrt{\frac{L}{V}}\,.$$

Et, dans le cas d'un sifflet cylindrique *(sifflet de police)*, on trouve ainsi:

$$V = \frac{\pi\,d^2\,L}{4} \text{ donc } f = k'\sqrt{\frac{4\,L}{\pi\,d^2\,L}} = \frac{2\,k'}{\sqrt{\pi}}\,\frac{1}{d} = \frac{K}{d}\,. \qquad (3)$$

Où d est le diamètre de la base, L la longueur de la cavité cylindrique et K *une constante, facile à déterminer expérimentalement.*

Dans le cas d'un sifflet toroïdal *à cavité sifflante «intérieure»* (tel que celui représenté sur la Fig. 6), en désignant par D le diamètre moyen du tore (diamètre du cercle décrit par le centre de la section qui engendre le tore) et par d le diamètre de la section, on a

$$V = \frac{\pi^2\,D\,d^2}{4} \text{ et } L = \pi(D+d) = \text{longueur de l'ouverture,}$$

donc (3 a)

$$f = k'\sqrt{\frac{4(D+d)}{\pi\,D\,d^2}} = \frac{2\,k'}{\sqrt{\pi}}\sqrt{\frac{D+d}{D\,d^2}} = \frac{K}{d}\sqrt{\frac{D+d}{D}}\,.$$

Dans le cas d'un sifflet toroïdal *à cavité sifflante «extérieure»* (sifflet analogue à celui représenté sur la Fig. 6, mais dans lequel la cavité sifflante se trouve à l'extérieur et la cavité auxiliaire à l'intérieur), on a

$$V = \frac{\pi^2\,D\,d^2}{4} \text{ et } L = \pi(D-d) = \text{longueur de l'ouverture,}$$

donc (3 b)

$$f = k'\sqrt{\frac{4(D-d)}{\pi\,D\,d^2}} = \frac{2\,k'}{\sqrt{\pi}}\sqrt{\frac{D-d}{D\,d^2}} = \frac{K}{d}\sqrt{\frac{D-d}{D}}\,.$$

Un grand nombre de mesures faites sur des sifflets de police et sur des sifflets toroïdaux de différentes dimensions, ont donné des résultats extrêmement concordants:

Pour les sifflets sans cavité auxiliaire

$K = 51\,000$ *environ.*

Pour les sifflets avec cavité auxiliaire

$K = 70\,350$ *environ.*

Toutes les dimensions, c'est à dire D et d, étant exprimées en millimètres.

4. Calcul des pavillons annulaires émettant des ondes planes

Pour qu'un sifflet toroïdal émette des ondes parfaitement planes on calcule son pavillon exponentiel annulaire de la façon suivante: soient (Fig. 11) R_1 et R_2 les rayons des deux cercles limitant l'entrée annulaire du pavillon (c'est à dire les rayons des bords de la cavité sifflante et de la cavité auxiliaire).

Soit R le rayon du cercle qui partage cette aire annulaire en deux parties égales

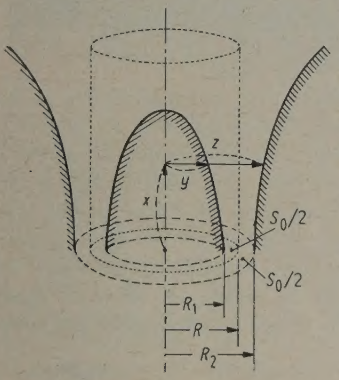

Fig. 11. Calcul d'un pavillon exponentiel annulaire.

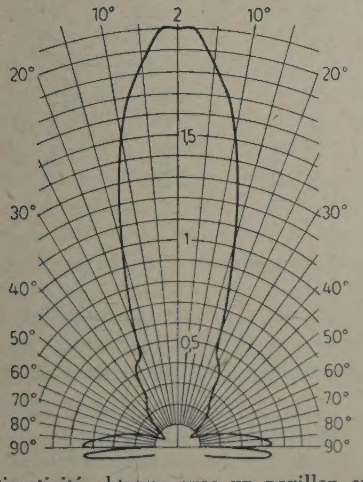

Fig. 12. Directivité obtenue avec un pavillon exponentiel correctement calculé.

$$\pi(R_2^2 - R^2) = \pi(R^2 - R_1^2)$$

d'où

$$R = \sqrt{\frac{R_1^2 + R_2^2}{2}}. \tag{4}$$

On considère le cylindre passant par ce cercle de rayon R et ayant ses génératrices parallèles à l'axe du sifflet et on calcule les surfaces limitant le pavillon annulaire exponentiel de telle façon que les sections comprises entre chacune de ces surfaces et ce cylindre de rayon R soient toujours égales.

Désignons par y le rayon de la surface exponentielle intérieure et par z le rayon de la surface exponentielle extérieure dans une section se trouvant à une distance x de l'entrée du pavillon, on a

$$y = \sqrt{R^2 - \frac{S}{2\,\pi}} \quad \text{et} \quad z = \sqrt{R^2 + \frac{S}{2\,\pi}} \tag{5}$$

avec

$$S = S_0\,\mathrm{e}^{mx}. \tag{6}$$

S_0 étant la surface *totale* de la section annulaire à l'entrée du pavillon.

Théoriquement [7], un tel pavillon devrait avoir une «fréquence de coupure»

$$f_0 = 2710\ m \tag{7}$$

(en Hz) et ne devrait pas transmettre les sons de fréquence inférieure à f_0. En fait, l'expérience montre qu'il n'en est rien: la «fréquence de coupure» n'existe pas. Et les constructeurs de sirènes ultrasonores utilisant des pavillons trop largement ouverts, conformes à cette théorie erronée, obtiennent de très mauvais rendements: en fait, c'est juste le contraire qu'on doit faire, — utiliser *des pavillons très allongés dans le cas des ultra-sons, pour éviter le décollement du faisceau ultra-sonore des parois du pavillon.*

D'ailleurs, le rôle du pavillon exponentiel n'est pas du tout le même dans le cas des haut parleurs et dans le cas des sirènes et sifflets: dans le cas d'un haut-parleur, le pavillon réalise une «adaptation des impédances», permettant à une petite membrane métallique de mettre en mouvement un grand volume de gaz. Dans le cas des sifflets le son étant engendré dans le gaz lui même, on n'a pas besoin d'une telle adaptation. Le rôle du pavillon est alors complètement différent: il transforme en son ou en ultrason [8] un jet d'air simplement interrompu dont les tronçons auraient tendance à se recoller, freinés par l'air ambiant.

On calcule le pavillon exponentiel en se donnant la hauteur de la basse centrale; connaissant la diamètre de la base on en déduit la valeur de m. Comme exemple de valeur de m, utilisée pour le calcul d'un sifflet de 10 kHz, on peut indiquer $m = 0{,}0491$ dans l'un des sifflets réalisés.

5. Rendement et puissance des sifflets

Dans un article publié précédemment [6] nous avons établi les formules théoriques donnant le rendement et la puissance des sifflets, et montré qu'il était possible d'obtenir pratiquement des rendements aussi bons que ceux des sirènes. Nous nous contenterons ici de rappeler très brièvement les résultats de cette étude:

Le rendement théorique d'un sifflet est donné par la formule:

$$\eta = \frac{p_0^2}{\varrho^2 c} \, \frac{a^2 b^3 \delta}{q_0^3} \left[\frac{\left(V + \frac{2\,q_0}{\omega_0}\right)^{\gamma} - V^{\gamma}}{\left(V + \frac{2\,q_0}{\omega_0}\right)^{\gamma} + V^{\gamma}} \right]^2 , \qquad (8)$$

où $p_0 = 1\,013\,000$ dyne/cm^2 est la pression atmosphérique,
$\varrho = 0{,}001205$ gr/cm^3 est la masse spécifique de l'air à 20° C,
$c = 34\,000$ cm/s est la vitesse de propagation du son dans l'air,
q_0 est le débit de l'air en cm^3/s ($q_0 = 2000$ cm^3/s pour un sifflet de police ordinaire),
a est l'épaisseur du jet ($a = 0{,}15$ cm pour un sifflet de police ordinaire),
b est la largeur de la fente (hauteur du volume résonnant cylindrique) ($b = 1{,}56$ cm),
δ est la hauteur de l'ouverture ($\delta = 0{,}73$),
f est la fréquence ($f = 2900$ Hz donc $\omega = 18\,230$ dans le cas du sifflet de police étudié),
V est le volume de la cavité résonnante ($V = 4{,}15$ cm^3 dans le cas du sifflet de police étudié).

Dans les cas du sifflet de police étudié, on trouve comme valeur théorique maximum du rendement

$$\eta = 21\%\,,$$

et, expérimentalement, on a trouvé $\eta = 13{,}25\%$. Dans le cas d'un petit sifflet de type «simplifié» (émettant un son de 3900 Hz), *on a trouvé, expérimentalement, un rendement* $\eta = 28{,}4\%$.

La puissance acoustique d'un sifflet, par centimètre de longueur de couteau est d'autant plus grande que la pression d'alimentation est grande. Pour un bon sifflet de police, $p = 40$ gr/cm^2 et on trouve:

$$w_0 = \frac{1{,}13\ \mathrm{W}}{1{,}56\ \mathrm{cm}} = 0{,}725\ \mathrm{W/cm}\,.$$

Pour le sifflet Levavasseur No. 4, $p = 400$ gr/cm^2 et on a trouvé:

$$w_0 = \frac{262\ \mathrm{W}}{\pi \times 13\ \mathrm{cm}} = 6{,}42\ \mathrm{W/cm}\,.$$

L'intensité du son émis dépasse toujours 150 dB dans le voisinage du sifflet par exemple pour le sifflet No. 4 de diamètre = 30 cm elle est

$$I = \frac{262}{\frac{\pi}{4}\,(30)^2} = 0{,}37\ \mathrm{W/cm^2} \ \text{ soit } \ 156\ \mathrm{dB}.$$

Et dans une «colonne de traitement», dans les conditions de résonance, elle atteint facilement 160 dB[6].

6. Batteries de sifflets («panneaux sifflants»)

Dans le cas des sifflets, tout comme dans le cas des sirènes, on est obligé d'utiliser des fréquences moins élevées lorsqu'on veut émettre des puissances plus grandes. Le son des grands sifflets industriels est parfaitement audible et on ne peut pas les utiliser à l'air libre, par exemple pour dissiper le brouillard: l'intensité du son est absolument insupportable.

C'est pourquoi, pour pouvoir émettre de grandes puissances acoustiques aux fréquences élevées, nous avons cherché à grouper en batteries[7] des sifflets Levavasseur de dimensions moyennes.

Pour fonctionner avec un bon rendement, sans court-circuits acoustiques, et émettre des ondes planes, directives, *tous les élements* d'un panneau sifflant *doivent être parfaitement synchronisés en fréquence et en phase.*

Les sifflets sont des oscillateurs acoustiques et, comme tous les oscillateurs, ils peuvent être synchronisés par couplage, comme le montre la Fig. 13. Ce couplage peut être réalisé de deux façons: soit en prévoyant une petite ouverture faisant communiquer les cavités résonnantes des deux sifflets, soit en établissant une communication entre ces cavités résonnantes au moyen de tubes de longueur convenable (accordés à la fréquence des sifflets).

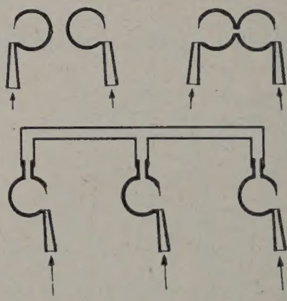

Fig. 13. Couplage direct et indirect de sifflets.

Un tel couplage permet la réalisation de sifflets Levavasseur à deux cavités sifflantes concentriques, permettant d'obtenir des intensités et des puissances plus grandes que les sifflets simples. Toutefois, nous avons abandonné la construction de tels sifflets multiples, car nous avons trouvé un procédé de synchronisation bien meilleur, beaucoup plus efficace, qu'un simple couplage: c'est la synchronisation par «buse auxiliaire».

---

[6] Les puissances acoustiques et les rendements invraisemblables indiqués par certains constructeurs de sirènes, s'expliquent par des mesures erronées.

[7] Brevet C.N.R.S., Invention de MM. V. Gavreau et A. Calaora.

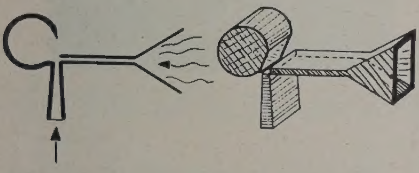

Fig. 14. Schéma d'un sifflet à buse auxiliaire.

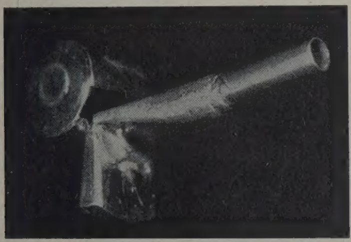

Fig. 15. Sifflet ordinaire à buse auxiliaire.

Un sifflet à buse auxiliaire, Fig. 14 et 15, est un sifflet ordinaire dans lequel un son synchronisant est appliqué transversalement à la base du jet d'air; ce son est guidé par une canalisation aplatie; la «buse auxiliaire» se trouve très près de la buse principale par laquelle s'échappe le jet d'air.

Voici le principe de la synchronisation par buse auxiliaire: nous avons vu [6], Fig. 2, que dans un sifflet ordinaire, l'oscillation périodique du jet d'air est due à l'addition géomètrique des vitesses du jet d'air et des «vitesses des particules» dans les ondes sonores émises par la cavité résonnant. En intégrant les vitesses transversales («vitesses des particules dans l'onde sonore») le long du parcours du jet d'air entre la buse et le couteau, on obtient le déplacement transversal résultant au niveau du couteau.

Comme il s'agit d'une fonction sinusoïdale, son intégrale le long du parcours du jet, est également une fonction sinusoïdale dont l'amplitude dépend de la distance entre la buse et le couteau et de la vitesse du jet d'air (cette dernière déterminant le temps de parcours, donc la durée de l'intégration des vitesses pour chaque particule d'air). Cette amplitude d'oscillation du jet au niveau du couteau doit s'annuler pour certaines valeurs de la vitesse du jet; ce fait a été confirmé expérimentalement.

Si, au lieu d'appliquer une onde sonore tout le long du parcours du jet d'air entre la buse et le couteau, on applique une onde sonore seulement à l'origine du jet, près de sa sortie de la buse, le phénomène est différent: *tout le jet* (qui est sinusoïdal sous l'effet du son émis par le sifflet, ou droit, en absence de ce son) *s'incline et l'amplitude des déplacements au niveau du couteau est beaucoup plus grande*. Ainsi un son très faible suffit pour synchroniser les oscillations d'un jet puissant, à condition d'être appliqué très près de la buse émettant ce jet. Ce résultat est obtenu au moyen d'une deuxième buse (la buse auxiliaire) amenant le son de synchronisation dans le voisinage de l'origine du jet, perpendiculairement à ce jet.

Le rôle de la buse auxiliaire est donc absolument analogue à celui de la grille dans une lampe triode: de même que la grille placée dans le voisinage immédiat de la cathode émettant un puissant flux d'électrons permet de commander ce flux par des tensions électriques très faibles, — la buse auxiliaire, placée dans le voisinage immédiat de la buse principale émettant un puissant jet d'air, permet de commander ce jet d'air par des ondes sonores très faibles. Un sifflet à buse auxiliaire est donc *une véritable «triode acoustique»*.

L'expérience montre que la buse auxiliaire permet une synchronisation parfaite non seulement des sifflets à basse pression mais également des sifflets à haute pression et que le son émis par un sifflet Levavasseur permet la synchronisation d'une vingtaine de sifflets Levavasseur de mêmes dimensions munis de buses auxiliaires. Il est donc possible de réaliser des panneaux synchronisés de sifflets à basse ou à haute pression. Un élément de tel panneau est représenté sur la Fig. 16. La buse auxiliaire est annulaire, tout comme la buse principale. Le son de synchronisation est amené par un tube (un tube de 18 mm de diamètre intérieur dans le cas de sifflets de 40 W fonctionnant à 10 kHz).

Pour que tous les sifflets d'un panneau fonctionnent en synchronisme parfait, il faut évidemment que les tubes de synchronisation soient accordées à la fréquence du sifflet pilote et que leurs longueurs diffèrent d'un nombre entier de longueurs d'ondes

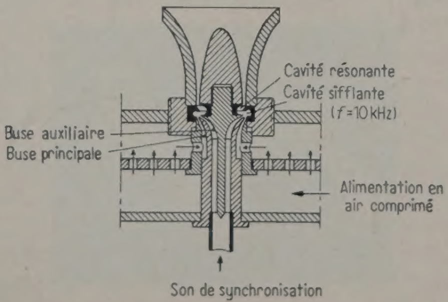

Fig. 16. Sifflet Levavasseur à buse auxiliaire (élément d'un panneau sifflant).

de ce son. On voit le schéma d'un tel panneau de 19 sifflets synchronisés par un 20^{me} sur la Fig. 17 et l'aspect extérieur de ce panneau sur la Fig. 18.

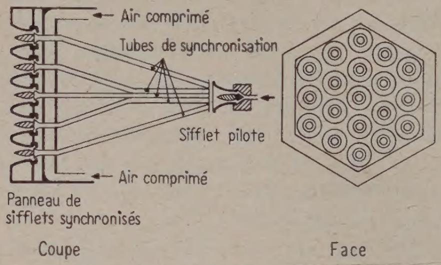

Fig. 17. Panneau de 19 sifflets synchronisés par un vingtième.

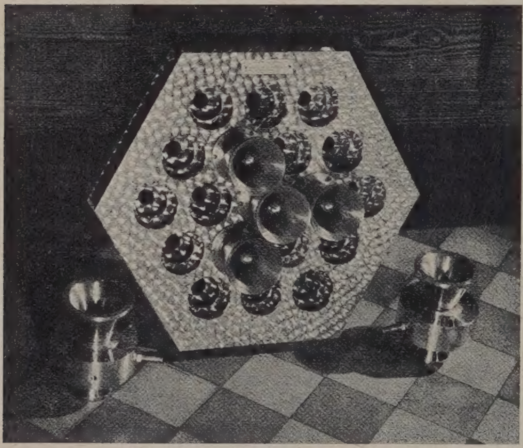

Fig. 18. Vue d'un panneau de 19 sifflets synchronisés avec quatre éléments en place. Devant le panneau deux autres éléments synchronisés.

La synchronisation a été contrôlée expérimentalement en captant le son émis par un microphone connecté à un oscilloscope cathodique: sur la Fig. 19 on voit les battements (d'ailleurs parfaitement audibles) en absence de la synchronisation; sur la Fig. 20, les sifflets sont synchronisés, il n'y a plus de battements, un son unique est émis.

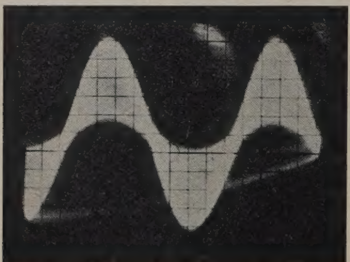

Fig. 19. Battement entre le son émis émis par deux sifflets non synchronisés (vu sur l'écran d'un oscilloscope cathodique).

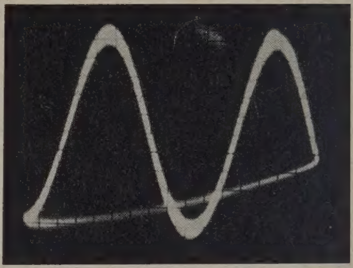

Fig. 20. Son unique émis par deux sifflets synchronisés.

7. Mesure de la puissance des sifflets

La puissance acoustique de la composante audible est mesurée au moyen d'un microphone étalonné placé à une assez grande distance du sifflet, dans une chambre sans échos. On tourne le sifflet ce qui permet d'obtenir un diagramme de rayonnement et, en intégrant les intensités dans différentes directions, on détermine la puissance acoustique totale aux fréquences audibles.

La difficulté de cette mesure vient de la très grande intensité du son à mesurer: la membrane d'un microphone placé trop près du sifflet est très rapidement brisée, et même à une distance de plusieurs mètres le son dépasse 145 dB. Or, les résultats obtenus en utilisant des microphones «protégés» (placés dans une boite) sont généralement faux, probablement à cause des résonances des parois de la boite, des vibrations parasites du support du microphone relié à cette boite protectrice, etc. . . . Il est préférable d'utiliser pour ces mesures un microphone très robuste, peu sensible, «nu».

La mesure de la composante ultra-sonore se heurte à une autre difficulté. L'expérience montre que les microphones dits «ultra-sonores» étalonnés donnent des résultats peu sûrs[8] et seul le procédé de la pression de radiation sonore [9], [10] convient pour ces mesures. Or, le son émis par des sifflets et par des sirènes s'accompagne toujours d'un jet d'air et ce jet, même lorsqu'il est très faible (sifflets à séparation du jet et du son) risque de fausser les mesures. Mais il est possible de séparer complètement les ultrasons et ce jet d'air au moyen d'un miroir (plaque métallique lourde) à 45°, comme le montre la Fig. 21. En effet, la longueur d'onde de l'ultra-son étant très inférieure aux dimensions du «miroir», ils se réfléchissent à 90°, tandis que le jet d'air suit la surface du miroir. On vérifie facilement en déréglant le sifflet (ou en arrêtant la sirène) que le jet d'air seul n'influe nullement sur la balance. On utilise toujours un obstacle conique, pour éviter

---

[8] Des mesures faites «à quelques décibels près» ne présentent aucun interêt lorsqu'il s'agit d'évaluer la puissance acoustique en Watt.

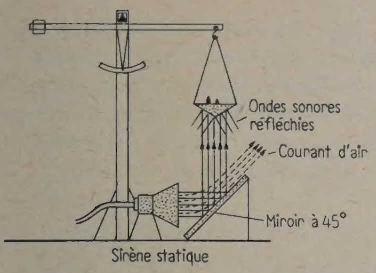

Fig. 21. Mesure de l'intensité du son émis par un sifflet par le procédé de la pression de radiation sonore.

tout risque d'ondes stationnaires et de résonance entre le générateur du son et l'obstacle. La formule à utiliser est

$$I = 1{,}7\,\frac{P}{S\cos^2\Theta}\ \mathrm{W/cm^2}, \qquad (9)$$

où P est le poids en grammes mesuré par la balance, S la surface de la base du cône en cm^2 et Θ l'angle que font les génératrices du cône avec sa base.

8. Sirènes industrielles [8], [11]

Contrairement à une opinion assez repandue, *il ne suffit pas d'interrompre périodiquement un jet d'air pour le transformer intégralement en énergie sonore.* Les tronçons d'un tel jet, freinés par l'air ambiant se recollent et reconstituent un jet d'air continu silencieux. C'est pourquoi, le rendement d'une sirène est déplorable lorsqu'elle n'est pas munie d'un pavillon suffisamment allongé. C'est dans le pavillon que prennent naissance, sous l'effet de l'inertie du jet brusquement interrompu, les dépressions périodiques engendrant les ondes sonores.

Pour cette raison, les sirènes pour les alertes antiaériennes à pavillons multiple allongés, sont très efficaces. Par contre les sirènes industrielles, surtout les sirènes dites «ultra-sonores» à pavillon très évasé [12], [13], ont généralement un très mauvais rendement et une faible puissance[9].

Des sirènes bien meilleures, à pavillon allongé, ont été cependant réaliées aussi bien aux États-Unis [15] qu'en Allemagne [16] ces dernières ont un rendement entre 25 et 30% à 5 kHz.

En même temps que des dépressions périodiques dans le pavillon, l'inertie du jet d'air brusquement interrompu, produit des compressions périodiques à l'intérieur même de la sirène et ces compressions contribuent également à l'émission sonore, mais seulement à certaines fréquences: les sirènes présentent des fréquences de résonance très prononcées, pour lesquelles le rendement est meilleur que pour les autres fréquences.

Une difficulté particulière aux sirènes est la nécessité d'assurer une étanchéité parfaite entre le rotor et le stator, sans provoquer un frottement excessif.

9. Avantages et inconvénients des sifflets et des sirènes

Les sirènes permettent une émission de très grande puissance acoustique, surtout aux basses fréquences. Elles peuvent être facilement synchronisées et utilisées en batteries. Mais elles exigent un ajustage de haute précision et le fait qu'elles comportent des organes tournants et exigent un moteur d'entrainement, rend pratiquement impossible leur emploi à hautes températures et sous fortes pressions (bruleurs de charbon pulvérisé et de mazout, synthèse de l'ammoniac).

Les sifflets permettent d'obtenir très facilement des ultrasons de très haute fréquence (plus exactement, des sons complexes à forte proportion de composantes ultra-sonores), convenant bien pour la coagulation de fumées et de poussières. On peut utiliser pour leur construction n'importe quel métal (acier inoxydable, bronze, etc. . . .) ce qui permet leur emploi pour différents traitements chimiques, même à hautes temperatures et fortes pressions, en les alimentant au besoin directement par le mélange gazeux à traiter.

Le principal inconvénient des installations à sirènes et à sifflets est une consommation assez importante d'énergie, nécessaire pour assurer leur fonctionnement. Mais des progrès importants ont été réalisés récemment et ont permis d'accroitre considérablement leur rendement, donc de réduire la consommation de l'énergie.

10. Applications pratiques

Les premières applications envisagées ont été *la précipitation des fumées, et poussières industrielles [17], [18] et la précipitation des brouillards.* Mais on est rapidement arrivé à la conclusion que seuls certains types de poussières et de fumées pouvaient être précipitées par ce procédé: les poussières humides ou grasses, collantes, et les fumées goudronneuses (telles que la fumée de tabac, la fumée de caoutchouc, la fumée des usines fabriquant l'oxyde de zinc, etc. . . .). Dans d'autres cas, on est obligé d'utiliser une pulvérisation d'eau pour permettre le collage et la précipitation de la poussière par les ultrasons.

Une application assez intéressante paraît être la précipitation des goudrons «non-coagulables» par tous les autres procédés, notamment *des goudrons très finement pulvérisés contenus dans le gaz des gazogènes.* Dans ce cas, le sifflet est alimenté en gaz comprimé purifié, pour éviter la formation d'un mélange explosif avec l'air. Nous avons également utilisé dans ce but un sifflet alimenté en vapeur sous pression fournie par une chaudière ordinaire.

---

[9] Le calcul du rendement [14] basé sur l'hypothèse inexacte d'une transformation totale, de 100% de l'énergie du jet interrompu en énergie sonore, ne correspond à aucune réalité physique.

La précipitation des brouillards naturels a été réalisée au moyen de sirènes, mais le son audible de 3 à 5 kHz émis par de telles sirènes est absolument insupportable et on a été obligé d'abandonner ce procédé. Il sera peut-être possible de précipiter le brouillard par des batteries de sifflets, à fréquence plus élevée, beaucoup moins pénible et d'ailleurs fortement absorbée par le brouillard en déhors de la zone «nettoyée»: La fréquence de 10 kHz parait être particulièrement efficace. (Plus exactement, il s'agit d'un mélange de 10 kHz et de 150 kHz émis par un sifflet Levavasseur; les essais ont été faits sur un brouillard d'eau produit artificiellement, au laboratoire.)

Mais les applications les plus intéressantes des sifflets (les sirènes ne pouvant pas être utilisées dans ce but) sont la combustion accélérée et la catalyse accélérée. Les essais préliminaires ont donné des résultats absolument remarquables et des sifflets-bruleurs industriels ont été construits.

11. Conclusion

Une très longue et difficile mise au point des émetteurs pneumatiques d'ultra-sons intenses (sirènes et sifflets) a permis d'accroitre considérablement leur rendement et les puissances acoustiques émises. Leur emploi industriel a ainsi été rendu possible et un certain nombre d'installations sont en cours de réalisation dans différents pays (en France, en Pologne, en Hongrie).

Il s'agit de dépoussièrage et de précipitation de fumées, pour lesquels on peut utiliser indifféremment des sirènes ou des sifflets, mais il faut que la poussière ou la fumée ne soit pas «sèche», car seule la poussière collante et la fumée goudronneuse peuvent ainsi être précipitées.

Les applications de loin les plus importantes et les plus intéressantes concernent l'accélération de certaines réactions chimiques: combustion, catalyse. Pour ces application seuls les sifflets conviennent, les sirènes tournantes ne pouvant pas être utilisées aux temperatures élevées et sous très grandes pressions.

Une autre application, peut-être possible, est la précipitation des brouillards. Là encore, seuls les sifflets peuvent être utilisés, car les sirènes de grande puissance émettant des sons de fréquence peu élevée, sont insupportables pour le personnel travaillant dans les ports et sur les aérodromes.

Bibliographie

[1] Seljakov, N. V., Catalyseurs pour la synthèse d'ammoniaque et pour l'hydrogénation. Brevet soviétique No. 48.210 (1936).

[2] Seljakov, N. V. et Frost, A. W., Réactions catalytiques. Brevet soviétique No. 50.985 (1936).

[3] Richardson, C. N., Ammonia synthesis. Brevet américain No. 2.500.008 (1950).

[4] Pschenytzin, N. N., Sidorov, N. W. et Sternina, D. G., Traitement des catalyseurs d'ammoniaque par les ultra-sons. J. Chim. Appl. (URSS) **13** [1940], 76.

[5] Handbuch der Experimentalphysik, Vol. XVII, 3, Akustik II, p. 231.

[6] Gavreau, V., Sifflets, théorie de fonctionnement et rendement. Acustica 4 [1954], 555 et Note du C.R.S.I.M. No. 350 du 11 Julliet 1953.

[7] Davis, A. H., L'acoustique moderne. Ed. Dunod, Paris 1936, p. 59.

[8] Gavreau, V., Caractéristiques de fonctionnement et rendement des sirènes. Note du C.R.S.I.M. No. 354 du 21 Août 1953.

[9] Gavreau, V. et Miane, M., Étude theorique et expérimentale de la pression de radiation sonore. Note du C.R.S.I.M. No. 389 du 2 Janvier 1957 (Bibliographie).

[10] Gavreau, V., Pression de radiation sonore d'après la théorie cinétique des gaz. J. Phys. Radium **17** [1956], 899.

[11] Gavreau, V., Brevet français No. 1.111.527 du 2 Mars 1954 du C.N.R.S.

[12] Horsley, C. B. et Seavey, G., Brevet américain No. 2.514.129 et Brevet français No. 934.086.

[13] Pimonow, L., Un nouveau modèle amélioré de sirène ultra sonore. Ann. Télécommun. **6** [1951], 337.

[14] Jones, R. C., A fifty horsepower siren. J. acoust. Soc. Amer. **18** [1946], 371.

[15] Allen, C. H. et Rudnick, I., A powerful high frequency siren. J. acoust. Soc. Amer. **19** [1947], 857.

[16] Brevet allemand No. 823.716 de la société Atlas-Werke, Bremen.

[17] Porter, R. W., High intensity sound waves harnessed for industry. Chem. Engrg. **55** [1948], Mars, 100.

[18] Danser, H. W. et Neumann, E. P., Systèmes industriels d'agglomération sonique et de recueil des poussières. Industr. Engrg. Chem. **41** [1949], Novembre, 2439 (Traduction No. 13–50 du Centre d'Études et de Recherches des Charbonnages de France).

PULSE TECHNIQUES
FOR MEASURING ULTRASONIC ABSORPTION IN LIQUIDS

by J. H. Andreae°, R. Bass+, E. L. Heasell+ and J. Lamb+

Summary

The paper is concerned with the construction and operation of equipment for the measurement of the ultrasonic absorption in liquids by the pulse method over a range of frequencies from 1 to 200 Mc/s. General considerations of the design of experimental systems are discussed together with the practical limitations.

Details are given of the electrical and mechanical parts of three systems which are in current use, and permit the measurement of ultrasonic absorption within an accuracy of ±2%. The first two systems, A and B, are designed to operate up to a frequency of 200 Mc/s and illustrate alternative lines of approach to the problem. The third system C can be used for measurements on liquids under pressures up to 100 atm. It incorporates a common transmitter-detector system and provides a longer ultrasonic path than do the first two systems: thus smaller absorption coefficients can be measured or measurements made at correspondingly lower frequencies, down to a minimum of 1 Mc/s.

Attenuation measurements are referred to various piston attenuators which have been constructed and checked against each other.

Sommaire

On traite de la réalisation et de l'utilisation d'un appareillage destiné à mesurer l'absorption des ultra-sons dans les liquides, par la méthode des impulsions, entre 1 et 200 MHz. On en discute les lignes générales, ainsi que les limites pratiques.

On décrit en détail les parties électriques et mécaniques de trois systèmes couramment utilisés, qui permettent de mesurer l'absorption des ultra-sons à ±2% près. Les deux premiers dénotés A et B, sont destinés à fonctionner jusqu'à 200 MHz et représentent deux façons différentes d'aborder le problème. Le troisième système dénoté C peut être utilisé pour des mesures dans des liquides soumis à des pressions allant jusqu'à 100 atm; il comporte un système transmetteur-détecteur commun et un trajet d'ultra-sons plus long que dans les deux premiers; ceci permet de mesurer des coefficients d'absorption plus faibles, ou encore de descendre à des fréquences plus basses (jusqu'à 1 MHz).

Les mesures d'affaiblissement sont données par comparaison avec différents affaiblisseurs à piston, qui ont été construits à cet effet, et que l'on a comparés entre eux.

Zusammenfassung

Die Arbeit befaßt sich mit Aufbau und Wirkungsweise einer Apparatur zur Messung der Ultraschallabsorption in Flüssigkeiten nach der Impulsmethode für Frequenzen zwischen 1 und 200 MHz. Es werden allgemeine Gesichtspunkte zur Konstruktion der Apparatur und die praktisch gegebenen Grenzen diskutiert. Einzelheiten des elektrischen und mechanischen Aufbaues dreier Systeme werden angegeben, die Absorptionsmessungen mit einer Genauigkeit von 2% gestatten. Die ersten beiden Systeme arbeiten bis zu Frequenzen von ca. 200 MHz und benutzen verschiedene Methoden. Das dritte System kann für Drucke bis 100 atm benutzt werden. Es enthält ein gemeinsames Sende- und Empfangssystem und benutzt eine längere Ultraschall-Wegstrecke als die ersten beiden Systeme. Somit können kleine Absorptionskoeffizienten gemessen oder Frequenzen bis hinunter zu 1 MHz benutzt werden. Die Dämpfungswerte wurden auf verschiedene geeichte Dämpfungsglieder bezogen.

1. General considerations

1.1. Features of the different possible experimental arrangements

In principle, a short radio-frequency pulse containing an appreciable number of oscillations at the frequency f, is generated by a suitably modulated oscillator and is fed to a piezoelectric transducer. The resulting ultrasonic pulse from the transducer passes through the liquid to be measured and is reconverted into an electrical pulse by a detecting transducer. After suitable amplification and demodulation the envelope of the received pulse is displayed on an oscilloscope. By varying the distance between the launching and detecting transducers and by measuring the change in amplitude of the detected pulse, a plot of attenuation versus path length is obtained which gives the absorption coefficient α

° Imperial Chemical Industries Ltd., Akers Research Laboratories, Welwyn, Herts.

+ Electrical Engineering Department, Imperial College, London.

directly. From this and the known frequency, f, the quantity α/f^2 may be calculated.

Measurements of the attenuation in the liquid are referred to a precision attenuator. The attenuator may be placed (i) in series with the detecting transducer, or (ii) in series with the oscillator. In both these cases variations in the attenuation in the ultrasonic path are compensated for by equivalent changes in the setting of the attenuator, maintaining a constant signal level on the oscilloscope. A disadvantage of these arrangements is that the accuracy depends on the gain of the electrical receiver remaining constant during the period of a measurement (10 – 15 minutes). The amplitude of the received signal before it reaches the receiver input is reduced by losses in the acoustic system and by the insertion loss and added attenuation of the attenuator. Thus, for a given oscillator output and receiver noise level, the signal to noise ratio is determined by the sum of these attenuations and remains constant throughout a measurement. Considerable improvement may be obtained with arrangement (i) if a preamplifier can be placed between the receiving transducer and the attenuator. The signal to noise ratio is then determined by the attenuation in the acoustic system and the noise level in the preamplifier only, provided that the gain of the latter is large compared with the insertion loss of the attenuator. It is, however, essential that the pre-amplifier should have a linear gain characteristic over the required dynamic range of input signals and this is not easily combined with a high gain. On the other hand arrangement (ii) has obvious advantages over (i) if the permissible output from the oscillator is limited by "spark-over" at the transducer.

A third arrangement which is particularly satisfactory at high frequencies requires the addition of an electronic delay circuit and a second (comparison) oscillator tuned to the same frequency as the main oscillator. The pulse from the comparison oscillator is delayed with respect to that from the main oscillator so that the envelopes of the two pulses are displayed adjacently when they reach the oscilloscope. Both pulses pass through the same amplification path. The receiver is operated at maximum gain only for the highest attenuator settings, the gain being reduced successively as the attenuation decreases, with a consequent improvement in the signal/noise ratio. There is no need for the receiver to have a constant gain over the period of time required for a measurement.

The detecting transducer can be dispensed with by using a reflector, in which case the ultrasonic wave is returned to the transmitting transducer for detection. In this common transmitter-detector system the receiver must be capable of recovering from the application of the oscillator output. The double path length provided by this arrangement can be advantageous at low frequencies when the absorption is low. Also at high frequencies the problem of producing transducers with identical harmonic resonant frequencies is avoided.

1.2. Practical limitations to the design of experimental systems

A variety of practical limitations must be considered in the design of experimental systems utilising the pulse technique:

(i) At any one frequency there is a wide variation in the absorption coefficient of different liquids. For example, in water (which has a low absorption coefficient), $\alpha/f^2 = 25 \cdot 10^{-17}\,\mathrm{s^2\,cm^{-1}}$, and at a frequency of 50 Mc/s a liquid path of 5.5 cm would be required to reduce the amplitude of an ultrasonic wave by 30 dB; in carbon tetrachloride ($\alpha/f^2 = 550 \cdot 10^{-17}\,\mathrm{s^2\,cm^{-1}}$) the absorption is high and the corresponding path length would be 0.25 cm. This means that separate mechanical systems may be needed for measurements on different liquids at the same frequency.

(ii) For a specific liquid, in the absence of relaxation processes, the absorption coefficient is proportional to the square of the frequency: thus, to reduce the amplitude by, say, 30 dB, the path length required at 10 Mc/s would be one hundred times that at 100 Mc/s. In the case of carbon tetrachloride cited above the path length for 30 dB attenuation would be 6.25 cm at 10 Mc/s and only 0.0625 cm at 100 Mc/s. These two conditions could not easily be dealt with in the same mechanical system.

(iii) At low frequencies diffraction effects due to the finite radius, a, of the transmitting transducer may have to be taken into account. The sound field can be divided approximately into the Fresnel region near the transducer and the more distant Fraunhofer region. The boundary between these two lies at a distance of about a^2/λ from the transmitting transducer. In the Fresnel region, the total ultrasonic energy radiated from the transducer is still confined to a narrow beam, but the pressure amplitude fluctuates rapidly both across the beam and along its axis. If, however, the receiving transducer is made somewhat larger than the transmitting transducer and so covers the whole cross section of the beam, constant signal is obtained throughout the Fresnel region in the absence of absorption. This is not exactly true for transmitting and receiving transducers of equal radius, but even then diffraction effects are in practice usually negligible at frequencies above 5 Mc/s and with ultrasonic pathlengths not exceeding $a^2/2\,\lambda$ [1]. On the other hand, in the Fraunhofer, or diverging, region of the sound field the aperture of the detecting transducer may be restricted so as to record as nearly as possible the pressure on the axis; it is then necessary to apply a correction to the measured attenuation to allow for the divergence of the sound beam in order to obtain the true ultrasonic absorption. A discussion of these corrections has been given by PINKERTON [1].

(iv) When the time taken for the ultrasonic pulse to traverse the liquid path is less than the pulse duration an additional time delay must be provided in the ultrasonic system. This serves to separate on a time scale the required signal from the transmitted pulse which, if two transducers are used, by-passes the ultrasonic system by radiation, or if a common-transmitter-detector system is employed, is fed directly to the receiver. Owing to the high power of the oscillator and the sensitivity of the receiver, it is not generally feasible to eliminate this 'pick-up' pulse. The necessary time delay may be provided conveniently by introducing a length of fused quartz rod into the ultrasonic path. Fused quartz possesses a low attenuation coefficient and gives a delay of about 1.7 µs/cm. In practice further advantages accrue from the use of such delay rods and these will be discussed in chapter 2.

(v) The temperature of the test liquid must be kept constant to within ±0.1° C in order to prevent local thermal fluctuations from causing variations in the received signal. Heating of the liquid by the dissipation of ultrasonic energy does not present a problem because the duty cycle (on/off ratio) may be kept as small as necessary, say, 10^{-3}.

1.3. *Standards of attenuation*

The overall accuracy of the absorption measurements depends upon the accuracy of the attenuator employed. Piston attenuators have been used throughout this work [2], [3] and in order to verify the theoretical attenuation constants various attenuators have been constructed and compared with each other. These include types operating in the E_{01} (circular), H_{11} (circular) and H_{01} (rectangular) modes. Two attenuators of different transverse dimensions have been built to operate in each of these modes. The design of the H_{11} attenuators followed the description by GAINSBOROUGH [2]. Diagrams illustrating the construction of the E_{01} and H_{01} attenuators are shown in Fig. 1. In all cases the calculated attenuation constants were found to agree to within better than ±0.5%, which was the limit of accuracy of the method of comparison.

1.4. *Transducers*

X-cut quartz crystals are normally used as transducer elements at all frequencies from 1 to 200 Mc/s, but polarised barium titanate discs are suitable below about 10 Mc/s. The electrical impedance presented to an oscillator by a quartz transducer becomes excessive at the lower frequencies and power is more readily transferred from the oscillator to the lower impedance offered by a barium titanate transducer. However, this advantage of the barium titanate transducer is not particularly significant since there is no need for large amounts of ultrasonic power at the lower frequencies. In fact, there is little difficulty in obtaining a wide range of attenuation (e. g. 50 dB) for measurements taken with apparatus operating below 100 Mc/s.

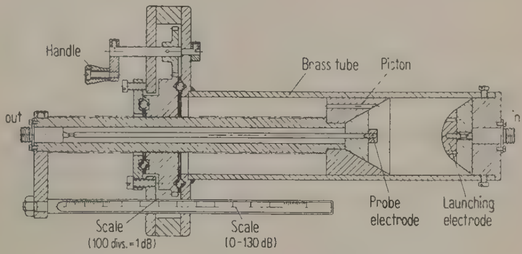

Fig. 1a. E_{01} (circular) piston attenuator.

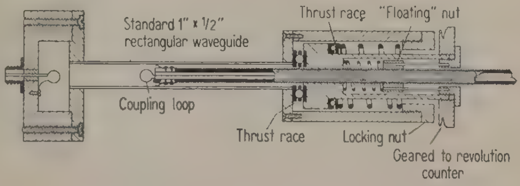
Standard 1" x 1/2" rectangular waveguide
Thrust race
"Floating" nut
Coupling loop
Thrust race
Locking nut
Geared to revolution counter

Fig. 1b. H_{01} (rectangular) piston attenuator.

The thickness-vibration of an X-cut quartz crystal disc is resonant when the thickness of the disc is equal to one half wavelength or an odd number of integral half wavelengths. One half wavelength is about 0.014 in. at 20 Mc/s in quartz so this frequency is about the highest at which a crystal can be operated conveniently in a fundamental frequency, or half wavelength, mode. Higher frequencies are reached by using the odd harmonic resonances of the crystals and, by selecting a crystal with a convenient fundamental frequency, a complete range of discrete frequencies can be covered. The bandwidth of a crystal increases with the frequency of its fundamental vibration but is the same at all harmonic frequencies for the same fundamental: therefore it is advisable to select crystals with the highest possible fundamental frequency if a reasonably broad frequency response is required at harmonic frequencies above 100 Mc/s. This is important in two-crystal systems which depend on the optimum behaviour of two crystals at the same frequency. Fundamental frequencies of 10 and 20 Mc/s have proved to be suitable for operation up to 200 Mc/s.

In order to apply an alternating voltage across a quartz crystal, an electrode is provided on each side of the disc and the area of at least one of the electrodes is limited to the area of the required ultrasonic beam. The electrodes may be metallic layers evaporated on to the surfaces of the crystal, or they may consist of conducting surfaces between which the crystal is clamped. When fused quartz delay rods are employed, one electrode is conveniently provided by evaporating a layer of chromium or gold on to the optically flat end of the rod before pressing the crystal disc against it. Also, to permit ultrasonic propagation from the crystal to the rod, it is necessary to indroduce a drop of non-volatile liquid (e. g. vacuum oil) between the crystal and the rod. Methods of mounting quartz crystals are illustrated in Figs. 2, 7 and 8.

Experience with the ultrasonic systems A and B of section 2 has shown that it becomes increasingly difficult above 100 Mc/s to obtain the desired attenuation range of 30 dB for measurements. Neither of the systems allows a useful variation in the amplitude of the received signal for more than 25 dB at frequencies above 200 Mc/s. The reason for this decrease in the available attenuation range is not clear at present, but it is likely to be connected with the operation of the crystals, the efficiency of the coupling between the crystals and the delay rods and the attenuation in the latter [4], [5], [6].

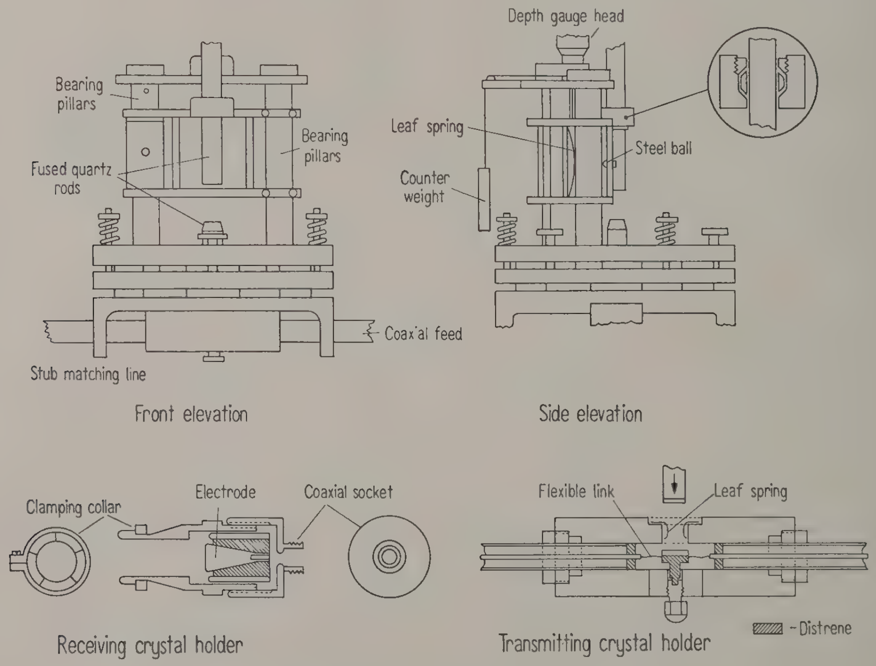

Fig. 2. Mechanical design of system A.

2. Detailed description of experimental systems

Three of the experimental systems used by the authors have been selected to illustrate the salient features of apparatus employing the pulse technique. The first two systems, A and B, were designed for the purpose of measuring ultrasonic absorption in small quantities of liquids up to 200 Mc/s; both are included so that alternative lines of appreach to the design of equipment can be emphasized. The third system, C, is used for measuring the absorption in liquefied gases at pressures up to 100 atm. It incorporates a common transmitter-detector system and provides a longer usable ultrasonic path than do the first two systems. These three sets of apparatus are described in turn.

2.1. *System A*

2.1.1. Mechanical design

Two considerations arise in the design of the mechanical system, namely, the production of small displacements and the alignment of the two transducers. It is desirable to obtain ten, or more, points on the final graph of attenuation plotted against distance and the points should be accurate to ±1%, so it is necessary to produce measurable displacements of, say, 0.2% of the total path length covered in the measurement. Also, to obtain the maximum ultrasonic signal through the system, parallelism of the transducers must be achieved and maintained to within a fraction of an acoustic wavelength during displacement. These problems can be illustrated by the case of carbon tetrachloride at a frequency of 200 Mc/s. For a measuring range of 30 dB, the total change in path length is only 0.016 cm and so measurable displacements of the order of a micron must be possible. Also the ultrasonic wavelength is only 6 microns so parallelism should be maintained to within about one wavelength of visible light. At lower frequencies the problem is proportionately simpler.

The mechanical design of system A is illustrated in Fig. 2. The detecting transducer and its associated fused quartz delay rod are supported in a rigid steel framework which slides upon two steel pillars, the surfaces of which are hardened and ground to be accurately straight and cylindrical. The framework is kinematically mounted, being supported by five hardened steel balls, which are held in firm contact with the bearing pillars by two flat phosphor-bronze springs: as can be seen from Fig. 2, there are four point contacts on one pillar and one on the other. The whole moving system is counterbalanced by a brass weight and is driven by a micrometer depth gauge. The transmitting crystal, quartz rod and matching lines are rigidly fixed to the base of the apparatus and alignment is achieved by tilting the two bearing pillars with respect to the base. These pillars are fixed into accurately matched holes in the two end plates, the lower plate being spring-loaded against the base of the apparatus and tilted by means of three fine-pitched screws (40 t.p.i.). The displacement of the upper fused quartz rod is measured by a dial gauge, the sensitivity of which is chosen to suit the absorption of the test liquid.

The design of the vessel containing the liquid is influenced by the need to isolate the temperature-controlling liquid from the test sample. The controlling liquid flows between the inner and outer walls of a double wall container (Fig. 3), which fits on to the lower fused quartz rod by a tapered ground joint. This seal is found to be liquid tight without the use of any grease, which might contaminate the test sample and has proved to be satisfactory over the temperature range -60° to $+100^\circ$ C. The temperature of the liquid is measured by a thermocouple attached to the upper fused quartz delay rod. The diameter of the fused quartz rods is 9/16″ and, when these are touching, less than 10 cm^3 of test liquid are needed to fill the vessel.

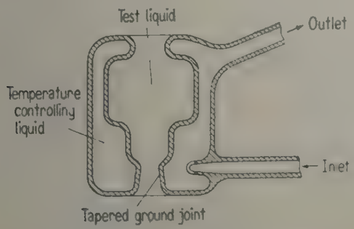

Fig. 3. Liquid vessel for system A.

2.1.2. Electrical design

In order to achieve simplicity of design and construction, self-excited oscillators are employed. By using the push-pull oscillator circuits of Fig. 4 only a single tuned-circuit is required. Normal inductances and condensers are satisfactory for the tuned-circuit up to about 120 Mc/s and above this frequency Lecher lines are used. The output coupling consists of a coil or loop placed close to the tuned circuit. The valve chosen for these oscillators is the double tetrode type QQV 06/40. The anode voltage for normal operation should not exceed 600 V, but, since modulation is applied to the anodes in pulses of 5 μs duration and at a repetition rate of 500 per second, voltages up to 5 kV have been employed.

The circuit of the high power modulator built to generate the 5 kV pulses in shown in Fig. 5. A delay cable (Telcon Type Z 3 M) of characteristic im-

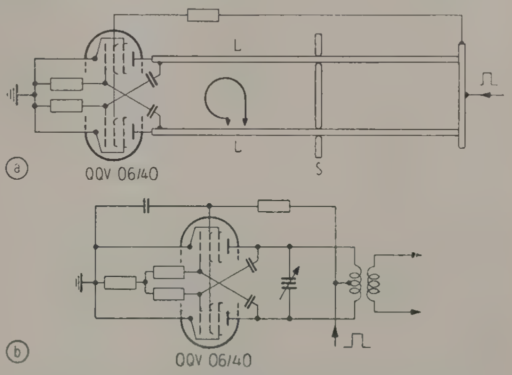

Fig. 4. (a) Tuned-line oscillator, for use above 120 Mc/s (LL Twin Lecher line, S Movable short circuit);

(b) Lumped circuit oscillator, for use up to 120 Mc/s.

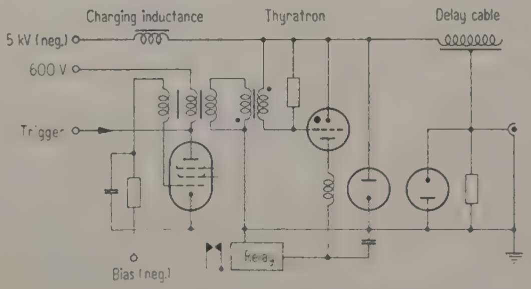

Fig. 5. Modulator circuit system 'A'.

pedance equal to 330 ohms is used for the storage element and this is discharged in series with the load resistance through an hydrogen thyratron type BT 83. The impedance of the combined load formed by the load resistance in parallel with the oscillator must be matched to the characteristic impedance of the delay line for correct operation [7]. In order to overcome the effect of fluctuations in the impedance presented by the various oscillators it is desirable that the characteristic impedance of the delay line should be small compared with the impedance of the oscillator. It may be noted that the use of a pulse transformer which would require more careful impedance matching is avoided in this circuit.

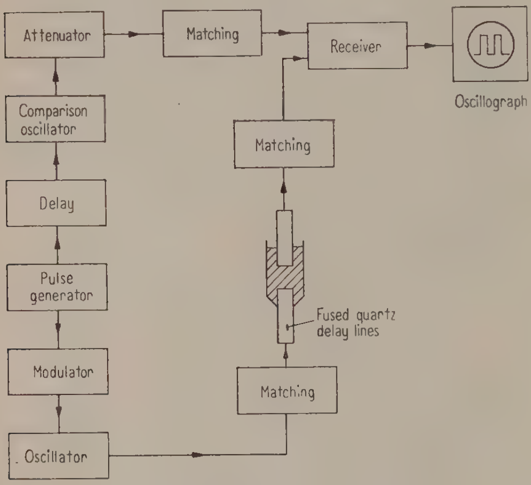

Fig. 6. Schematic diagram of system ‘A’.

A block diagram of system A is given in Fig. 6. The pulse generator, which triggers the modulator and the comparison oscillator, is of conventional design and this is also true of the delay circuit. The matching indicated in Fig. 6 is achieved by the use of coaxial lines of variable length. The transducers are X-cut quartz crystals having a fundamental frequency of 20 Mc/s and a capacity of 45 pF. In the case of the transmitting transducer an additional ‘stub’ line is provided to tune out this capacity. At frequencies below about 100 Mc/s matching to the attenuator is more easily accomplished by the use of tapped tuning coils across the input and output capacities.

Modified Radar receivers have been employed to provide the necessary amplification for the detected pulse. The GEE receiver type R 1355 has been used up to 130 Mc/s and the receiver R 1359 for the higher frequencies. In order to obtain a better signal-to-noise ratio in the latter, the initial stage of intermediate frequency amplification has been replaced by a Cascode low-noise amplifier [8].

Use of a comparison pulse for attenuation measurement implies that both comparison and ultrasonic signals shall follow identical paths through the amplifier. To achieve this a small coupling coil or probe is introduced near the input radio-frequency tuning circuit of the receivers for injection of the comparison signal. This circuit is very loosely coupled and little interaction occurs between the two signal paths.

To reduce the effects of receiver paralysis resulting from overloading by the transmitter ‘pick-up’ pulse, ‘blanking’ techniques may be employed. While the oscillator is generating power, a pulse is applied to the grids or cathodes of the initial amplifying stages of the receiver to reduce their gain to zero. As a further precaution a clipping network may be inserted after the second detector to prevent pulses of more than a predetermined height from entering the video-frequency amplifier.

2.1.3. Measuring procedure

The piston attenuator is set to minimum attenuation and, using its known calibration, the comparison oscillator is tuned to the required frequency (an odd harmonic of the fundamental frequency of the crystal transducer). No matching is attempted at this stage but sufficient signal reaches the receiver to permit it to be tuned. Next an absorption wavemeter is tuned to the output of the signal generator and this is now used to check the tuning of the transmitting oscillator.

The transmitter and receiver are connected to the ultrasonic system and the tuning of the former is checked. A small quantity of a liquid of low absorption, for example, alcohol, is put in the vessel and the two fused quartz rods are brought into contact. Under these conditions it is usually possible to observe a small signal which has passed through the ultrasonic system. The electrical system is now tuned and the matching lines adjusted to provide maximum signal. The final frequency does not necessarily correspond to an exact harmonic of the fundamental frequency of the transducer. The fused quartz rods are then separated to increase the ultrasonic path length and to reduce the signal amplitude to a little above noise level and the mechanical alignment is carried out as follows. The levelling screws are adjusted in turn to maximise the signal passing through the system: when an apparent maximum is obtained the apparatus is tilted grossly out of alignment in two directions at right angles to ensure that this is the largest maximum. The nuts controlling the compression springs are then tightened to prevent accidental alteration of the alignment and, finally, the tuning of the electrical system is rechecked.

It now remains to adjust the comparison oscillator. This is set to its pulse modulation position and the comparison pulse is made to overlap the first received ultrasonic pulse on the oscilloscope. Under these conditions beating between the two pulse envelopes can be observed and this is reduced to a minimum by tuning the comparison oscillator. Although there is no phase coherence between the transmitting and comparison oscillators, their stability permits the reduction of the beat to a very low rate, implying operation at identical frequencies. Now the attenuation in the comparison path is gradually increased and the attenuator matching is adjusted simultaneously to an optimum position.

The frequency of the oscillations is measured by means of a heterodyne wavemeter [9], the reference crystal of which is periodically checked against the Droitwich transmitter as a standard. Generally the frequency of the comparison oscillator is measured directly: this produces a narrower frequency spectrum having a longer pulse length than the main oscillator or it can be switched to continuous wave operation.

It is found that mechanical alignment at the higher frequencies above 100 Mc/s is complicated by the change in path length produced during the angular adjustment. For this reason the alignment procedure is performed at about 100 Mc/s and only residual corrections are made at higher frequencies. After careful alignment at any one frequency, note is made of all electrical settings so that the conditions can be repeated readily at a later date.

In conclusion it may be remarked that the system has been used successfully as a continuous wave interferometer for velocity measurements. The comparison oscillator is then employed to drive the ultrasonic system, internal sine-wave modulation being used to render the received signal suitable for display on the oscilloscope.

2.2. System B

2.2.1. Mechanical system

The precise mechanical movement (Fig. 7) is obtained by the sliding of one Invar steel cylinder A inside a second Invar cylinder B. One of the two fused quartz rods, C_1, is held in a conical hole along the axis of the cylinder, A, and the top end of this rod is also ground to take a small glass container. D, for the liquid to be measured. The other quartz rod C_2 is fixed into the Invar block E, which can be tilted about the centre point of the lower face of this rod; this is achieved by giving part of the block E a spherical surface F, which is held against the inside conical surface of the upper part of the cylinder B by four screws G. The adjustment of these screws tilts the axis of the fused quartz rod C_2 without varying the distance of it from the rod C_1.

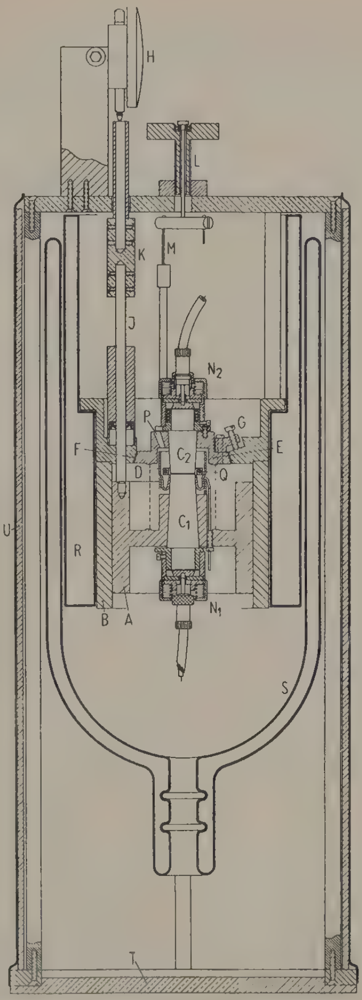

Fig. 7. Mechanical design of system 'B'.

The displacement of the cylinder A is transmitted to the dial gauge H through a vertical rod J, the two sections of which are thermally insulated from each other by a Bakelite connector K. For very short ultrasonic paths in the liquid between the fused quartz rods an accurate Swiss dial gauge is used having graduations down to 0.001 mm. For longer ultrasonic paths up to a maximum of about 1 cm a less accurate gauge is employed. The displacement of the cylinder A is controlled by the screw L which supports the cylinder through two thin steel wires, M. These wires act as thermal insulators so that the driving screw L can project outside the thermal insulation.

The generating and detecting X-cut quartz crystals of 10 Mc/s fundamental frequency are pressed against the outer ends of the fused quartz rods by means of the crystal holders N_1 and N_2. When the crystal holders and crystals are removed and the tilt screws G are loosened, it is found that optical interference fringes can be observed through the rods as the lower quartz rod is raised to touch the upper one. However, this method of alignment is insufficiently precise for operation above 100 Mc/s when it is necessary to adjust the tilt screws for maximum ultrasonic signal.

About 12 cc of the liquid to be measured is introduced into the container D. A heavy copper wire coil is wound around the outside of the container and a periodically interrupted current of about 15 amperes is fed to the coil by a thermostat. This on-off cycle of current provides heating for proportional temperature control and also generates an intermittent magnetic field to drive a small annular magnetic stirrer Q.

Three tapered holes P are ground to take standard B 7 glass cones and these are used, respectively, for the insertion of two thermistors (Standard Telephones and Cables, type F) – one for measuring the temperature and the other for controlling the thermostat bridge – and for the introduction and removal of liquid from the container D. Since some liquids cannot be exposed to the atmosphere, the apparatus can be fitted with chromium-plated brass bellows which seal off the space around the tank between the upper and lower steel cylinders, A and B. When the bellows are in position the apparatus can be connected directly to a distillation plant via a B 7 cone in one of the holes P, and air can be completely excluded from the space above the tank. Although the liquid is in direct contact with glass and fused quartz only, the vapour of acids will attack the Invar steel between the bellows and the quartz rods and it is necessary to dismantle the apparatus afterwards to clean off the slight corrosion. This involves the loss of the alignment between the fused quartz rods so, if corrosive liquids are to be used regularly, the steel should be coated or plated for protection.

The apparatus was designed to operate over the temperature range from +100° to −150° C and low temperatures are attained by means of liquid nitrogen. The outer Invar cylinder B is surrounded by a copper jacket R, which is partially filled with a low melting-point liquid, and liquid nitrogen is forced into it by a cooling system similar to that described by Vajda and Hart [10]. Around the copper jacket is a Dewar vessel, S, having a hole in the bottom to take the coaxial cable from the detecting crystal and the heater wire from the liquid container. The hole in the bottom of the Dewar vessel is fitted with glass bellows to allow for thermal contraction of the inner wall. The thermal insulation of the apparatus is completed by two Paxolin discs, T, a Paxolin tube, U, which is hinged for removal, and a rubber tube which is rolled down over U. Before lowering the temperature of the system it is essential to dry the air inside and, in particular, to insure that the graphite lubricant between the sliding cylinders is quite dry. A separate thermostat regulates the temperature of the cooling liquids in the copper jacket. For temperatures above room temperature the jacket R and the Dewar vessel S are unnecessary and an additional heater coil is wrapped around the outer cylinder B to raise the mean temperature of the apparatus to a few degrees below that required for the liquid in the container D.

2.2.2. Electrical system

The electrical arrangement is similar to that of system A apart from a few relatively unimportant details.

2.3. *System C*

2.3.1. General considerations

A hermetically sealed system has been constructed for measurements in liquids and liquefied gases at pressures up to 100 atm. over the frequency range 1 to 100 M/s. As discussed in Section 1.2. comparatively large ultrasonic path lengths are required for absorption measurements in the region of 1 Mc/s while at the same time a simple and compact design is required for pressure applications. By employing a common transmitting and receiving transducer the effective ultrasonic path is doubled and the mechanical layout is considerably simplified. In addition this avoids the difficulty of producing electrical connections of constant impedance to a moving transducer.

A disadvantage of the common T-R system, however, is the unavoidable paralysis of the electrical receiver for a short time following the transmitter pulse. Further, the transducer itself will continue to vibrate after the termination of the transmitter pulse and will therefore be unsuitable for the detection of weak echoes during a certain recovery period.

An ordinary plane reflector is unsuitable for the measurement of relatively high absorption coefficients since if the reflector is set at sufficiently short range the reflected signal arrives at the transducer before the system has recovered from the transmitter pulse. This difficulty is overcome by the use of a fused quartz delay line as a reflector [11]. On the other hand, with low absorption coefficients, the delay line is unsatisfactory because pulses reflected several times within the liquid remain strong enough to interfere with the delayed signal; further the length of the delay line restricts the available liquid path. The two reflectors are therefore used in turn.

Pulse systems working as common T-R arrangements at 7.5 Mc/s and above have been described by Pellam and Galt [12] and by Pinkerton [1]. In the present discussion attention is particularly focussed on the problems associated with the application of pressure and the measurement of low absorption coefficients in liquids at relatively low frequencies.

2.3.2. The mechanical system

A cross-section of the apparatus is shown in Fig. 8. The thick-walled cylindrical tube A, in the following referred to as the cylinder, has an inside diameter of 2″, an outside diameter of 5″ and is 8″ long. The top-plate B and baseplate C are both 3/4″ thick and held to the cylinder by means of 5/8″ diameter high tensile steel bolts. All metal parts, except for the bolts, are made of FMB grade stainless steel. The bore of the cylinder and the surface of the piston D are ground to secure smooth and strictly parallel movement of the latter. The reflector E has an accurately machined and polished surface and is screwed into the piston D. The piston is moved by turning the screwed rod F. The thread has 26 turns per inch and the position of the reflector can be read from an externally mounted revolution counter, which counts 100 units per turn of the drive.

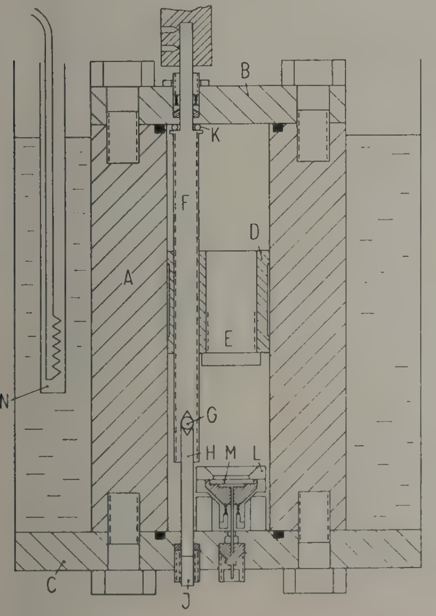

Fig. 8. Mechanical design of system 'C' (for description see text).

The drive is supported by the ball G and the rod H, the height of the latter being adjusted by means of the screw J in order to maintain a slight pressure on the ball bearing K and thus fix the position of the drive. The crystal holder (with the transducer M) is supported in such a way that it can be tilted about the centre of the top surface of the transducer. The tilting is carried out by means of two screws operated from outside which do not appear in the cross-section shown. By the eccentric arrangement of both ultrasonic path and drive with respect to the cylinder axis the maximum possible ultrasonic pathlength – in this case approximately 23 cm – is obtained for a given length of the cylinder. For the measurements of high absorptions the reflector E in Fig. 8 is replaced by a fused quartz delay line. The quartz rod has a diameter of 17.5 mm and a length of 128 mm providing a time delay of 43 μs per double journey. The end faces are ground parallel to each other to within 1′ and perpendicular to the axis to within 2′.

The cylinder is surrounded by a liquid bath which is kept at the desired temperature by circulating the liquid through a thermostat. The resistance element N is connected to a Sunvic resistance thermometer controller type RT. 2 operating in conjunction with the thermostat. In this way the temperature of the liquid is maintained constant to within ±0.1° C at temperatures between −60° C and +60° C. The temperature of the liquid bath is measured with mercury or alcohol in glass thermometers and is assumed – after about one hour has been allowed for equilibrium to be established – to be identical with the temperature inside the cylinder.

The whole assembly is well insulated thermally and is supported by two pieces of angle steel which in turn are mounted on a rigid wooden framework. O-rings are placed in annular grooves in the base and top plate to accomplish a pressure tight seal. The O-rings are made of synthetic rubbers especially selected for the substances to be measured. Alternatively, polythene or P.T.F.E. rings can be used. All other parts are sealed by suitably compressed washers made of either P.T.F.E. or polythene. It should be noted that due to the relatively high thermal expansion of the materials involved, all these gaskets are only effective over a limited temperature range unless they are readjusted at different temperatures (which is impracticable in the present arrangement) or are spring loaded as shown in Fig. 8 where the drive is led through the top plate.

Two stainless steel tubes enter the apparatus through the baseplate. One tube ends inside the baseplate and is normally used for feeding in or extracting the substances to be measured. The other projects inside the cylinder through a hole in the piston and is terminated immediately below the top plate. This second pipe line is connected to a pressure gauge and can be used alternatively for evacuating the apparatus by means of a rotary pump or for pressurising the system from a high pressure nitrogen supply via a reducing valve. This provides a convenient means for producing a constant working pressure well above the saturation point, and over a temperature range, without having to fill the entire system with the liquid under investigation. It is necessary, however, to take a number of test measurements before and after the admission of the nitrogen, in order to ensure that any nitrogen, which may be dissolved in the liquid, does not unduly influence the measured absorption. Needle valves are incorporated in both pipelines to disconnect the apparatus from the external supply system.

2.3.3. The electrical system

A block diagram of the electrical system employed in the frequency range 1 to 20 Mc/s is shown in Fig. 9. The trigger pulse generator has a repetition rate of 500 per second and produces trigger pulses for the time base of the oscilloscope and for the pulse generator incorporated in the transmitter. The latter provides switching pulses of 8 to 40 µs duration and of variable delay. The main part of the transmitter is formed by an EF 91 Colpitts oscillator and a QV 04/7 power amplifier. Both these stages can be pulsed independently and are, in normal operation, cut off during the intervals between transmitter pulses. The two stage transmitter is chosen in preference to a single stage pulsed oscillator because it enables accurate measurements of ultrasonic velocity to be carried out at low frequencies in the following manner: The oscillator is operated continuously, while the power stage is pulsed. A certain amount of CW breaks through the power stage and enters the receiver, there interfering with the signal pulse which is received in the usual way. If a measurement is taken over an ultrasonic path of, say, 10 cm and the corresponding number of beats (about 300 at 3 Mc/s) is counted then, in principle, the ultrasonic wavelength can be measured with an accuracy of ± 3 parts in 10^4. In practice, however, the accuracy of a velocity measurement is limited by the frequency stability of the oscillator and is estimated to be ± 2 parts in 10^3. This procedure for measuring velocity is not applicable at frequencies above 5 Mc/s, because sufficient CW then breaks through the power stage to overload the receiver permanently.

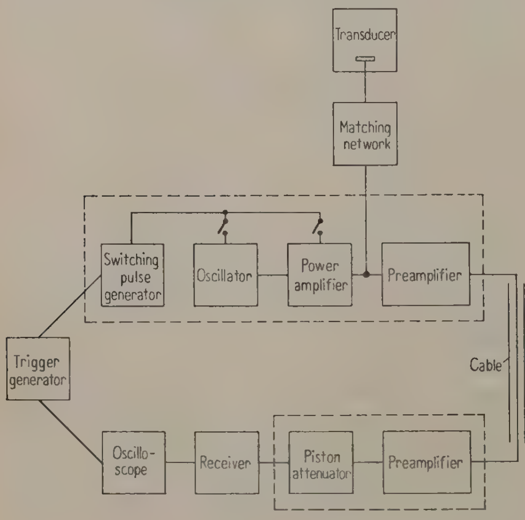

Radio frequency pulses of approximately 100 V peak amplitude appear at the output of the power stage and are fed to the transducer via a matching network. The latter is mounted in a small box as near as possible to the mechanical system without interfering with controls or thermal insulation. An H_{11} (circular) piston attenuator is placed between the transducer and the receiver input. This arrangement is chosen, because at low frequencies pulses with a duration of up to 40 µs have to be used and sufficiently long time intervals between transmitter pulse, received echo and subsequent reflections are not normally available for the accommodation of a comparison pulse.

Two stages of pre-amplification are used which provide a net gain of 25 dB, sufficient to compensate for the insertion loss of the attenuator. No deviations from linearity can be detected, within the experimental accuracy, for input voltages up to about 0.1 V. Thus if 100 µV is considered as a minimum signal voltage, a range of 60 dB is available for measurements. The GEE receiver type R 1355 is used as a receiver for frequencies above 10 Mc/s. This receiver is slightly modified to improve its overload performance and recovery time and plug-in RF-units have been adapted to cover the required frequency ranges. For frequencies below 10 Mc/s a T.R.F. receiver is used which consists of three tuned stages and three stages of wide band amplification. The tuned stages operate at the five spot frequencies 1, 3, 5, 7 and 9 Mc/s. The low frequency receiver is completed by a diode detector and the video amplifier in the R 1355 receiver.

At frequencies above 20 Mc/s the system remains essentially the same, but the transmitter is replaced by a self-excited push-pull oscillator driven from a high power pulse modulator as described in section 2.1.2. and illustrated by Figs. 4 and 5.

2.3.4. Recovery after the transmitter pulse

Using a transmitter output voltage of 100 V the receivers described in section 2.3.3. recover in about 5 µs, which at low frequencies is much less than the mechanical recovery time of the transducer. No further improvement is obtained by ‘blanking’ the first two receiver stages and this is only performed as an occasional check. In connection with the mechanical recovery time of the transducer, three different effects have to be distinguished:

(i) The decay of the thickness vibration of the transducer.
(ii) The decay of cross modes having resonance frequencies near the resonance frequency of the thickness mode and excited simultaneously with the latter.
(iii) Interaction between the transducer and the crystal holder.

The first of these effects is always present and the resulting recovery time depends mainly on the fundamental frequency, f_0, of the transducer, but very little on the actual harmonic frequency, at which it is operated. Practical values lie around 50 μs for $f_0 = 1$ Mc/s and 10 μs for $f_0 = 5$ Mc/s, in fair agreement with theoretical expectations. Abnormally long and irregularly shaped decays are produced by the second and third effects which are generally more troublesome than the first one and may, under certain conditions, make accurate measurements impossible. In order to study these effects and to find ways for their elimination, a number of different transducers have been used under different mounting conditions, and the following points have emerged from practical experience:

1. At any given frequency of operation a transducer with the highest practicable fundamental frequency is used because the recovery time due to both the thickness mode and to spurious modes decreases with increasing fundamental frequency, f_0, of the transducer.

2. When a fundamental frequency of 1 Mc/s is considered essential, barium titanate ceramic transducers are used in preference to X-cut quartz crystals, because the former have been found to exhibit less tendency for excitation in cross modes, and shorter decay times of the thickness mode. In addition, electrical matching is much more easily achieved at frequencies up to about 11 Mc/s. The high capacity of the transducers presents some difficulty at higher frequencies but, if special care is taken to avoid unnecessary line inductance, satisfactory signal strength can be obtained up to 15 Mc/s. No attempt has been made to use barium titanate transducers with fundamental frequencies higher than 1 Mc/s because of the inconveniently high capacities involved.

3. Three different arrangements of the exciting electrodes have been used:

a) The two opposite surfaces of the transducer are plated in full and each surface forms one electrode;
b) One of the electrodes covers only a central area of one of the surfaces, the other surface being plated in full;
c) As with (b) except that on the surface which is completely plated the plating is extended around the edge of the transducer on to the outer part of the opposite surface occupied by the smaller electrode.

Arrangement (a) produces a negligible electric field in the radial direction and is preferable for transducers having a low value of fundamental frequency (e. g. barium titanate at 1 Mc/s, X-cut quartz at 1 and 3 Mc/s), where there is strong excitation of cross-modes owing to the comparatively large ratio of thickness to diameter. Any of these arrangements can be employed with transducers of higher fundamental frequency but (c) is preferred since it reduces the influence of the clamping.

2.3.5. Limitations of the system

A low frequency limit is imposed on measurements of the absorption in liquids by the pulse method as a result of diffraction effects associated with the source of finite diameter ($= 2a$). Pinkerton [1] has found experimentally that with a common $T-R$ system operating above 7.5 Mc/s no correction to the measured absorption is required provided the path length is confined to the Fresnel region of the sound beam and does not exceed $a^2/2\lambda$. Recent calculations of Seki et al. [13] show that the recorded output of the transducer should fall slightly and also fluctuate inside the Fresnel region, the last of a series of maxima occurring at a path length equal to $2.4\,a^2/\lambda$. The calculations show that these effects would have little influence at the higher frequencies of Pinkerton's experiments but below about 5 Mc/s they become increasingly important. Preliminary investigations on the present system indicate that diffraction effects can be taken into account at frequencies above 1 Mc/s and do not constitute a fundamental limitation to the measurements.

A maximum change in ultrasonic path-length of 20 cm is possible with system C and this requires a volume of liquid of 250 cm³. If a minimum signal range of 10 dB is considered necessary the absorption in the liquid must exceed 0.5 dB/cm.

Finally, an upper frequency limit is imposed on the measurements. This depends upon the precision of the reflector movement and its accurate measurement and is further determined by the absorption in the liquid. In practice the maximum absorption which can be measured with reasonable accuracy is about 250 dB/cm.

The above considerations can be illustrated by considering as a typical example carbon tetrachloride in which $\alpha/f^2 = 550 \cdot 10^{-17}\,\mathrm{s^2\,cm^{-1}}$ at

25° C: measurements in this liquid can be made at frequencies between 3 Mc/s and 70 Mc/s to within an estimated accuracy of ±2%.

Acknowledgments

The work carried out at Imperial College was supported by a grant from the Department of Scientific and Industrial Research. The authors gratefully acknowledge this assistance and E. L. H. wishes to thank the same body for provision of a maintenance grant during the course of this work: R. B. is indebted to the Worshipful Company of Clothworkers for their award of a Bursary. J. H. A. whises to record his appreciation of the technical assistance rendered by members of the Akers Research Laboratories.

References

[1] Pinkerton, J. M. M., Proc. Phys. Soc. London **B 62** [1949], 286.
[2] Gainsborough, G. F., Proc. Inst. Elect. Engrs. (III) **94** [1947], 203.
[3] Brown, J., Proc. Inst. Elect. Engrs. (II) **96** [1949], 491.
[4] Redwood, M. and Lamb, J., Proc. Inst. Elect. Engrs. (B) **103** [1956], 773.
[5] Redwood, M. and Lamb, J., Proc. Phys. Soc. London **B 70** [1957], 136.
[6] Redwood, M., Proc. Phys. Soc. London, in the press.
[7] Heins, H., Electronics **19** [1946], No. 7, 96.
[8] Wallman, H., Macnee, A. B. and Gasden, C. P., Proc. Inst. Radio Engrs. **36** [1948], 700.
[9] Essen, L., Proc. Inst. Elect. Engrs. (III) **92** [1945], 291.
[10] Vajda, J. and Hart, D. P., Rev. Sci. Instrum. **24** [1953], 354.
[11] Rapuano, R. A., Phys. Rev. **72** [1947], 78.
[12] Pellam, J. R. and Galt, J. K., J. Chem. Phys. **14** [1946], 608.
[13] Seki, H., Granato, A. and Truell, R., J. acoust. Soc. Amer. **28** [1956], 230.

FORMATION OF AIR BUBBLES IN AIR-SATURATED WATER AT REDUCED PRESSURE AND THEIR INDICATION BY AN ACOUSTICAL MEASURING PROCEDURE

by H. J. Naake, K. Tamm, P. Dämmig and H. W. Helberg

III. Physikalisches Institut der Universität Göttingen

Summary

With the aid of sound-absorption measurements the formation of bubbles in water saturated with air is investigated. The bubbles occur when the static air pressure in the sample holder is reduced gradually or in steps. The formation of bubbles is reduced when the water is subjected to a pressure greater than atmospheric before commencing the experiment.

The behaviour of air pockets adhering to solids and of air-filled pores in the walls of the container or in solid particles under conditions of increased or of decreased pressure is considered. Calculations of the growth and ascent of bubbles and the sound absorption caused thereby are compared with measurements.

Sommaire

On a étudié la formation de bulles dans l'eau saturée d'air, en recourant à des mesures d'absorption du son. Les gouttes se forment lorsqu'on réduit, graduellement ou de façon discontinue, la pression statique de l'air sur l'éprouvette; il y en a moins si, avant l'expérience, l'eau a été soumise à une pression supérieure à la pression atmosphérique.

On s'est penché sur le comportement des poches d'air accolées aux solides, et à celui des pores remplis d'air dans les parois de l'éprouvette ou des particules solides, lorsque la pression est augmentée, ou bien diminuée. On a calculé la croissance et l'ascension des bulles, ainsi que l'absorption du son qui en résulte, et l'on a comparé les résultats de ces calculs avec ceux des mesures.

Zusammenfassung

Mit Hilfe von Messungen der Schallabsorption wird die Blasenbildung in luftgesättigtem Wasser untersucht, die auftritt, wenn der statische Druck über dem Meßgefäß allmählich oder in Stufen reduziert wird. Die Blasenbildung wird verringert, wenn man vor Beginn des Versuches einen Überdruck auf das Wasser einwirken läßt.

Weiterhin werden Überlegungen über das Verhalten von Luftansammlungen an Festkörpern und von luftgefüllten Poren in der Gefäßwandung oder in festen Partikeln bei Anwendung von Über- oder Unterdruck angestellt. Berechnungen über das Anwachsen und Aufsteigen von Luftblasen und die dabei zu erwartende Schallabsorption werden mit den Messungen verglichen.

1. Introduction

Under certain physical conditions, e. g. a rapid decrease of pressure, vapour or gas bubbles are formed in liquids and may give rise to considerable changes in their physical behaviour. A change in the absorption and velocity of sound is an example of this. If the physical properties of the liquid such as pressure, temperature, surface tension and degree of saturation with gas – all of which affect the formation of bubbles – are known, it is relatively easy to describe qualitatively the behaviour of bubbles already existing. Within certain limits it is possible, in addition, to calculate the rate at which the size of the bubbles changes. On the other hand no satisfactory explanation of the mechanism of origination of gas or vapour bubbles in a liquid has yet been found.

This last mentioned problem has already been investigated from various directions. Becker and Döring [2], [4], Turnbull and Fisher [21] and others have attempted to give a theory explaining the origination of a bubble or the cavitation of a liquid from a purely thermodynamical viewpoint. The conclusion of all these considerations is that a gas or vapour bubble which appears spontaneously will again vanish immediately unless considerable heating or high tensional stresses occur or unless the liquid is highly supersaturated with gas. In practice, however, formation of bubbles may already occur at much lower temperatures, without the application of tension and with slight supersaturation.

The new point of view is obtained by taking into consideration the properties of solid surfaces which are in contact with the liquid either as a wall of the containing vessel or as a solid impurity. For every combination of solid and liquid an angle of adhesion exists. S. Takagi [18] has shown that the negative pressure required for the formation of a bubble on a wall or on a solid particle depends on the adhesion angle. In the case of an ideal non-wetting liquid (angle of adhesion 180°) spontaneous accumulations of gas occur at the boundary between liquid and solid, according to his theory. Assuming an angle of 179°, a tensile stress of 0.2 $\mathrm{kg/cm^2}$ is sufficient for the formation of bubbles. The angles of adhesion observed in practice are, however, without exception smaller and call for appreciably higher tensile stresses.

In another group of investigations it is assumed that accumulations of gas are already present in the liquid before the negative pressure is applied. This conception was already arrived at by C. Tomlinson [19], [20] whose publication dating back to 1867 is probably the oldest systematic investigation of the problem. Tomlinson observed that bubbles were formed on an immersed sample when the latter was in an „active“ condition for the formation of bubbles. In the case of some materials treatment with alcohol or heating until red-hot destroyed the activity, whereas in the case of others (e. g. waxes, resins) it did not. Tomlinson concluded that the active condition was probably caused by the presence of adsorbed gas films.

The view that accumulations of gas on solids (walls of the container, impurities) contribute to the formation of bubbles was also held at a later date by E. Meyer and E. Skudrzyk [13]. Skudrzyk regards, in particular, small air-filled cavities in the bounding surfaces as being the nuclei for the formation of bubbles. This possibility will later be examined in greater detail.

Takagi also points out that the wetting effect, which he examined very thoroughly, is not by itself sufficient to explain all the phenomena that occur. In addition, effects due to the micro-structure of the walls have to be taken into account. The effect that pores in the walls of the vessel have on the resistance of the liquid against cavitation is examined by Fisher [7]. He considers two idealized cross-sections of pores and calculates the negative pressure required for the formation of a gas bubble.

Another possibility, suggested by Fox and Herzfeld [8], is that accumulations of air in liquid may be stable over long periods of time. According to this suggestion organic impurities in water, in particular proteins, whose presence can never be fully avoided, may form a film around an air bubble and thereby prevent its complete solution. According to the authors there are therefore always sufficient nuclei present in the liquid that can grow to macroscopic bubbles when a negative pressure is applied.

R. B. Dean [3] developed a theory for the formation of bubbles that does not require the presence of nuclei foreign to the liquid. He suspects that turbulence phenomena caused by impacts or sound waves play a decisive role and provide the forces necessary to overcome the surface tension. According to the theory rotation-free eddies are capable, at their moment of origination, of creating large tensile stresses in the liquid since they are accompanied by a negative pressure proportional to $1/r^2$ (r = distance from eddy centre). Sound waves of relatively low intensity may, according to Dean, give rise to appreciable tensile stresses in the liquid if viscosity effects cause turbulence in the boundary layers.

The object of the investigation to be described was to contribute to the explanation of the formation of bubbles and to investigate the further behaviour of the bubbles in the liquid. Certain considerations of G. Kurtze [10], which are based on conceptions similar to those of Skudrzyk, served as basis for this work. They will be briefly described here.

2. The behaviour of air bubbles in water containing air

If an air bubble is floating freely in water, a continuous exchange between the air of the bubble and the air in the water occurs due to diffusion. The preferential direction of the diffusion process depends on the partial pressure p_i of the air in the bubble and the partial pressure p_a of the air dissolved in the water. The partial pressure of the air inside the bubble is equal to the total pressure in the bubble if the vapour pressure of the liquid can be neglected, and is made up by the hydrostatic pressure p_0 and the additional pressure $2\alpha/r$ due to the surface tension α: $p_i = p_0 + 2\alpha/r$. The partial pressure p_a of the dissolved air is dependent on the degree of saturation.

In undersaturated water bubbles of all sizes dissolve, whereas in oversaturated water ($p_a > p_0$) an equilibrium radius

$$R = \frac{2\alpha}{p_a - p_0}$$

exists, for which the partial pressures of the air inside and outside the bubble are equal. This equilibrium is, however, unstable, i. e. should the bubble radius increase, the internal pressure decreases, with the result that air diffuses into the bubble and the radius is increased still further ($\partial V/\partial r > 0$ where V is the volume of the bubble). A limit to this increase exists in practice in that the bubble rapidly rises to the surface of the liquid, and bursts. Should the radius of a bubble that is in equilibrium decrease slightly, the internal pressure increases, air diffuses out of the bubble and the latter dissolves completely within a few seconds. One may say, therefore, that free bubbles cannot exist for long either in under- or in supersaturated water.

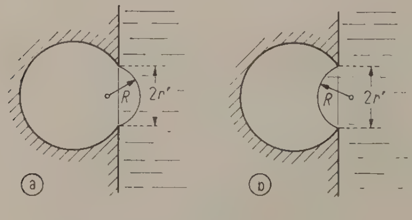

Fig. 1. Behaviour of an air-filled pore with the radius r' of the opening; (a) $p_0 < p_a$, (b) $p_0 > p_a$.

Different relations exist for bubbles clinging to solid surfaces. Consider an air-filled pore in the container wall, with an opening assumed to be circular with radius r' (Fig. 1). The spherically shaped air-water boundary that stretches across the pore opening can have positive or negative radii of curvature. The absolute values of these cannot, however, be less than the radius r' of the pore

$$|r| \geqq r' .$$

Equilibrium of the air diffusion exists as above, when the boundary surface has a radius of curvature

$$r = R .$$

In contrast to the case of a free bubble, the equilibrium is now stable over the range

$$|R| > r'$$

since here the radius decreases when the volume increases ($\partial V/\partial r < 0$). An equilibrium condition can therefore exist for undersaturated water also, when the boundary surface curves slightly into the pore (see Fig. 2). The reason for the stability is that with decreasing air volume the additional pressure due to surface tension also decreases, thereby decreasing the diffusion of air into the water. However, if the radius of the pore opening is greater than the absolute value of the equilibrium radius, no equilibrium can exist.

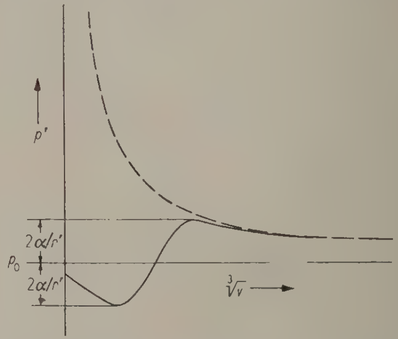

Fig. 2. Schematic representation of the course of the total pressure p' in a free air bubble — — — and in an air-filled pore ——— as functions of the volume. Stable equilibrium is possible for $dp'/dV > 0$. α surface tension, r' radius of the pore opening.

In the case of large external pressures ($p_0 > p_a + 2\alpha/r'$) the entire pore is filled with water and is lost as nucleus, provided that no part of the wall inside the pore has a radius of curvature less than r'.

With sufficient reduction of the external pressure ($p_0 < p_a - 2\alpha/r'$) the bubble swells outwords, becomes more than hemispherical and than grows to such an extent — since now the radius of curvature is increasing — that a large part of the air volume is detached and rises to the surface as a free bubble. The remaining part continues to grow, i. e. according to this mechanism the nucleus is continually producing bubbles and is continuously extracting air from the water through diffusion. This phenomenon may be observed very well when a bottle of soda-water is opened, it frequently occurs that a continuous stream of bubbles rises from a definite point in the wall or in the liquid.

In view of the behaviour of the pores under conditions of excess and reduced pressures as described above, it is to be expected that the application of an excess pressure will render the water insusceptible to degassing by pressure reductions up to the value of the initial pressure excess. This idea has already been mentioned by Skudrzyk [13].

A further possibility for the stabilization of air accumulations may be thought of as being provided by structures with smooth surfaces and cohering together due to adhesive or electrostatic forces. If one assumes that at the point of contact both particles have a convex curvature and that an air cushion is present, no pressure increase whatsoever will theoretically cause complete solution of the air cushion. Such a model could possibly be used to explain the micro-photos published by Liebermann [11], in which the pore-model cannot be described due to the minuteness of the solid particles visible in the picture.

One may also, in addition, imagine a solid particle having a rough surface as being surrounded by a layer of air. In this case also, the small, negative radii of curvature that arise when the air-water boundary is stretched across the surface roughnesses result in a stabilization of the surrounding air layer.

3. Methods of measurement

Two methods were employed to investigate the effects occurring during the degassing of water: an acoustical and an optical method. Only the acoustical method will be described here. A description of the optical method will be given in a later paper [22].

In the acoustical method, reverberation time measurements were carried out to measure the sound absorption, thereby enabling the presence of air bubbles to be determined. Whereas dissolved air causes no measurable increase in sound absorption [14] the formation of bubbles immediately causes an increase in absorption. The increase depends on the number and the size of the bubbles in the vessel as well as on the freqency of the sound wave. The acoustical method has the advantages that even a few bubbles produce an effect that is easily measured and that the degree of damping can easily be recorded over fairly long periods of time. Its disadvantage is that the damping is determined by two independant quantities – number of bubbles and bubble radius – and that a further measurement is required to determine one of these before an unambiguous result is obtained.

To carry out the absorption-measurements by the reverberation time method, the liquid sample under test was poured into a glass vessel suspended inside a pressure-flask. A piezo-electric crystal, attached to the outer side of one wall of the vessel and driven by pulsed oscillations, was used to excite numerous characteristic modes of vibration in the liquid. The decaying reverberation that commences when the driving signal is switched off, was picked up by a second crystal similarly attached to the wall. This receiver voltage was given a logarithmic characteristic, rectified and applied to the vertical deflection amplifier of the display C. R. O. which had a calibrated constant-velocity sweep. The decay constant in dB/second of the entire system, consisting of container plus liquid, could be read off directly from the slope of the straight line drawn on the C. R. O. screen. Similar measurements with water that was completely devoid of bubbles were always carried out in order to eliminate the constant losses due to the containing vessel, thereby enabling the effect of oscillating bubbles to be determined.

4. Preparatory treatment of the water

A large number of preparatory experiments were necessary before reproducible conditions could be obtained. Distilled water was used, which was drawn through a very fine glass filter. Subsequently, a large quantity of the water (180 l) was poured into a vessel and saturated with air. The air used for this purpose was filtered through cotton-wool to remove dust particles etc., and then allowed to bubble through a distributing filter.

Two methods were used to determine the air content of the water. In the first method, the air contained in a given quantity of water was displaced by the same quantity of a saturated potassium hydroxide solution, and its volume was measured. In the second method, the air contained in a known volume of water was driven off by carbon dioxide produced within the water from calcium carbonate and hydrochloric acid. The volume of air was measured after the carbon dioxide had been removed by a concentrated potassium hydroxide solution.

The air content was always adjusted so that the water was just saturated before the experiments began. The temperature of the water was kept at about 20° C. After being saturated with air, the water required was transferred through a glass tube to the testing vessel. To the water, hitherto cleaned of or kept free from contaminating substances, a weighed quantity (100 mg) of defined „contaminating“ particles was added. For this purpose jeweller's rouge was used at first, and later a powder was employed consisting of pure aluminium oxide and having a mean particle diameter of approximately 4 μm.

5. Calculation of the expected damping in the measuring vessel

5.1. Damping caused by one bubble

The calculation of the damping caused by a bubble is based on a theory due to Pfriem [15]. This theory has been confirmed by measurements carried out on single bubbles by M. L. Exner [5], W. Hampe [6] and H. Haeske [9].

An air bubble in water represents a system capable of performing oscillations. The compliance is due to the air enclosed in the bubble, the mass due to the medium taking part in the oscillation. The resonant frequency is given by the relation

$$f_0 = \frac{1}{2\pi r}\sqrt{\frac{3\gamma(p_0+2\alpha/r)}{\varrho_w}}, \tag{1}$$

where $\gamma = c_p/c_v$ is the ratio of specific heats and ϱ_w the density of water.

For a constant radius, the resonant frequency is therefore proportional to $\sqrt{p_0+2\alpha/r}$. The damping due to the bubble has two components: a thermal component, caused by the non-adiabatic compression of the air in the bubble, and a radiation component due to the spherically symmetrical radiation of energy into the surrounding medium. Both components in combination essentially determine the amplitude of oscillation of the bubble near its resonant frequency. An irreversible loss of acoustical energy in the container is, however, caused only by the thermal component, since in the diffuse sound field existing in the vessel the reradiated energy is to all intents and purposes equivalent to that previously present.

The energy absorbed per unit time by thermal processes by the bubble has a value of

$$\dot{E}_{th} = \frac{\eta_{th}}{F\omega} v_B^2,$$

where v_B is the R. M. S. velocity at surface of bubble, $F = \delta r/S\,\delta p$ the compliance constant of bubble, S the surface area of bubble and η_{th} the loss factor of thermal damping.

The relation between the velocity at the bubble surface v_B and the free-field sound pressure p is given by the impedance of the bubble:

$$Z = \frac{1}{F\omega}(\eta_{th}+\eta_r) + j\left(\omega M - \frac{1}{\omega F}\right) \tag{2}$$

(where η_r is the damping factor due to radiation and $M = 4\pi\varrho_w r^3$ the oscillating mass) so that the relation between the thermally absorbed energy and the sound pressure in the container is (3)

$$\dot{E}_{th} = \frac{\eta_{th}}{(1/\omega F)^2(\eta_{th}+\eta_r)^2 + (\omega M - 1/\omega F)^2}\,\frac{S^2}{\omega F}\,p^2 .$$

If one now assumes that per unit volume one bubble of radius r is present and one introduces the acoustical energy present per unit volume at a sound pressure of p_0, the decay constant of the entire system is

$$\delta = 4.34\,\frac{\eta_{th}}{(\eta_{th}+\eta_r)^2 + (\omega^2/\omega_0^2-1)^2} \times S^2\omega F(\varrho_w c_w^2)\ \mathrm{dB/s}, \tag{4}$$

where $(\varrho_w c_w^2)$ is the compressibility of water. This assumes that the losses in the water itself are negligible, and that the sound energy in the bubbles is negligible in comparison to the sound energy in the water.

That the first condition is fulfilled, is immediately evident when the damping of distilled water quoted in the literature (0.8 dB/s at 50 kc/s) is compared to the damping due to air bubbles that was measured. (Order of magnitude 100 to 1000 dB/s.) Since furthermore a bubble by itself, with a resonant frequency of 50 kc/s, should have a decay constant of 150,000 dB/s the only explanation that can be offered for the much lower values of damping constant actually measured is that by far the greater part of the energy is stored outside the bubble, i. e. in the water. Hence the second condition is also fulfilled.

To apply the above equation for the decay constant to bubbles that are undergoing a slow growth, it is also necessary to know the damping factors η_{th} and η_r for bubbles excited at a frequency other than the resonant frequency. Pfriem [15] gives the value for the thermal damping factor η_{th} as function of the dimensionless quantity $\psi = 2r\sqrt{\pi f/a}$, where $a = \lambda/c_p\,\varrho_A$ the thermal conductivity of air. The mass of the medium participating in the oscillation does not enter into Pfriem's calculation, so that the results are also applicable to bubbles excited outside their resonant frequency.

The loss factor due to radiation may easily be calculated from the compressional energy in the bubble and from the power radiated by the bubble as a spherical radiator [17]. We obtain

$$\eta_r = \frac{8\pi^3\varrho_w(f_0R)^3}{3c_w\varrho_a c_a^2}\,\frac{f^3}{f_0^3}, \tag{5}$$

where ϱ_w, c_w are the density and sound velocity respectively for water, ϱ_a and c_a the density and sound velocity for air, and R the resonance radius.

5.2. Damping caused by a given number of bubbles

The optical investigations of the degassing process have shown that under the test conditions that existed the concentration of bubbles was always less than 1.5 per cc. The absorptional cross-section of a bubble at resonance, on the other hand, is only

0.5 cm² at 50 kc/s and for bubbles not in resonance it is even less. Therefore, and also because of the great difficulties encountered when the problem is treated theoretically, the mutual reaction of bubbles on one another was not considered, even though under unfavourable circumstances the statistical distribution of the distances between bubbles may result in an effect. The increase in the decay constant of the system, caused by the bubbles, is therefore given by the expression (4) in the case of one bubble per cm³, and is proportional to the bubble concentration.

5.3. *Rate of growth of the air bubbles*

If the air pressure over a given volume of water saturated with air is suddenly or gradually reduced, the water becomes supersaturated with air. The decrease in the hydrostatic pressure results, on the one hand, in an increase in the volume of the gas accumulations existing as thin layers, or in the pores of solid particles or stabilised in some other way by their shape. In many cases this results in an increase in the radius of curvature of the air-water boundaries. On the other hand, the critical radius

$$R = \frac{2\,\alpha}{p_a - p_0} = \frac{2\,\alpha}{\Delta p} \tag{6}$$

is decreased because of the increase in Δp. Both effects have as result that some air accumulations may increase beyond the equilibrium point, and from there on grow still further due to diffusion. If during this growth the radius does not again become less than the critical radius (e. g. when the opening of an air-filled pore is sufficiently large) the growth will continue steadily. The rate of growth may be calculated if the diffusion constant of air in water is known.

Measurements of the diffusion constant have hitherto only been carried by observation of bubbles dissolving in undersaturated water. The bubbles concerned were either clinging to a wall, or rising freely in an observation tube, dissolving as they rose. Liebermann [11] observed that the rate of growth was larger for freely rising bubbles than for bubbles attached to some surface. He obtains a diffusion constant apparently 2 to 3 times larger for freely rising bubbles using in both cases the formula (7) given below for resting bubbles. Similar results, i. e. an apparent diffusion constant ($D' = 5.4 \cdot 10^{-5}$ cm²/s) 2.7 times as large as the known value ($D = 2.0 \cdot 10^{-5}$ cm²/s) for diffusion of air in resting water, have recently been observed by Martini [12] who also gives a simple model for explaining this fact.

If one assumes that the diffusion constant observed when a bubble dissolves also holds good for the case of a bubble growing in supersaturated water, the size of the bubble can be expressed as a function of time. Disregarding the effect of surface tension for the present, we find for resting bubbles

$$r^2 = r_0^2 + 2\,D\,s\,\delta\,t\,, \tag{7}$$

where r_0 is the initial radius, D the diffusion constant, s the solubility of air in water and δ the degree of supersaturation. If surface tension is taken into account, one obtains (see ref. [10]) (8)

$$r^2 - r_0^2 + R\left(\tfrac{4}{3}\,\delta + 2\right)\left(r - r_0 + R \ln \frac{r - R}{r_0 - R}\right) = 2\,D\,s\,\delta\,t\,,$$

where R is the critical radius.

It is important that for small bubbles the surface tension be taken into consideration, since it reduces the rate of growth of small bubbles. In both equations the initial radius of the bubbles at the time $t = 0$ appears. This is, to begin with, an unknown quantity. If, however, one reduces the external air pressure in small steps (e. g. by 100 mm Hg at a time) the range of values assumed by the initial radii may be confined. Additionally one must make the plausible assumption that in the time between two pressure steps the radii of nuclei with $r < R$ do not alter appreciably. The bubble size as function of time for the individual pressure steps is given in Fig. 3. For the time $t = 0$ the value $r = 2\,R$ was assigned arbitrarily. Deviations of the initial radius from this value result merely in a shift of the abscissa. From these curves it is possible for example, to determine the time required for the bubble to become just visible ($r = 30$ µm) or to attain the resonance radius (e. g. 60 µm at 50 kc/s and 600 mm Hg, see Fig. 4).

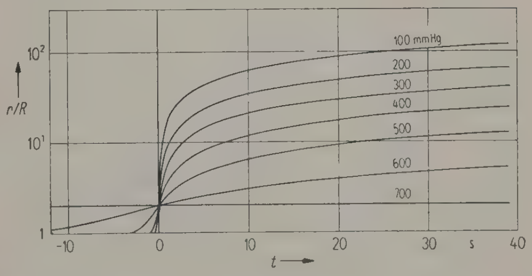

Fig. 3. Growth of bubbles by diffusion. Radius r of the bubbles, referred to the critical radius $R = 2\,\alpha/(p_a - p_0)$, as a function of the time t, for different pressures p_0 in water saturated for $p_a = 750$ mm Hg, calculated for $D' = 5{,}4 \cdot 10^{-5}$ cm²/s. $r_0/R = 2$ has been chosen arbitrarily.

5.4. *Velocity of ascent of the bubbles*

The frictional force acting on a solid sphere moving in a viscous medium has been calculated by Stokes as

$$K = 6\,\pi\,\nu\,r\,v \quad (\nu\text{: viscosity}). \tag{9}$$

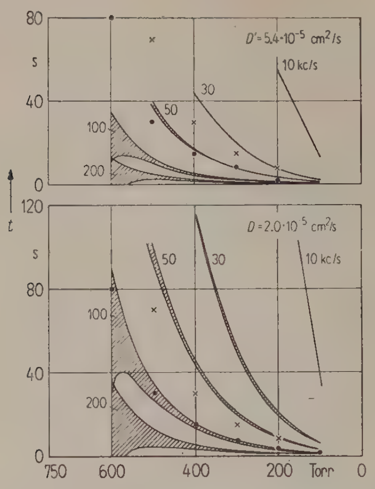

Fig. 4. Time t necessary for the growth of a bubble up to its resonance radius starting with a radius between two limiting values corresponding to $r/R(p_0) = 1.05$ and $r/R(p_0 + 100\ \text{mm Hg}) = 1$ resp. calculated for the normal and for the larger apparent diffusion constant i. e. for resting and for freely rising bubbles. × measured at 50 kc/s, ● measured at 100 kc/s.

According to Oseen and Goldstein this formula is the first term of a series of powers of the Reynolds number. Deviations for larger Reynolds numbers, i. e. for higher velocities (onset of turbulence) may therefore be expected.

Allen [1] confirmed the validity of Stoke's formula for ascending bubbles of small radius, and found deviations tending in the direction of Oseen and Goldstein's corrections for larger bubbles (r between 50 and 200 μm): for bubbles having these radii the measured velocity of ascent is less than that calculated from Stokes's formula. The applicability of Stokes's law to bubbles is not immediately obvious, since it is not known if the layer of liquid immediately at the boundary of the bubble moves with the latter so that it acts as a rigid sphere, or whether it flows around the bubble and is constantly renewed. Rybczynski [16] therefore proposed a new formula for the force acting on a moving bubble. The measurements of Allen, which have recently been confirmed by Exner and Hampe [6] and by Liebermann [11] appear, however, to justify the use of Stokes's formula.

5.5. *Concentration of bubbles in the measuring vessel*

Because bubbles slowly rise during measurements and reach the surface of the liquid, the number of bubbles in the vessel decreases. The decrease in the bubble concentration can be found, since the bubble radius as function of time, the relationship between bubble radius and rate of ascent and the dimensions of the containing vessel are known.

If q_0 is the number of bubble nuclei that form growing bubbles at the application of the stepwise pressure reduction, $v(t)$ is the velocity of ascent of the bubbles as a function of time and h is the mean height of the container, then the mean concentration of bubbles referred to the total volume of liquid is given by

$$q(t) = q_0 \left[1 - \frac{1}{h} \int_0^t v(t)\,\mathrm{d}t \right]. \tag{10}$$

The expected variation of the concentration with time is shown in Fig. 5 for the two different values of the apparent diffusion constant (resting and rising bubbles resp.). In each case two curves were computed for the two limiting values (see below) of the bubble nuclei. It frequently happens that the concentration does not decrease according to the above function, because a number of bubbles cling to the walls and do not rise. A degree of damping is then measured that does not return, even after a considerable period of time, to the value originally existing before commencement of the experiment.

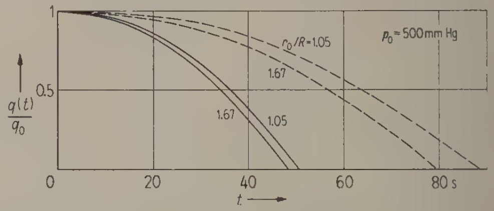

Fig. 5. Relative bubble concentration in the measuring vessel as a function of time at the 500 mm Hg pressure step. Initial radii of the nuclei: $r_0 = 1.05\,R$ or $1.67\,R$ resp., calculated for the normal (– – –) and for the larger (———) apparent diffusion constant corresponding to resting and to freely rising bubbles.

Starting with the known initial bubble concentration c_i (determined by optical methods [22] and given in the following table) the course of the damping in the measuring vessel then can be calculated by the aid of the curves given in Fig. 5:

p_0	600	500	400	300	200	100	mm Hg
c_i	1.4	1.3	0.64	0.31	0.36	0.36	1/cm³

6. Measurements

Two methods of pressure reduction were employed for the acoustical measurements. In the first, the air pressure was continuously reduced with an oil pump from normal (approx. 750 mm Hg) to about 100 mm Hg within a time of approximately 120 seconds. The rate of decrease of pressure was, in this case, determined by the capabilities of the pump and the volume of the pressure flask. In a second series of measurements, the pressure was reduced in one sudden step first to 700 mm Hg and then in six further steps of 100 mm Hg to a final pressure of 100 mm Hg. By connecting the pressure flask briefly to an evacuated reservoir of adequate volume, the pressure reductions could be effected in less than one second, between each of the individual pressure steps a pause of a few minutes allowed completion of the degassing process that occurred. Before degassing begins, the damping measured in the vessel is determined principally by the losses in the vessel itself and in the suspension. With the set-up used, this damping was about 150 dB/s. When bubbles begin to form, this damping increases more or less strongly. With the apparatus available it was possible to measure rates of decay up to 2000 dB/s in very rapid succession.

6.1. *Measurement of the pressure-dependence of the onset of degassing*

The onset of degassing as a function of the previously applied pressure excess was measured under conditions of a steady reduction of pressure. The excess pressure could be varied from 0 to 1.2 atmospheres, the upper limit being set by the maximum permissible loading of the pressure flask. The amount of air that diffused into the water through its undisturbed free surface during application of the excess pressure was so small that the degree of saturation of the water remained practically unaltered. The defined impurities used in these measurements consisted of jeweller's rouge and aluminium oxide. Measurements were carried out with frequencies between 10 and 100 kc/s. The results obtained with aluminium oxide are shown in Fig. 6. In this figure the shift in the point of initiation is shown that occurs when the results of a test are compared to the results obtained with a trial measurement carried out on the same sample without an initial excess pressure being applied. This method of measurement was necessary because large fluctuations in the pressures at which damping commenced were observed between different fillings of the measuring vessel. In spite of this precaution, Fig. 6 still shows a large spread in the measured values. Systematic differences between the different frequencies at which measurements were performed cannot be found. The direction in which the point of initiation shifts agrees with the prediction that the higher the initial excess pressure, the lower the pressure to which the water may be subjected before degassing begins. The view that excess pressure and pressure reduction are equal could not, however, be confirmed.

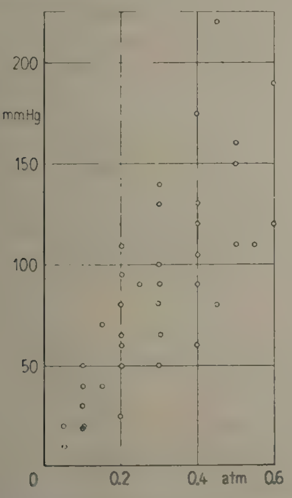

Fig. 6. Shift of the onset pressure of degassing against that of the trial measurements as a function of the applied overpressure.

6.2. *Measurement of the maximum value of damping*

During evacuation the damping in the vessel could be measured continuously. The values of greatest damping occurring with jeweller's rouge and aluminium oxide are plotted as a function of the previously applied excess pressure in Fig. 7. The measurements were carried out with frequencies between 10 and 200 kc/s. The effect was found to be strongly frequency-dependent. It is noteworthy that at high frequencies (200 kc/s) no measurable damping occurs after application of a slight pressure excess, whereas for low frequencies an increase in damping is still found even for high initial excess pressures. The explanation for this is that the few nuclei remaining after application of the excess pressure undergo a steady change in size and thereby

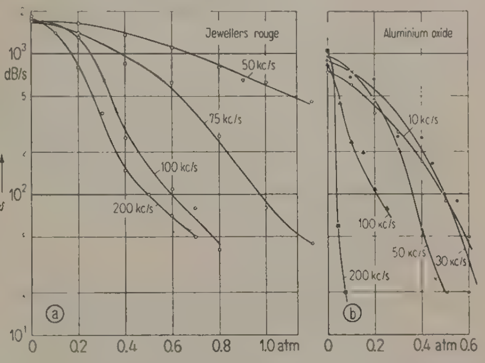

Fig. 7. Maximum of the measured additional damping as a function of the previously applied excess pressure. Impurity: (a) jeweller's rouge, (b) aluminium oxide powder.

in resonance frequency and are less effective as small bubbles than as large bubbles. A larger fraction of the sound energy is therefore absorbed the larger the bubbles are, and the lower therefore their frequency of resonance. After a high initial pressure the effect of the remaining bubbles is only noticeable when they have a large diameter, i. e. at low frequencies. At low frequencies and after the application of a small initial excess pressure the maximum damping is appreciably greater than could be measured with the apparatus (2000 dB/s).

6.3. Effect of the duration of the pressure excess

One series of tests was performed to investigate the effect of the duration of the previous excess pressure on the degassing process. The degree of degassing was again determined from the value of the observed damping maximum. In every test the excess pressure used was 0.6 atm. The results are shown in Fig. 8. It will be seen that with increasing duration of subjection to the excess pressure, the degassing at first is reduced rapidly and then attains a steady value depending only on the value of the excess pressure. This steady value may be measured after a time of about 10 min, and therefore all the experiments in which the point of initiation and the maximum value of the damping were measured, were performed after application of an initial pressure excess of 10 min duration.

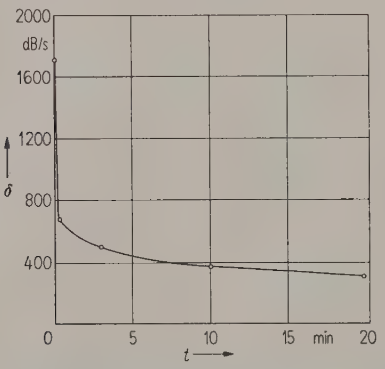

Fig. 8. Maximum attenuation measured as a function of the duration of the application of an excess pressure of 0.6 atm.

A possible explanation may be advanced to account for the relatively long time required by the initial pressure before it becomes fully effective: It is possible that wetting effects inside a pore play a part in the process, i. e. that for complete inhibition of a nucleus it is necessary that certain parts of a pore wall be gradually wetted by the water, which would not reach those parts during the course of the deformation of the air-water boundary determined by the ratios of the partial pressures. One may well imagine this gradual progress of a film of water requiring times of the order magnitude of minutes.

6.4. Effect of elapsed time between initial pressure excess and evacuation

In general, experiments were commenced with immediately after application of the initial pressure excess. In one series, however, the water was subjected to an excess pressure of 1 atm and then stored for 15 days. It was found that nuclei, once inhibited, were not capable of producing bubbles even after such a long recovery period, i. e. no greater increase in damping could be observed. This result is in agreement with the idea of Dean [3] that no subsequent adsorption of air occurs at a surface once it has been wetted.

6.5. Measurements with degassing carried out in steps

To obtain closer information regarding the sizes of the nuclei present, a few series of measurements were carried out in which the pressure was not reduced gradually but in steps of 100 mm Hg at a time. For this purpose the pressure flask was connected to a previously evacuated container through a tube of large cross-section. In this way the pressure could be reduced almost instantaneously by the required amount, and then held constant during degassing. In addition this method possesses the advantage that clear distinction is made possible between pressure and time effects occurring during degassing. It then becomes possible to compare the measured damping curves with the calculated values.

Very little air is extracted from the water by the formation of bubbles, in spite of the large effect on the absorption of sound. For each pressure step one may therefore be certain to have a nearly unaltered air content of the water, corresponding to a degree of saturation of 1 at 750 mm Hg due to the preparatory treatment. Fig. 9 shows how the additional damping obtained from the experiment varies with the time elapsed after the application of the corresponding pressure step. Noteworthy in these „curves" is the time t_i which elapses between the initiation of the pressure reduction and the onset of an increase in the damping. The higher the pressure in the vessel, the longer this time becomes. This relation is in agreement with the theoretical expectations and it can easily be seen that the lower the pressure in the vessel is made, the higher the degree of supersaturation of the water becomes and the faster therefore the growth of the bubbles. The following table shows the times that were measured:

p_0	600	500	400	300	200	100	mm Hg
t_i	20	10	4	2.5	2.5	1.5	s

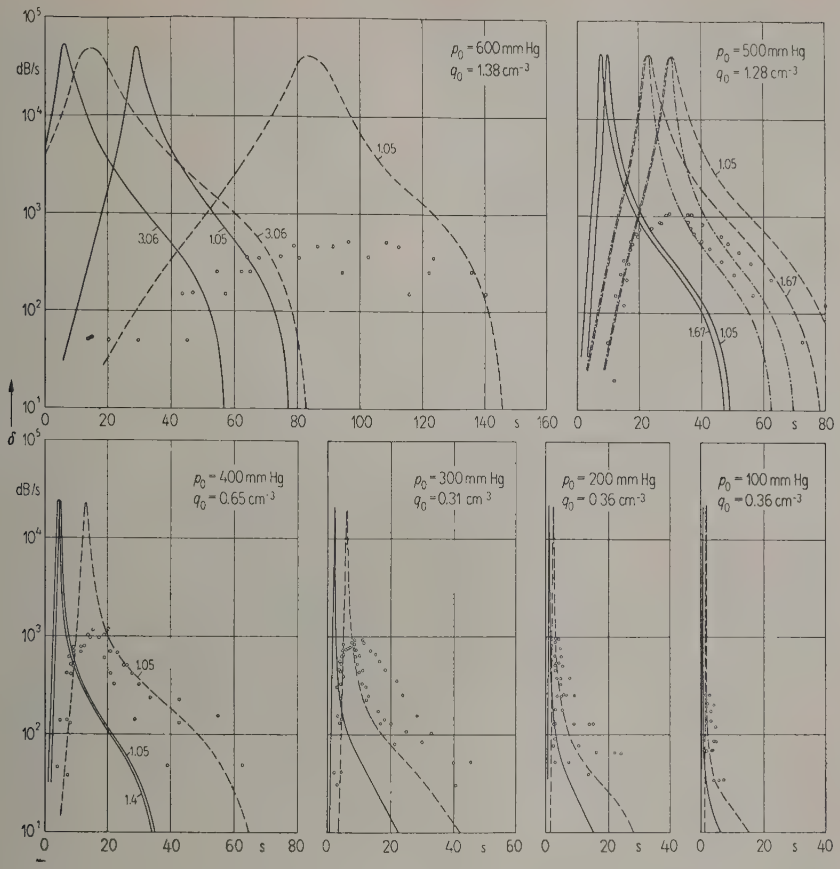

Fig. 9. Course of the damping as a function of time during stepwise degassing ($f = 100$ kc/s);
——— calculated for the normal diffusion constant ($D = 2.0 \cdot 10^{-5}$ cm^2/s),
— — — calculated for the larger apparent diffusion constant ($D' = 5.4 \cdot 10^{-5}$ cm^2/s),
○ measured values.
(—•— For the pressure step to 500 mm Hg an additional theoretical curve is shown, calculated with $D = 2.0 \cdot 10^{-5}$ cm^2/s below and with $D' = 5.4 \cdot 10^{-5}$ cm^2/s above the resonance size.)

The maximum value of the additional damping is determined by the number of bubbles formed in the vessel. When the degassing occurs in steps, the damping is always much less than the maximum value which can be measured with the apparatus (2000 dB/s) so that the measured values may be compared to the calculated values. The number of bubbles formed during each step was obtained from the optical measurements. The resulting „theoretical" curves, as calculated, are also plotted in Fig. 9. Two pairs of curves were computed for each pressure step: One pair using the normal diffusion constant D, the other pair using the higher apparent diffusion constant D'. One of the two curves, each pair consists of, is calculated for the largest and one for the smallest nuclei in question. The largest nucleus radius was taken to be the critical radius of the previous step i. e. these bubbles could just not be induced to grow during the previous pressure level. The smaller value of radius was assumed to be $r/R = 1.05$, i. e. a radius 5% greater than the critical radius for the existing pressure level. Nuclei with a radius only just above the critical value (r/R between 1 and 1.05) grow extremely slowly and contribute a negligible amount to the absorption.

These curves would have to be applied if all the bubbles had either the one or the other of the two initial radii considered. In actual fact the initial radii have values lying between these limits, and the curve to be expected will therefore lie somewhere between the computed boundary curves.

A comparison between the experimental and the theoretical curves shows that surprisingly the course of the experimental values first follows much better the theoretical curves calculated for resting bubbles (i.e. with the diffusion constant $D = 2.0 \cdot 10^{-5}$ cm^2/s) than those for freely rising bubbles (with a larger apparent diffusion constant $D' = 5.4 \cdot 10^{-5}$ cm²/s). This fact agrees with the results of the optical method [22] which show a slow growth for bubbles smaller than the limit of visibility ($r = 30$ µm) and a fast one for larger bubbles. A theoretical damping curve (see Fig. 9, $p_0 = 500$ mm Hg) calculated according to this rule indeed shows best relative agreement with the experimental results. While there is a quite good agreement with respect to the relative course of the curves, a discrepancy must be stated between their absolute values; the theoretical ones being too high. A reason for this deviation cannot be advanced at present with certainty. It may be assumed the theoretical values are too high because of the neglection of the interaction of the bubbles between each other (see section 5.1). Further theoretical investigations seem desirable here.

The work described in this paper was carried out under arrangements with the Department of Scientific and Industrial Research, London, whose assistance and interest are gratefully acknowledged. It is published with the permission of the Department.

(Received 7th July, 1957.)

References

[1] Allen, H. S., The motion of a sphere in a viscous fluid. Phil. Mag. (5) **50** [1900], 323 and 519.
[2] Becker, R. and Döring, W., Kinetische Behandlung der Keimbildung in übersättigten Dämpfen. Ann. Phys., Lpz. (5) **24** [1935], 719.
[3] Dean, R. B., The formation of bubbles. J. appl. Phys. **15** [1944], 446.
[4] Döring, W., Die Überhitzungsgrenze und Zerreißfestigkeit von Flüssigkeiten. Z. phys. Chem. (B) **36** [1937], 371; **38** [1937], 292.
[5] Exner, M. L., Messung der Dämpfung pulsierender Luftblasen in Wasser. Acustica **1** [1951], Beiheft 1, AB 25.
[6] Exner, M. L. and Hampe, W., Experimental determination of the damping of pulsating air bubbles in water. Acustica **3** [1953], 67.
[7] Fisher, J. C., The fracture of liquids. J. appl. Phys. **19** [1948], 1062.
[8] Fox, F. E. and Herzfeld, F. K., Gas bubbles with organic skin as cavitation Nuclei. J. acoust. Soc. Amer. **26** [1954], 984.
[9] Haeske, H., Experimental determination of the damping of pulsating air bubbles in water in the frequency range 100 to 300 kc/s. Acustica **6** [1956], 266.
[10] Kurtze, G., Über die Bedingungen von Kavitation in Flüssigkeiten. Nachr. Akad. Wiss. Göttingen, Math.-Phys. Klasse IIa [1958], Nr. 1.
[11] Liebermann, L., Air bubbles in water. J. appl. Phys. **28** [1957], 205.
[12] Martini, W., Thesis, still to be published.
[13] Meyer, E. and Skudrzyk, E., Chapter II of: Sound absorption and sound absorbers in water (1946).
[14] Mukhopadhyay, S. K., Ultraschallabsorption in Wasser und ihre Abhängigkeit von Temperatur und Luftgehalt des Wassers. Acustica **6** [1956], 25.
[15] Pfriem, H., Zur thermischen Dämpfung in kugelsymmetrisch schwingenden Gasblasen. Akust. Z. **5** [1940], 202.
[16] Rybczynski, W., Bull. Acad. Sci. Cracovie (1911), 40.
[17] Smith, F. D., Phil. Mag. **19** [1935], 1147.
[18] Takagi, S., Theory of the formation of bubbles. J. appl. Phys. **24** [1953], 1453.
[19] Tomlinson, C., On the so-called "inactive" condition of solids. Phil. Mag (4) **34** [1867], 136.
[20] Tomlinson, C., On the action of solid bodies on gaseous supersaturated solutions. Phil. Mag. (4) **45** [1873], 276.
[21] Turnbull, D. and Fisher, J. C., Rate of nucleation in condensed systems. J. Chem. Phys. **17** [1949], 71.
[22] Naake, H. J., Tamm, K., Dämmig, P. and Helberg, H. W., Observation of the formation and growth of bubbles in water containing air by optical methods. Acustica **8** [1958], in the press.

BEITRÄGE ZUR DEUTUNG DER SCHALLGESCHWINDIGKEIT IN BINÄREN FLÜSSIGKEITSMISCHUNGEN

von R. Genähr

I. Physikalisches Institut der Technischen Hochschule, Stuttgart

Zusammenfassung

Fußend auf den bekannten, von M. R. Rao und W. Schaaffs aufgestellten halbempirischen Beziehungen $R=\sqrt[3]{u}\cdot M/\varrho$ und $u=u_\infty\cdot s\,B/V$ wird an Hand eigener und fremder Messungen die Abhängigkeit der Schallgeschwindigkeit von der Konzentration in binären Flüssigkeitsmischungen diskutiert. Es zeigt sich, daß der Verlauf der Schallgeschwindigkeit über der Konzentration qualitativ gedeutet werden kann. Bei Mischungen, deren Komponenten keine schweren Atome enthalten bzw. keine extrem hohe Schallgeschwindigkeit besitzen, läßt sich auch ein quantitativer Zusammenhang zwischen der Schallgeschwindigkeit und der Dichte in Abhängigkeit von der Konzentration angeben. Zum Schluß wird auf eine Möglichkeit hingewiesen, bei schalldispergierenden Flüssigkeiten die Dispersion bei konstanter Frequenz in Abhängigkeit von der Temperatur zu messen.

Summary

The dependence of the velocity of sound on the concentration in binary fluid mixtures is discussed in terms of the well-known semi-empirical relations $R=\sqrt[3]{u}\cdot M/\varrho$ and $u=u_\infty\cdot s\,B/V$ established by M. R. Rao and W. Schaaffs. When the velocity of sound is plotted against the concentration, the result permits a qualitative interpretation. In cases of mixtures with components not having heavy atoms or extremely high velocities of sound, it is also possible to establish a quantitive interrelation between the velocity of sound and the density as a function of the concentration. For sound-dispersing fluids, finally, the possibility is pointed out of measuring the dispersion at constant frequency as a function of the temperature.

Sommaire

Le rapport entre la vitesse du son et la concentration de mélanges de liquides binaires est discuté sur la base des relations semi-empiriques connues, établies par M. R. Rao et W. Schaaffs: $R=\sqrt[3]{u}\cdot M/\varrho$ et $u=u_\infty\cdot s\,B/V$, et à l'aide de mesures effectuées par les auteurs et de mesures de sources étrangères. Il est démonstré que la variation de la vitesse du son peut être interprétée qualitativement en fonction de la concentration. Pour les mélanges dont les composantes ne contiennent pas d'atomes lourds et dans lesquels la vitesse du son n'est pas extrèmement élevée, on peut également établir un rapport quantitatif entre la vitesse du son et la densité en fonction de la concentration. A la fin, on indique la possibilité de mesurer, pour les liquides qui dispersent le son, la dispersion en fonction de la température, la fréquence restant constante.

1. Einleitung

Für die Schallgeschwindigkeit in reinen organischen Flüssigkeiten hat W. Schaaffs [1] die empirische Formel

$$u=u_\infty\cdot s\,B/V \tag{1}$$

angegeben. In ihr bedeuten u_∞ eine Konstante für alle organischen Flüssigkeiten mit der Dimension einer Geschwindigkeit, s ein die Elastizität der Molekülstöße bestimmender Stoßfaktor, der den für elastische Kugeln geltenden Wert $s=4$ nicht übersteigen kann, B das Eigenvolumen der Moleküle und V das Molvolumen. Die zunächst unbekannten Größen s und B setzen sich, wie Schaaffs zeigt, additiv aus den entsprechenden, die Flüssigkeitsmoleküle aufbauenden Atomgrößen zusammen. Schaaffs hat an über 180 organischen Flüssigkeiten die Brauchbarkeit von Gl. (1) geprüft.

1940 fand M. R. Rao [2] folgende, ebenfalls empirische Beziehung zwischen Schallgeschwindigkeit u, Dichte ϱ und Molekulargewicht M in reinen, nicht assoziierten Flüssigkeiten:

$$R=\sqrt[3]{u}\cdot M/\varrho=\sqrt[3]{u}\cdot V\,. \tag{2}$$

R ist eine temperaturunabhängige Stoffkonstante, die von Lagemann und Corry [3] den unglücklichen Namen „molekulare Schallgeschwindigkeit" erhielt. Ihre Dimension ist $\mathrm{cm}^{10/3}\cdot\mathrm{s}^{-1/3}$. Wie schon Rao [4] und auch Lagemann und Corry [3] zeigten, ist R eine additive Größe, d. h., die molekulare Schallgeschwindigkeit einer Verbindung setzt sich additiv aus den sogenannten Atominkrementen (bei Lage-

MANN und CORRY: Bindungsinkrementen) zusammen. Um dieser Additivität eine Deutung geben zu können, geht SCHAAFFS [5] von Gl. (1) aus und erhält aus ihr eine Größe mit der Dimension eines Volumens:

$$S = \sqrt[3]{u/u_\infty} \cdot V = \sqrt[3]{s\,B\,V^2}\,. \tag{3}$$

Sie hängt mit der molekularen Schallgeschwindigkeit R in folgender Weise zusammen:

$$S = R/\sqrt[3]{u_\infty}\,.$$

In der vorliegenden Arbeit wird S als Schallvolumen bezeichnet. Da sich R und S nur durch einen konstanten Faktor unterscheiden, gelten alle Überlegungen, die sich auf die molekulare Schallgeschwindigkeit R beziehen, auch für das Schallvolumen S, womit die erwähnte Additivität etwas plausibler gemacht ist.

Ersetzt man in Gl. (2) mittels der Beziehung $u^2 = (\varrho\,\beta)^{-1}$ die Schallgeschwindigkeit u durch die adiabatische Kompressibilität β, so wird

$$R = \varrho^{-7/6}\,\beta^{-1/6}\,M$$

oder

$$W = R^{6/7}\,M^{1/7} = \beta^{-1/7} \cdot M/\varrho = u^{2/7} \cdot M/\varrho^{6/7}\,. \tag{4}$$

Die Größe W, von Y. WADA [6] als „molekulare Kompressibilität“ eingeführt, ist ebenfalls temperaturunabhängig und additiv. Ihre Dimension ist $\mathrm{g} \cdot \mathrm{cm}^{20} \cdot \mathrm{s}^{-2}$.

2. Messungen

Den nachstehenden Überlegungen liegt folgendes experimentelle Material zugrunde:

1. Vom Verfasser wurden von den vier Mischungen

Benzol – t-Butylalkohol (1)
Cyclohexan – Essigsäure (2)
Dekalin – n-Propylalkohol (3)
Chlorbenzol – n-Propylalkohol (4)

Dichte und Schallgeschwindigkeit als Funktion der Konzentration bei 20° C gemessen; die erstere mit einem Satz Aräometer (Meßgenauigkeit: ±0,1%), die letztere mit einem Ultraschallinterferometer der Fa. Steeg & Reuter (Meßfrequenz 2 MHz, Meßgenauigkeit ebenfalls ±0,1%). Diese Meßwerte sind in Tabelle I zusammengestellt.

Die Flüssigkeiten wurden jeweils in der reinst erhältlichen Form von der Fa. Merck, Darmstadt, bezogen und anschließend wie folgt gereinigt:

Benzol und Cyclohexan:
über Na fraktioniert destilliert,
Dekalin:
getrocknet mit Na, dann zweimal einfach destilliert,
n-Propylalkohol und t-Butylalkohol:
einen Tag über CaO gekocht,
Essigsäure:
gekocht mit Essigsäureanhydrit, dann fraktioniert destilliert,
Chlorbenzol:
fraktioniert destilliert.

2. Ferner wurden Messungen anderer Autoren ausgewertet, und zwar an folgenden Mischungen:

Heptan – Dichlormethan (5)
Tetrachlorkohlenstoff – Äthylalkohol (6)

Tabelle I

Benzol-t-Butylalkohol

Mol-%	0	4,10	9,87	21,25	45,80	60,20	78,98	100	
u	1318,0	1308,7	1290,2	1256,0	1201,9	1175,3	1155,2	1141,3	m/s
ϱ	0,8790	0,8738	0,8666	0,8538	0,8285	0,8143	0,8010	0,7868	g/cm³

Cyclohexan-Essigsäure

Mol-%	0	4,68	23,60	36,50	56,30	63,00	75,70	86,20	92,20	100	
u	1280,3	1267,0	1223,7	1195,4	1161,7	1149,3	1136,0	1133,5	1142,0	1164,3	m/s
ϱ	0,7784	0,7829	0,8077	0,8293	0,8754	0,8937	0,9337	0,9804	1,0083	1,0550	g/cm³

Dekalin-n-Prophylalkokol

Mol-%	0	2,80	5,56	24,56	40,30	59,40	87,00	100	
u	1413,6	1403,3	1393,3	1374,0	1352,6	1320,4	1262,3	1221,2	m/s
ϱ	0,8778	0,8766	0,8754	0,8674	0,8596	0,8471	0,8215	0,8036	g/cm³

Chlorbenzol-n-Propylalkohol

Mol-%	0	3,60	8,72	15,10	27,75	42,50	60,00	77,30	96,00	100	
u	1286,7	1280,1	1273,8	1267,2	1260,1	1254,2	1248,1	1240,1	1226,2	1221,2	m/s
ϱ	1,1112	1,1017	1,0890	1,0737	1,0420	1,0029	0,9514	0,8933	0,8204	0,8034	g/cm³

Methylalkohol – Cyclohexanol (7)
n-Propylalkohol – Cyclohexanol (8)
iso-Propylalkohol – Cyclohexanol (9)
n-Butylalkohol – Cyclohexanol (10)
iso-Butylalkohol – Cyclohexanol (11)
Oktylalkohol – Cyclohexanol (12)
Glykol – Cyclohexanol (13)
Glyzerin – Cyclohexanol (14)

Diese Meßwerte stammen von Tuomikoski und Nurmi [7] (Mischung 5, entnommen einer Arbeit von D. Sette [8], Meßtemperatur 25° C), K. Sacher [9] (Mischung 6, Meßtemperatur 18° C) und F. Danusso [10] (Mischung 7 bis 14, Meßtemperatur 30° C). Die Genauigkeit dieser Messungen ist nicht bekannt.

3. Ergebnisse

3.1. Zusammenhang zwischen u und ϱ in binären Flüssigkeitsmischungen

In binären Mischungen gehorchen im allgemeinen weder die Dichte bzw. das Molvolumen noch die Schallgeschwindigkeit der Mischungsregel[1]. Irgendein Zusammenhang im Verlauf der Dichte und der Schallgeschwindigkeit in Mischungen konnte bisher nicht gefunden werden. Ist z. B. bei einer bestimmten Gruppe von Mischungen die Dichtekennlinie konvex nach oben gekrümmt, so können die Schallkennlinien dieser Mischungen konvex nach oben oder unten gekrümmt sein, sie können aber auch einen Wendepunkt besitzen. Entsprechendes gilt, wenn die Dichtekennlinie konvex nach unten verläuft bzw. einen Wendepunkt besitzt[2].

Ohne eine quantitative Annahme zu machen, kann man über den Verlauf der Schallkennlinie folgendes aussagen: Aus Gl. (1) sieht man, daß die Schallgeschwindigkeit in Mischungen auch dann nicht linear mit der Konzentration verläuft, wenn sowohl das Molvolumen V als auch das Volumen sB der Mischungsregel gehorchen. Bei bekanntem Verlauf des Molvolumens wird der Charakter der Schallkennlinie nur noch durch den Verlauf des Volumens sB in der Mischung bestimmt. Über den Stoßfaktor s kann man von Fall zu Fall qualitative Aussagen machen. Er wird im allgemeinen kleiner sein als es der Mischungsregel entspricht, und zwar um so kleiner, je mehr sich die Moleküle der reinen Flüssigkeiten in bezug auf Größe und Form voneinander unterscheiden. Da man annehmen kann, daß sich das Molekülvolumen B der reinen Substanzen in der Mischung nicht sehr ändert, bestimmt im wesentlichen der Stoßfaktor s den Verlauf des Volumens sB über der Konzentration.

In den Bildern 1 a bis 14 a sind über der Konzentration

$$\Delta V = V_{\mathrm{g}} - V_{\mathrm{m}}$$

und

$$\Delta(sB) = (sB)_{\mathrm{g}} - (sB)_{\mathrm{m}}$$

aufgetragen. Dabei ist V_{g} das gemessene Molvolumen, V_{m} bzw. $(sB)_{\mathrm{m}}$ sind die der Mischungsregel gehorchenden Werte, $(sB)_{\mathrm{g}}$ ist das mittels Gl. (1) aus der gemessenen Schallgeschwindigkeit berechnete Volumen sB. Man sieht, daß mit Ausnahme der Mischung 9 (iso-Propylalkohol – Cyclohexanol, vgl. Bild 9 a) in allen Fällen das Volumen sB in der Mischung kleiner ist als es der Mischungsregel entspricht, und zwar völlig unabhängig vom Verlauf des Molvolumens[3].

3.2. Berechnung der Schallgeschwindigkeit in binären Flüssigkeitsmischungen mittels S bzw. W

Es erhebt sich die Frage, ob ähnliche halbempirische Beziehungen wie sie die Gl. (2) bzw. (3) darstellen, auch zur Deutung der Konzentrationsabhängigkeit der Schallgeschwindigkeit binärer Mischungen herangezogen werden können, d. h., ob die zwei Komponenten der Mischung gewisse „Inkremente" zu irgendeiner geeignet zu definierenden Kenngröße, z. B. zum Schallvolumen S, additiv beisteuern.

Diese Frage hat O. Nomoto [13] an 37 binären Flüssigkeitsmischungen untersucht[4] und zwar derart, daß er aus den gemessenen Dichte- und Schallgeschwindigkeitswerten die Kenngröße (in diesem Fall die molekulare Schallgeschwindigkeit R) berechnet, über der Konzentration aufträgt und graphisch die Linearität prüft. Auf diesem Weg wird jedoch die zum Teil sehr beachtliche Meßgenauigkeit mancher Arbeiten nicht voll ausgenützt.

Eine viel schärfere Prüfung einer solchen halbempirischen Arbeitshypothese ergibt sich, wenn man umgekehrt verfährt. Man berechnet zunächst die Kenngrößen der reinen Flüssigkeiten aus den bekannten Daten (Dichte und Schallgeschwindigkeit), dann daraus mittels der Mischungsregel den Wert für eine beliebige Konzentration. Es gilt also für das Schallvolumen $S_{(x)}$ bei der Konzentration x:

---

[1] Vgl. Markgraf und Nikuradse [11], die die Abweichungen des Molvolumens von der Mischungsregel auf das Zusammenwirken eines rein geometrischen Packungseffektes mit zwischenmolekularen Kraftwirkungen zurückführen.

[2] In einzelnen Fällen versuchten Parshad [12], Sacher [10] u. a. den Verlauf der Schallkennlinie mit Hilfe von Assoziationen, Dipolwirkungen u. ä. zu deuten.

[3] Bei der genannten Mischung könnte die unterhalb 20 Mol-% Cyclohexanol auftretende Anomalie vielleicht auf das Vorhandensein besonderer Molekülkomplexe zurückgeführt werden, deren Stoßfaktor größer ist als der des reinen Cyclohexanol.

[4] Er stützt sich dabei auf Messungen von Tuomikoski und Nurmi, Gabrielli, Poiani, Parshad u. a.

$$S_{(x)} = S_1 (1-x) + S_2 x = \sqrt{\frac{u_{(x)}}{u_\infty} \frac{M_{(x)}}{\varrho_{(x)}}} .$$

Dabei bedeuten S_1 und S_2 die Schallvolumina der reinen Flüssigkeiten. Nun berechnet man aus dieser Gleichung die Schallgeschwindigkeit $u_{(x)}$ und vergleicht sie mit der gemessenen. Es ist (5)

$$u_{(x)\,S} = \frac{u_\infty \, \varrho_{(x)}{}^3}{M^3} \, S_{(x)}{}^3 = \frac{u_\infty \, \varrho_{(x)}{}^3}{M} \, [S_1 (1-x) + S_2 x]^3 .$$

In den Bildern 1 b bis 14 b ist von den oben erwähnten Flüssigkeitsmischungen die Größe $\Delta u_S = u_{(x)S} - u_{(m)}$ aufgetragen, also die Differenz zwischen der nach Gl. (5) berechneten Schallgeschwindigkeit $u_{(x)\,S}$ und der nach der Mischungsregel berechneten Größe $u_{(m)} = u_1 (1-x) + u_2 x$, wenn u_1 und u_2 die Schallgeschwindigkeiten der reinen Flüssigkeiten bedeuten. Die gemessenen Werte der Schallgeschwindigkeit, bzw. die Abweichung dieser Werte

Bilder 1 bis 14. Verlauf der Größen ΔV, $\Delta(s\,B)$, Δu_S bzw. Δu_W über der Konzentration in Mol-% der an zweiter Stelle genannten Komponente. Die Volumina sind in cm³, die Schallgeschwindigkeit ist in m/s angegeben. Bei den Bildern 1 b bis 14 b entsprechen die Kurven den berechneten Größen Δu_S bzw. Δu_W, die eingetragenen Punkte sind Meßwerte.

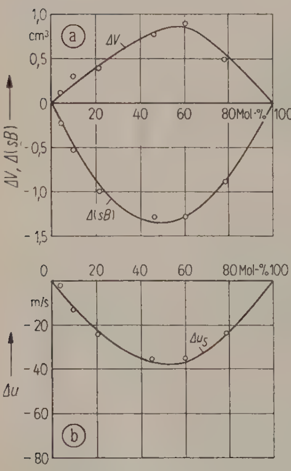

Bild 1. Benzol – t-Butylalkohol.

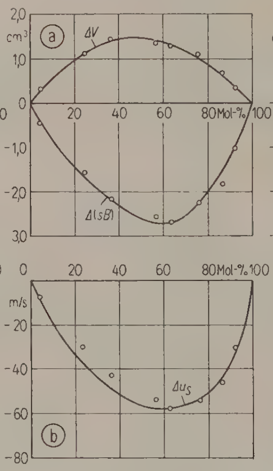

Bild 2. Cyclohexan – Essigsäure.

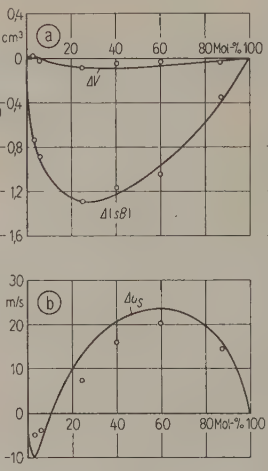

Bild 3. Dekalin – n-Propylalkohol.

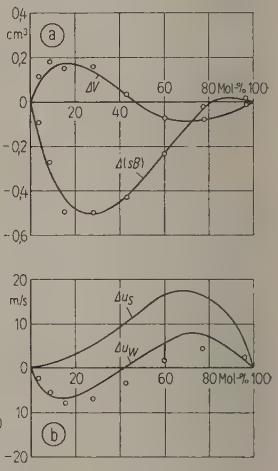

Bild 4. Chlorbenzol – n-Propylalkohol.

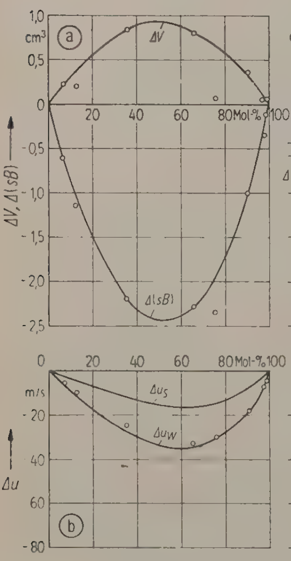

Bild 5. Heptan – Dichlormethan.

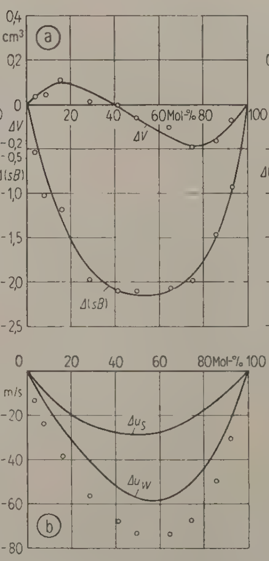

Bild 6. Tetrachlorkohlenstoff-Äthylalkohol.

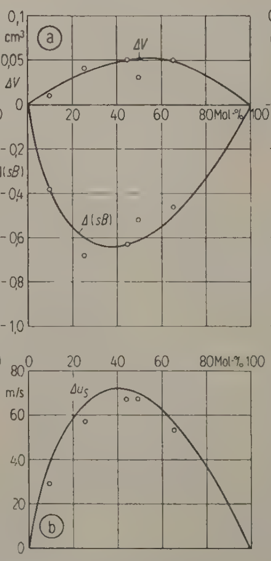

Bild 7. Methylalkohol – Cyclohexanol.

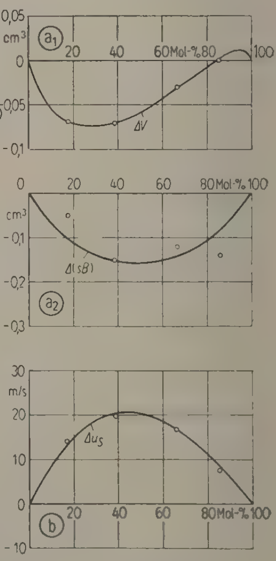

Bild 8. n-Propylalkohol – Cyclohexanol.

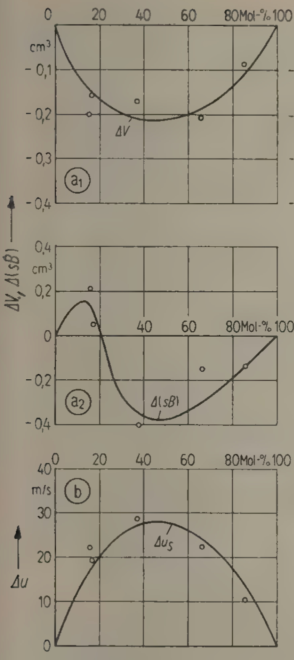

Bild 9. iso-Propylalkohol — Cyclohexanol.

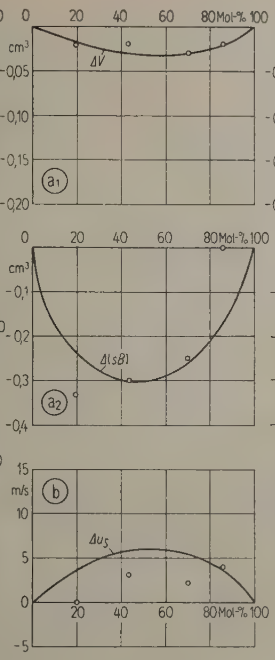

Bild 10. n-Butylalkohol — Cyclohexanol.

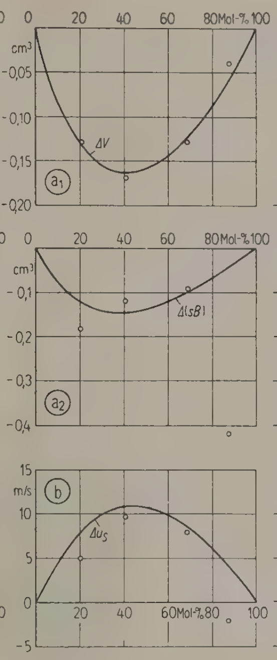

Bild 11. iso-Butylalkohol — Cyclohexanol.

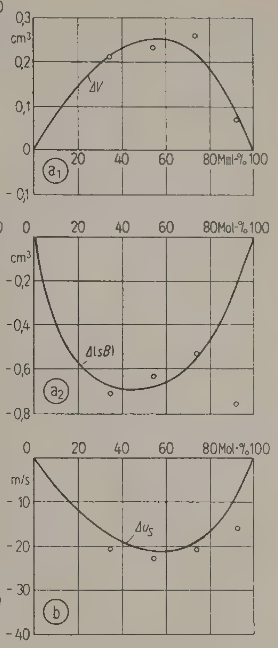

Bild 12. Octylalkohol — Cyclohexanol.

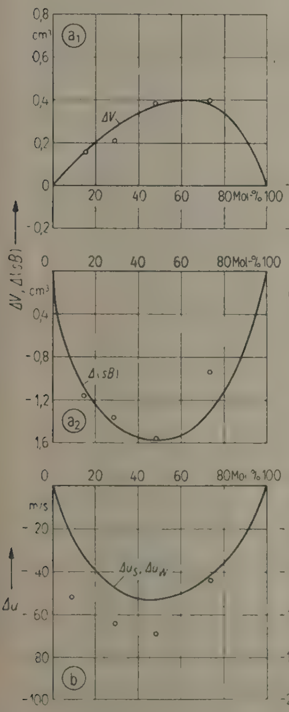

Bild 13. Glykol — Cyclohexanol.

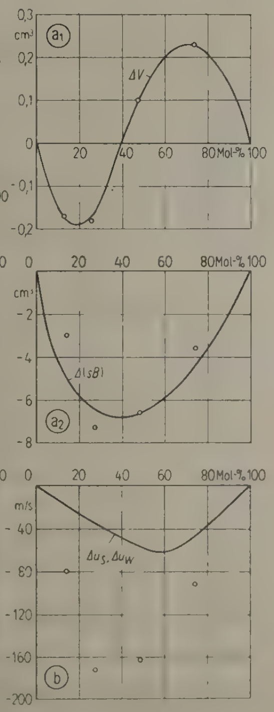

Bild 14. Glyzerin — Cyclohexanol.

von der Mischungsregel, sind in diesen Bildern ebenfalls eingetragen. Man sieht, daß mit Ausnahme der Mischungen 4, 5, 6, 13 und 14 die gemessenen Werte mit den berechneten innerhalb der Meßgenauigkeit übereinstimmen (siehe Bilder 4 b, 5 b, 6 b, 13 b und 14 b).

Wendet man die vorstehenden Überlegungen auch auf die molekulare Kompressibilität W (siehe Gl. (4)) an, dann erhält man

$$W_{(x)} = W_1 (1-x) + W_2 x = u_{(x)}^{2/7} \frac{M_{(x)}}{\varrho_{(x)}^{6/7}}$$

und daraus analog zu Gl. (5) (6)

$$u_{(x)W} = \frac{\varrho_{(x)}^3}{M^{7/2}} W_{(x)}^{7/2} = \frac{\varrho_{(x)}^3}{M^{7/2}} \left[W_1(1-x) + W_2 x\right]^{7/2}.$$

In den Bildern 4 b bis 6 b ist außer der Größe $\Delta u_S = u_{(x)S} - u_{(m)}$ auch die Differenz $\Delta u_W = u_{(x)W} - u_{(m)}$ aufgetragen, bei den Mischungen 13 und 14 (Bilder 13 b und 14 b) fallen die Δu_W- und Δu_S-Kurven innerhalb der Zeichengenauigkeit zusammen. Man sieht, daß bei den Mischungen 4 und 5, bei denen die nach Gl. (5) berechnete Schallgeschwindigkeit von der gemessenen abweicht, die nach Gl. (6) berechnete Größe $u_{(x)W}$ innerhalb der Meßgenauigkeit mit der gemessenen Schallgeschwindigkeit übereinstimmt. Das bedeutet, daß bei diesen Mischungen nicht das Schallvolumen S, sondern die Größe W linear mit der Konzentration verläuft.

Dies gilt jedoch nicht für die Mischungen 6, 13 und 14, bei denen auch die nach Gl. (6) berechnete Schallgeschwindigkeit $u_{(x)W}$ nicht mit der gemessenen übereinstimmt (siehe Bilder 6 b, 13 b und 14 b).

O. Nomoto [13] kommt zu dem Schluß, daß bei der Mischung Heptan – Dichlormethan (in der vorliegenden Arbeit Mischung 5) sowohl R als auch W linear mit der Konzentration verlaufen, bei der Mischung Tetrachlorkohlenstoff – Äthylalkohol (Mischung 6) dagegen nur W. Das liegt, wie schon erwähnt, daran, daß Nomoto die Linearität graphisch prüft. Geht man dagegen wie vorstehend beschrieben vor, dann sieht man aus den Bildern 5 b und 6 b, daß bei der Mischung 13 nur W, bei der Mischung 14 dagegen weder S (bzw. R) noch W der Mischungsregel gehorchen.

Bei den Mischungen, bei denen Gl. (5) bzw. (6) nicht erfüllt ist, fällt auf, daß eine Komponente der Mischung entweder schwere Atome (z. B. Chlor) enthält[5], oder aber ihre Schallgeschwindigkeit extrem hoch liegt (Glykol: $u = 1643$ m/s; Glyzerin: $u = 1911$ m/s). Davon unberührt bleibt jedoch das im vorigen Abschnitt dargestellte Verhalten des Volumens sB in der Mischung, d. h., auch bei den Mischungen, in denen das Schallvolumen S bzw. die molekulare Kompressibilität W nicht der Mischungsregel gehorcht, wird das Volumen sB in der Mischung kleiner.

3.3. Die Schallgeschwindigkeit als Funktion der Temperatur bei schalldispergierenden Flüssigkeiten

Die Schallgeschwindigkeit reiner organischer Flüssigkeiten und auch binärer Mischungen nimmt linear mit der Temperatur ab, falls bei der Meßfrequenz, bei der die Schallgeschwindigkeit gemessen wird, keine Schalldispersion auftritt. Ist letzteres jedoch der Fall (z. B. bei reiner Essigsäure bei einer Meßfrequenz von 2 MHz), so besitzt die Gerade, die den Verlauf der Schallgeschwindigkeit über der Temperatur beschreibt, einen Knick, wie folgende Überlegung zeigt.

In Bild 15 sind die Dispersionsstufen für mehrere Temperaturen eingezeichnet. Mißt man nun die Schallgeschwindigkeit im Dispersionsgebiet mit konstanter Frequenz bei steigenden Temperaturen T_1 bis T_5, so erhält man die Meßpunkte 1 bis 5, oder, wenn man die Schallgeschwindigkeit über der Temperatur aufträgt (siehe Bild 16), die doppelt geknickte Gerade I – II – III. Da mit steigender Temperatur die Dispersionsstufen größer werden, werden die Abstände der Parallelen oberhalb der Dispersionsstufen kleiner, d. h. die Geraden I und III in Bild 16 divergieren nach höheren Temperaturen.

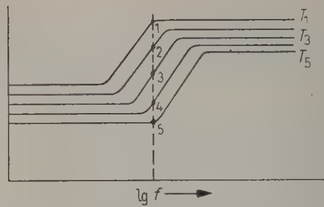

Bild 15. Verlauf der Schallgeschwindigkeit über der Frequenz im Dispersionsgebiet.

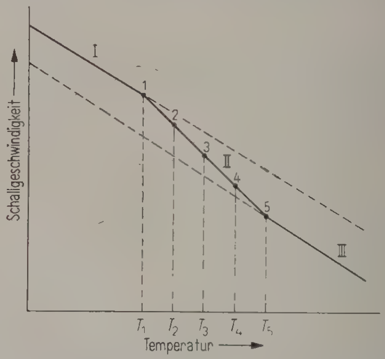

Bild 16. Die Schallgeschwindigkeit von Flüssigkeiten in Abhängigkeit von der Temperatur bei Schalldispersion.

Die Mischung 2 (Cyclohexan – Essigsäure) zeigt auffallend starke Schallabsorption [14], aus der man auf eine erhebliche Dispersion bei 2 MHz schließen kann. Deshalb wurde vom Verfasser in dieser Mischung die Schallgeschwindigkeit temperaturabhängig gemessen. Dabei wurde der zweite „Knick" (Übergang von I nach II in Bild 16) tatsächlich festgestellt, wie Bild 17 zeigt. Da mit der Schalldispersion zusammen auch eine erhöhte Schallabsorption auftritt, die mit steigender Essigsäurekonzentration und steigender Temperatur stark zu-

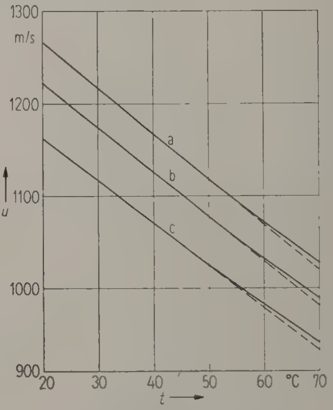

Bild 17. Verlauf der Schallgeschwindigkeit über der Temperatur in der Mischung Cyclohexan – Essigsäure. Kurve a: 4,68 Mol-%, Kurve b: 23,6 Mol-%, Kurve c: 56,3 Mol-% Essigsäure; Meßfrequenz $f = 2$ MHz.

---

[5] Hierauf hat Nomoto [13] bereits hingewiesen.

nimmt, war es mit dem zur Verfügung stehenden Ultraschall-Interferometer nicht möglich, auch bei höheren Essigsäurekonzentrationen bzw. bei reiner Essigsäure diesen Knick zu messen.

Lamb, Andreae und Bird [15] haben bei reiner Essigsäure die Schallgeschwindigkeit bei 0,5, 4,0 und 5,0 MHz temperaturabhängig gemessen (siehe Fig. 3 in [15]). Da ihre Meßfrequenzen unter- bzw. oberhalb der Dispersionsfrequenz liegen, haben sie innerhalb ihres Temperaturbereiches nur die Geraden I und III (vgl. Bild 16) gemessen, nicht aber die Verbindungsstücke II. Man sieht aber deutlich, daß diese Geraden mit steigender Temperatur divergieren.

Herrn Professor Dr. H. O. Kneser möchte ich für die Anregung zu dieser Arbeit und seine Unterstützung besonders danken. Der Deutschen Forschungsgemeinschaft verdanken wir einige der benützten Apparate.

(Eingegangen am 3. August 1957.)

Schrifttum

[1] Schaaffs, W., Ann. Phys. (5) **40** [1941], 393 und Z. phys. Chem. **194** [1944], 28, 39 und 66.
[2] Rao, M. R., Indian J. Phys. **14** [1940], 109.
[3] Lagemann, R. und Corry, J., J. Chem. Phys. **10** [1942], 759.
[4] Rao, M. R., J. Chem. Phys. **9** [1941], 682.
[5] Schaaffs, W., Acustica **4** [1954], 635.
[6] Wada, Y., J. Phys. Soc. Japan **14** [1949], 280.
[7] Tuomikoski, P. und Nurmi, U., Soc. Sci. Fenn. Comm. Phys. Math. **10** [1940], 1.
[8] Sette, D., Ric. Sci. **19** [1949], 1338.
[9] Sacher, K., Phys. Z. **41** [1940], 360.
[10] Danusso, F., Rend. Accad. Naz. Lincei **17** [1954], 114.
[11] Markgraf, H. G. und Nikuradse, A., Z. Naturforschg. **9 a** [1954], 27.
[12] Parshad, R., J. Chem. Phys. **15** [1947], 418.
[13] Nomoto, O., J. Phys. Soc. Japan **8** [1953], 553.
[14] Eppler, K. und Dieter, H., Naturwiss. **42** [1955], 122.
[15] Lamb, J., Andreae, J. H. und Bird, R., Nature **162** [1948], 993.

ZWECKMÄSSIGE EINTEILUNG DER ELEKTROMECHANISCHEN WANDLER MIT RÜCKSICHT AUF IHRE BERECHNUNG AUS IHREN ELEKTRISCHEN UND MECHANISCHEN DATEN

von A. Lenk

Mitteilung aus dem Institut für Elektro- und Bauakustik der Technischen Hochschule Dresden

Zusammenfassung

In dieser Arbeit wird eine Systematik der elektromechanischen Wandler angegeben, die sich in verschiedenen Punkten von den in der Literatur vorhandenen Einteilungen unterscheidet.

Für die vier Gruppen, in die sich die elektromechanischen Wandler unterteilen lassen, wird ein sehr einfaches Einteilungskriterium angegeben, das sich nur auf einfache konstruktive Eigenschaften des Wandlers bezieht. Jeder Gruppe ist dann ein Ersatzschaltbild zugeordnet, dessen Elemente sich aus dem Aufbau des Wandlers einfach bestimmen lassen.

Summary

In this paper a systematic is given for the electro-mechanical transducer, which differs in several points from that commonly given in the literature.

A very simple criterion for allotting such a transducer to one of four groups is given which depends only on simple properties of the construction. Each group is then classified into a substitute circuit, the elements of which can be derived from the construction of the transducer.

Sommaire

On donne dans le présent travail un classement systématique des transformateurs électromécaniques; ce classement diffère à certains égards de ceux déjà publiés ailleurs.

On indique un critère très simple de classement dans les 4 groupes proposés pour les transformateurs électromécaniques, ce critère ne faisant appel qu'à des caractéristiques de construction simples. On établit ensuite pour chaque groupe un schéma équivalent dont les éléments constitutifs peuvent être déterminés de façon simple à partir de la constitution du transformateur.

1. Einleitung

Die Frage der systematischen Einteilung der elektromechanischen Wandler wurde zuletzt in einer Arbeit von F. A. Fischer [1] angeschnitten. Einige Punkte dieser Arbeit waren der Anlaß zu einer Diskussion des Verfassers mit Herrn Dr. F. A. Fischer, in deren Verlauf ein großer Teil der hier wiedergegebenen Ergebnisse geklärt und formuliert wurde. Es besteht im übrigen über alle Punkte der hier veröffentlichten Arbeit vollständige Einstimmigkeit des Verfassers mit Herrn Dr. F. A. Fischer.

Zur Beschreibung von elektromechanischen Wandlern werden weitgehend elektrische Ersatzschaltbilder oder unter Verwendung der elektromechanischen Analogien elektromechanische Vierpolersatzschaltbilder verwendet [2], [3], [4].

Mit Rücksicht auf eine rationelle Beschreibung entsteht dabei die Frage, welche Gruppen von Wandlern jeweils durch ein gemeinsames Ersatzschaltbild dargestellt werden können, und darüber hinaus die weitere Frage, ob die so erhaltenen einzelnen Wandlerklassen durch irgendwelche gemeinsame konstruktive Eigenschaften oder gemeinsame physikalische Merkmale der Energieumsetzung gekennzeichnet sind.

Solche Einteilungen sind in [2], [5], [6] enthalten. Sie enthalten gemeinsam das Ergebnis, daß nach der Art des Ersatzschaltbildes vier verschiedene Klassen von Wandlern unterschieden werden müssen. Bezüglich der Frage, welche Wandler zu welcher Klasse gehören und welche gemeinsamen konstruktiven oder physikalischen Eigenschaften eine Klasse kennzeichnen, unterscheiden sich die obengenannten Arbeiten in einigen Punkten.

In der vorliegenden Arbeit sollen diese Unterschiede geklärt werden, und weiterhin wird ein neues, sehr einfaches Kriterium angegeben, nach dem die Zuordnung eines Wandlers zu einer der erwähnten vier Klassen ohne weiteres möglich ist.

2. Ersatzschaltbilder der elektromechanischen Wandler

Aus [2], [6], [7] kann man entnehmen, daß man im quasistatischen Zustand, der vorläufig betrachtet werden soll, sämtliche elektrischen Wandler durch die beiden miteinander identischen Ersatzschaltbilder nach Bild 1a und 1b, und sämtliche magnetischen Wandler durch die beiden ebenfalls miteinander identischen Schaltbilder nach Bild 2a und 2b darstellen kann. Unter elektrischen Wandlern sind solche zu verstehen, bei denen die Energieumwandlung mit Hilfe von elektrischen Feldern vor sich geht. Analog dazu geschieht bei magnetischen Wandlern die Energieumwandlung mit magnetischen Feldern.

In den Bildern 1 und 2 haben C_f und L_f die Bedeutung der Kapazität bzw. Induktivität im mechanisch festgebremsten Zustand. n_k und n_l sind die mechanischen Nachgiebigkeiten für konstante elektrische Feldstärke (elektrischer Kurzschluß) und konstante dielektrische Verschiebung (elektrischer Leerlauf). Entsprechend bedeuten im magnetischen Fall n_l die Nachgiebigkeit bei konstanter magnetischer Feldstärke (elektrischer Leerlauf) und n_k die Nachgiebigkeit bei konstanter Induktion (elektrischer Kurzschluß). k ist der elektromechanische Kopplungsfaktor.

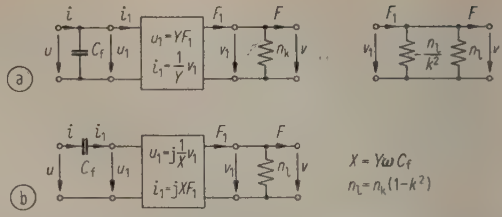

Bild 1. Ersatzschaltbild der elektrischen Wandler, (a) mit Parallelkondensator, (b) mit Reihenkondensator.

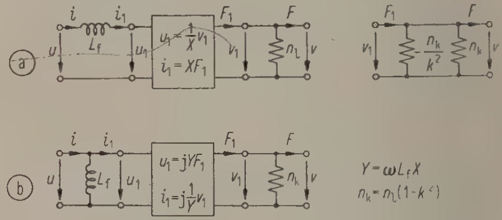

Bild 2. Ersatzschaltbild der magnetischen Wandler, (a) mit Reiheninduktivität, (b) mit Parallelinduktivität.

Auf der mechanischen Seite wird die Analogie $u \rightarrow v$, $i \rightarrow F$ verwendet.

3. Unterteilung der Wandler in vier Klassen

Interessiert man sich nur für Messungen an bereits fertigen Wandlern, so wären damit die aufgestellten Fragestellungen schon beantwortet. Es gibt danach zwei verschiedene Sorten von Wandlern, nämlich elektrische und magnetische, die durch die Ersatzschaltbilder nach den Bildern 1 und 2 dargestellt werden können. Die darin enthaltenen Konstanten C_f, L_f, X, Y, n_l, n_k können sämtlich durch geeignete Messungen an den Klemmenpaaren des Wandlers bestimmt werden. Es besteht also bis jetzt kein Anlaß für eine weitergehende Unterteilung.

Das ändert sich jedoch, wenn man sich die Aufgabe stellt, die Eigenschaften eines Wandlers aus seinem konstruktiven Aufbau zu bestimmen. Die Verhältnisse sollen zunächst einmal am Beispiel der elektrischen Wandler betrachtet werden.

Zu dieser Berechnung muß man den Zusammenhang der Größen C_f, X bzw. Y und n_l bzw. n_k mit den Konstruktionselementen kennen. Die Kapazität C_f läßt sich aus dem Aufbau des Wandlers in jedem Fall einfach bestimmen, ohne daß der Mechanismus der Energieumwandlung näher bekannt sein muß.

Es handelt sich dabei um ein rein elektrisches Problem. Nicht so einfach ist es auf der mechanischen Seite. Im System ist eine rein mechanisch bedingte Nachgiebigkeit n_s etwa in Form von Federn, gespannten Membranen o. ä. vorhanden, deren Zusammenhang mit n_l und n_k erst noch festzustellen ist.

An dieser Stelle ergibt sich nun eine nochmalige Unterteilung. Es zeigt sich nämlich, daß bei einem Teil der elektrischen Wandler die rein mechanisch bedingte Nachgiebigkeit n_s bei elektrischem Kurzschluß und bei einem anderen Teil im elektrischen Leerlauf an den mechanischen Klemmen gemessen werden kann. Im ersten Fall ist also $n_s = n_k$, und im zweiten Fall ist $n_s = n_l$. Der Zusammenhang zwischen n_l und n_k ist durch den elektromechanischen Kopplungsfaktor k bestimmt: $n_l/n_k = 1 - k^2$. Die Kopplungsfaktoren üblicher Wandler liegen zwischen 10 und 30%, so daß die beiden Nachgiebigkeiten um 1 bis 10% voneinander verschieden sind, was oft vernachlässigt werden kann.

Es zeigt sich nun weiter, daß bei allen Wandlern, bei denen die elektrischen Feldgrößen auf den mechanischen Größen v und F senkrecht stehen $n_s = n_k$ ist (tangential-dielektrische Wandler, piezoelektrische Längsschwinger). Bei allen Wandlern, bei denen elektrische und mechanische Größen parallel zueinander liegen, gilt $n_s = n_l$ (normal-dielektrische Wandler; piezoelektrische Dickenschwinger).

Die Richtigkeit dieser Behauptung läßt sich bei den dielektrischen Wandlern leicht nachprüfen, weil dort die Größe von n_s aus der mechanischen Konstruktion zu entnehmen ist. Man kann auch dann an den mechanischen Klemmen messen, wenn man die Polarisationsgröße abschaltet.

Bei den piezoelektrischen Wandlern ist das nicht so einfach einzusehen. Elektrischer Energiespeicher (Kapazität) und mechanischer Energiespeicher (Elastizität) sind hier untrennbar miteinander verknüpft, und es hat zunächst offenbar keinen Sinn, von einer rein mechanisch bedingten Nachgiebigkeit oder einer rein elektrisch bedingten Kapazität zu sprechen. Die Abschaltung der inneren Polarisation ist auch ohne gleichzeitige erhebliche Änderung aller anderen Eigenschaften nicht möglich, so daß nicht festgestellt werden kann, welche der beiden Nachgiebigkeiten n_l und n_k als die des mechanischen Systems zu betrachten ist.

Diese Entscheidung wird möglich, wenn man die stetige Massen- und Federungsverteilung längs der Schwingungsrichtung berücksichtigt, also die Beschränkung auf den quasistationären Zustand fallen läßt. Aus den Schaltungen des Bildes 1 werden dann die Schaltungen des Bildes 3 a, b. Man erkennt, daß sich Dickenschwinger und Längsschwinger verschieden verhalten. Beim Längsschwinger wird aus der Nachgiebigkeit n_k der mechanische Mitgang, den man nach der mechanischen Anordnung erwarten müßte. Die Wellengeschwindigkeit c ist hier durch die elastische Konstante bei fester Feldstärke bestimmt.

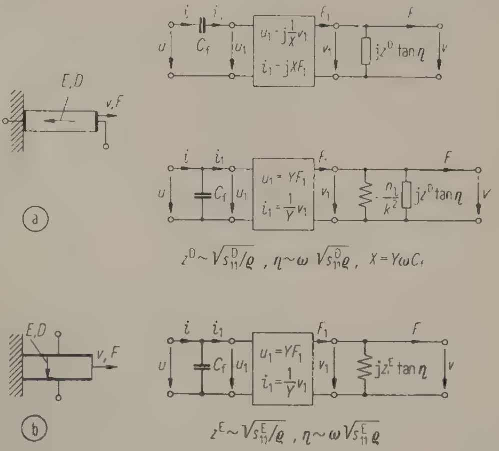
E,D
v,F
i
i_1
C_f
u
u_1
$u_1 = j\frac{1}{X}v_1$
$i_1 = jXF_1$
F_1
F
v_1
$jz^D \tan\eta$
v
$u_1 = YF_1$
$i_1 = \frac{1}{Y}v_1$
$\frac{n_l}{k^2}$
a
$z^D \sim \sqrt{s_{11}^D/\varrho}\,,\ \eta \sim \omega\sqrt{s_{11}^D\varrho}\,,\ X = Y\omega C_f$
$jz^E \tan\eta$
b
$z^E \sim \sqrt{s_{11}^E/\varrho}\,,\ \eta \sim \omega\sqrt{s_{11}^E\varrho}$

Bild 3. (a) Ersatzschaltbilder des einseitig eingespannten piezoelektrischen Dickenschwingers,
(b) Ersatzschaltbild des einseitig eingespannten piezoelektrischen Längsschwingers.

Beim Dickenschwinger tritt der gleiche Mitgang, der hier nur durch die elastische Konstante bei fester Verschiebung bestimmt ist, an die Stelle der Nachgiebigkeit n_l. Der Grund dafür ist, daß beim Längsschwinger die Feldstärke E längs der Schwingungsrichtung konstant ist, wohingegen beim Dickenschwinger dasselbe für die Verschiebung D der Fall ist.

Vergleicht man nun die entsprechenden dielektrischen Wandler (Bild 4 a, b), bei denen das Dielektrikum gleichzeitig die Rolle des mechanischen Systems übernimmt, so erkennt man, daß der piezoelektrische Dickenschwinger das vollständige Analogon zum normal-dielektrischen Wandler ist. Dasselbe gilt für den piezoelektrischen Längsschwinger und den tangential-dielektrischen Wandler. Der Unterschied besteht lediglich darin, daß man beim dielektrischen Wandler unmittelbar erkennt, was unter dem mechanischen System zu verstehen ist, wohingegen das bei den piezoelektrischen Wandlern erst aus dem dynamischen Verhalten zu sehen ist.

Bei den magnetischen Wandlern liegen die Verhältnisse ganz ähnlich. Infolge der Dualität zwischen elektrischen und magnetischen Vorgängen vertauschen sich jedoch die Zuordnungen.

Man mißt die mechanische Nachgiebigkeit im elektrischen Kurzschluß ($n_s = n_k$), wenn magnetische und mechanische Größen parallel zueinander sind (normal-elektromagnetischer Wandler). Stehen magnetische und mechanische Größen senkrecht aufein-

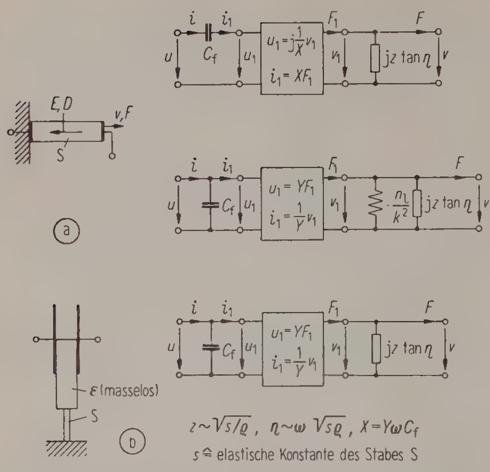

Bild 4. (a) Ersatzschaltbilder des normal-dielektrischen Wandlers,
(b) Ersatzschaltbild des tangential-dielektrischen Wandlers.

ander, so mißt man die mechanische Nachgiebigkeit n_s im elektrischen Leerlauf ($n_s = n_l$, tangential-elektromagnetischer Wandler, elektrodynamischer Wandler).

Die gleiche Unterteilung, wie sie eben beschrieben wurde, findet man durch die Betrachtung des Kraftgesetzes [2]. Sucht man eine Beziehung zwischen der erzeugten Kraft F und einer elektrischen Größe, in der die Schnelle nicht vorkommt, so erhält man sowohl bei den elektrischen als auch bei den magnetischen Wandlern die erwähnte Unterteilung in zwei Gruppen.

Bei der einen Gruppe hängt F auf die beschriebene Weise von der Spannung u, und bei der anderen Gruppe von dem Strom i ab.

Es gelten dabei im einzelnen die Zuordnungen:

$$n_s = n_l \rightarrow F \sim i\,,$$
$$n_s = n_k \rightarrow F \sim u\,.$$

Der Nachteil dieses Kriteriums liegt darin, daß man den physikalischen Mechanismus der Energieumsetzung schon kennen muß, was bei dem zuerst angeführten Kriterium (Richtung der Verkopplung) nicht nötig ist.

In der Literatur [2], [5] ist noch eine Reihe anderer Kriterien angegeben, die ebenfalls eine Unterteilung sowohl der elektrischen als auch der magnetischen Wandler in je zwei Gruppen liefern. Diese Unterteilungen stimmen jedoch nicht mit der oben behandelten, aus der Art der Ersatzschaltbilder folgenden Unterteilung überein.

Es handelt sich dabei erstens um die Frage nach der wesentlichen Beteiligung oder Nichtbeteiligung des elektrischen Energieträgers an der Energieumwandlung [5] und zweitens um die Frage, ob lineare oder quadratische Kraftgesetze vorliegen. Im ersten Fall ergibt sich, daß bei allen dielektrischen und elektromagnetischen Wandlern der Energieträger an der Energieumwandlung wesentlich beteiligt ist, wohingegen das bei den piezoelektrischen und elektrodynamischen Wandlern nicht der Fall ist. Im zweiten Fall, bei der Frage nach dem Grad des Kraftgesetzes, kann man keine so einfache Aussage machen. Obwohl bei den dielektrischen und elektromagnetischen Wandlern immer quadratische Kraftgesetze vorliegen, gibt es piezoelektrische Wandler sowohl mit linearem als auch mit quadratischem Kraftgesetz.

4. Zusammenfassung

Bei der Einteilung der elektromechanischen Wandler nach der Art ihres Ersatzschaltbildes ergeben sich vier Klassen. In zwei Klassen sind alle magnetischen Wandler und in zwei anderen Klassen alle elektrischen Wandler enthalten.

Die Unterteilung der elektrischen und magnetischen Wandler unter sich in zwei Klassen hat nur dann eine Bedeutung, wenn man nach dem Zusammenhang der im Ersatzschaltbild vorhandenen Nachgiebigkeiten n_k (elektrischer Kurzschluß) und n_l (elektrischer Leerlauf) mit der rein mechanisch bedingten Nachgiebigkeit n_s, die auch das dynamische Verhalten wesentlich bestimmt, fragt. Diese Fragestellung tritt auf, wenn ein Wandler berechnet wird, wohingegen sie bei der Messung eines vorhandenen Wandlers ohne Bedeutung ist.

Für die erwähnte Unterteilung kann man eine einfache Regel angeben, die darauf Bezug nimmt, ob die mechanischen Größen v, F auf den elektrischen bzw. magnetischen Feldgrößen senkrecht stehen oder mit ihnen parallel laufen.

Es gilt das Schema entsprechend Bild 5.

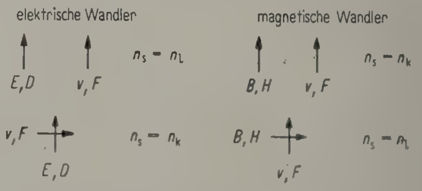

Bild 5. Richtungskriterium für die Einteilung von elektromechanischen Wandlern.

Da der Unterschied zwischen n_l und n_k bei üblichen Wandlern zwischen 1 und 10% liegt, kann er im allgemeinen, wenn es sich nicht um die Berechnung abgestimmter Wandler handelt, vernachlässigt werden, und man hat lediglich zwischen elektrischen und magnetischen Wandlern mit den Ersatzschaltbildern nach den Bildern 1a und 2a zu unterscheiden.

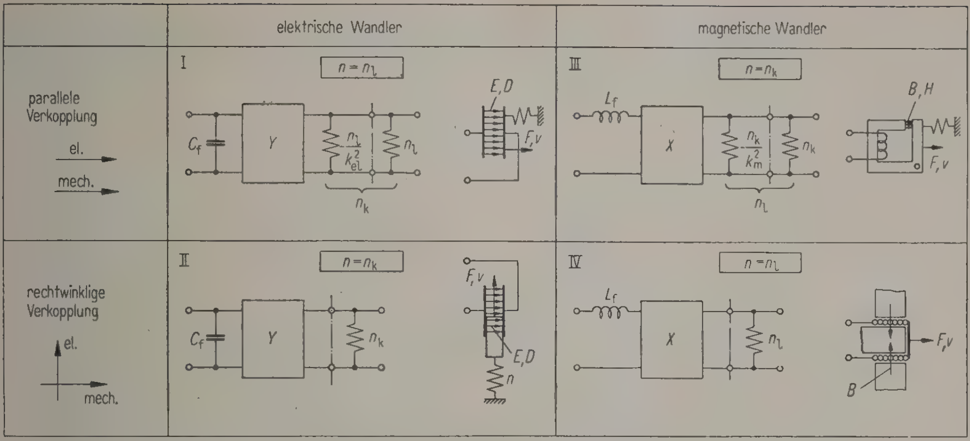

Bild 6. Zusammenfassung.

Für ihr förderndes Interesse an dieser Arbeit und viele wertvolle Ratschläge bin ich den Herren Dr. F. A. Fischer und Prof. Dr. W. Reichardt zu Dank verpflichtet.

(Eingegangen am 1. April 1957.)

Schrifttum

[1] Fischer, F. A., Die Idealform der elektroakustischen Wandler und die Eigenschaften der aus ihnen gebildeten Schaltungen. Acustica 6 [1956], 421.

[2] Fischer, F. A., Grundzüge der Elektroakustik. Fachverlag Schiele & Schön, Berlin 1950.

[3] Reichardt, W., Grundlagen der Elektroakustik, 2. Aufl. Akad. Verlagsges., Leipzig 1954.

[4] Mason, W. P., Electromechanical transducers and wave filters. D. van Nostrand Co., New York 1942.

[5] Fischer, F. A., Über die verschiedenen Darstellungen der elektroakustischen Wandler. Arch. elekt. Übertragung 7 [1953], 569.

[6] Reichardt, W. und Lenk, A., Die Vierpolersatzschaltbilder der elektromechanischen Wandler, Teil I. Acustica 5 [1955], 1.

[7] Lenk, A., Die Vierpolersatzschaltbilder der elektromechanischen Wandler, Teil II. Acustica 6 [1956], 304.

Buchbesprechung

K. Schubert, Sprachhörprüfmethoden, Grundlagen, Würdigung und Anwendung bei Begutachtung und Hörgeräteanpassung. G. Thieme Verlag, Stuttgart 1958, XVI, 361 Seiten, 187 Bilder, Gr. −8°, Ganzleinen DM 69,—.

Der Verfasser behandelt einleitend die Notwendigkeit der Sprachaudiometrie und schildert dann die Gesichtspunkte, die zur Aufstellung seiner Sprachprüfteste geführt haben. Diese Teste können durch Umgruppierung der Worte sowohl in sinnvoller als auch in sinnloser Form verwendet werden. Anschließend an die Beschreibung der Meßapparatur und der Hörprüfräume folgt eine Diskussion der Methodik der Sprachhörprüfung und der Ergebnisse von Untersuchungen des Verfassers. Die verschiedenen Einflüsse auf die Lautverständlichkeit werden analysiert; die Kenntnis dieser Zusammenhänge kann mitunter dazu dienen, Simulanten zu entlarven.

Eine neue Definition des Sprachhörverlustes und der dadurch bedingten Erwerbsminderung wird erläutert und den Definitionen von Hahlbrock, Meister u. a. gegenübergestellt. Daran schließen sich kritische Bemerkungen über Prüfmethoden und Sprachteste anderer Autoren.

Besonders eingehend wird das hallaudiometrische Verfahren des Verfassers dargestellt, bei welchem verschiedene Mischungsverhältnisse von Direktschall zu Indirektschall eingestellt werden können. Die Auswertung dieser verhältnismäßig schlecht zu verstehenden verhallten Teste ermöglicht eine Aussage über die Fähigkeit, aus einem Frequenzgemisch Sprache heraushören zu können, und damit über den vermutlichen Nutzen einer Hörhilfe. Abschließend wird u. a die Anpassung von Hörgeräten behandelt.

Der Berichter möchte anregen, bei einer Neuauflage des Buches die in der Einleitung aufgeführten Grundbegriffe und Formeln zu überarbeiten und auch konsequent im Text anzuwenden; außerdem sollte eine Reihe von Druckfehlern berichtigt werden. Das Verwenden verschiedener Symbole (z. B. große und kleine Buchstaben) für die gleiche physikalische Größe erschwert unnötig das Verständnis der Formeln. Die etwas uneinheitliche Darstellung ist vermutlich darauf zurückzuführen, daß das Buch — wie im Vorwort mitgeteilt wird — aus einzelnen Teilen eines langjährig gelesenen audiometrischen Kollegs des Verfassers entstanden ist.

Das Buch mit seinem sehr ausführlichen Literaturverzeichnis gibt einen interessanten Überblick über den gegenwärtigen Stand der Sprachaudiometrie und ihrer Prüfmethoden.

H. G. Diestel

FORCED BENDING AND EXTENSIONAL VIBRATIONS OF A TWO-LAYER COMPOUND LINEAR VISCOELASTIC BEAM

by F. Schwarzl

Centraal Laboratorium TNO, Delft, Netherlands

Summary

In the forced vibrations of a two-layer viscoelastic beam four basic cases are to be distinguished:

A pure tensile vibration excited by a tensile force and a bending moment.

A pure bending vibration excited by a bending moment and a tensile force.

A superposition of a bending vibration and a longitudinal vibration under a pure bending moment.

A superposition of a longitudinal vibration and a bending vibration under a pure tensile force.

The apparent stiffness against bending or tension, the damping and the energy dissipation in these four cases are discussed as functions of the elastic constants and the ratio of the layers.

Sommaire

Il y a lieu de distinguer quatre cas fondamentaux de vibrations forcées d'une poutre viscoélastique à deux couches:

Une vibration de traction pure, excitée par une force de traction et un moment de flexion.

Une vibration de flexion pure, excitée par un moment de flexion et une force de traction.

La superposition d'une vibration de flexion et d'une vibration longitudinale sous l'effet d'un moment de flexion pur.

La superposition d'une vibration longitudinale et d'une vibration de flexion sous l'effet d'une force de traction pure.

La rigidite apparente à la flexion ou à la traction, l'amortissement et la dissipation de l'énergie, sont étudiés dans ces quatre cas en fonction des constantes élastiques et du rapport des épaisseurs des couches.

Zusammenfassung

Bei den erzwungenen Schwingungen eines aus zwei Schichten zusammengesetzten viscoelastischen Stabes sind vier grundlegende Fälle zu unterscheiden: 1. Reine Dehnschwingung, erregt durch Dehnungskraft und Biegemoment. 2. Reine Biegeschwingung, erregt durch Biegemoment und Dehnungskraft. 3. Überlagerung von Biege- und longitudinaler Schwingung durch reines Biegemoment. 4. Überlagerung von Biege- und longitudinaler Schwingung durch reine Dehnungskraft.

Die Steife gegen Biegung oder Dehnung sowie die Dämpfung und die Energieverluste werden für die vier Fälle in Abhängigkeit von den elastischen Konstanten und dem Verhältnis der Schichtdicken diskutiert.

1. Introduction, Discussion of the concepts of "pure bending" and "neutral fibre", Relation to previous work

It is well known that the vibrational properties of linear viscoelastic materials may be described by means of a complex elasticity modulus $E^* = E' + \mathrm{i}\, E''$ which depends on the frequency ω of the vibration. The storage modulus E' and the loss modulus E'' represent the components of tensile stress in phase and out of phase with unit tensile strain. The absolute modulus $E = \sqrt{E'^2 + E''^2}$ and the loss tangent $\tan\delta = E''/E'$ give the ratio and the phase lag between stress and strain amplitudes.

The purpose of this investigation is a study of the vibrational behaviour of a rectangular beam consisting of two layers of different viscoelastic materials with the complex elasticity moduli E_1^* and E_2^*. The breadth of the beam is taken equal to unity and all forces and moments will be given per unit breadth. A discussion of bending vibrations only will turn out to be too restricted. Therefore the superposition of bending vibrations and longitudinal tensile vibrations will be considered.

The definitions of the physical concepts of "pure bending" and "neutral fibre" will meet with unexpected difficulties in our problem. Therefore we have to start with a careful investigation of the definitions concerning pure bending.

Up to now it has been usual to define pure bending of a rectangular beam as a state of strain which is obtained under the action of a pure bending moment. In addition the principle of St. Venant[1] is assumed to be valid: The amplitude of the longitudinal strain is linearly distributed over the cross-section[2]

$$\varepsilon_{zz} = \alpha(x+r). \qquad (1\,\mathrm{a})$$

The tensile strains in the transverse directions, ε_{xx} and ε_{yy} are assumed to be equal to $-\nu\,\varepsilon_{zz}$ (ν Poisson's ratio) and the shear strains are assumed to vanish. This ensures that only one component of the stress tensor, the longitudinal stress, σ_{zz}, is different from zero. There exists one fibre $x=-r$ (cf. eq. (1 a)), called the neutral fibre which remains undeformed and therefore unstressed. The position of this fibre, i. e. the value of r, is fixed by the condition that only a bending moment but no resulting tensile force is acting on the bar. Consequently the mean tensile force of the stress distribution σ_{zz}, must be equal to zero:

$$F = \int \sigma_{zz}\,\mathrm{d}x = 0. \qquad (1\,\mathrm{c})$$

This equation determines r. The bending moment is calculated as the moment of the stress distribution relative to the neutral fibre

$$M = \int (x+r)\,\sigma_{zz}\,\mathrm{d}x. \qquad (1\,\mathrm{b})$$

The conditions (1 a), (1 b) and (1 c) together form the usual definition of pure bending. This definition is a mixed one, partly consisting of conditions for the strain (eq. (1 a)) and partly of conditions for the stress (eq. (1 b) and (1 c)). One must be prepared that in certain cases the conditions (1 a) on the one hand and (1 b) and (1 c) on the other hand turn out to be no longer compatible. Anticipating the results of the following sections we mention three cases of increasing degree of intricacy. In two of these cases the definition (1) for pure bending is admissible, in the third case it fails.

1. A homogeneous rectangular bar of a linear elastic or viscoelastic material is subjected to the action of a periodic bending moment after (1 b) and (1 c). The bar undergoes periodic pure bending of the same frequency in the sense of (1 a). There exists a neutral fibre in the middle of the cross-section, which remains unstrained during the vibration.
2. Consider a compound beam consisting of two different linear viscoelastic materials. The elasticity moduli of both layers may be different, their, damping, however, is assumed to be equal, $\tan\delta_2 = \tan\delta_1$. Under the action of a periodic bending moment, again a certain fibre remains undeformed during vibration. This neutral fibre is not situated in the middle of the beam. Its position is determined by the ratio of the thicknesses and the elasticity moduli of both layers. Again eq. (1) are compatible and may be used for the definition of bending.
3. A compound bar with layers of different damping is considered, $\tan\delta_2 \neq \tan\delta_1$. It will be shown that a periodic bending moment without longitudinal force results in a vibration which is *not* of the simple form (1 a). No single fibre exists which remains unstrained during the *entire* period of vibration. At each particular instant a certain fibre of the beam is unstrained, but this will be a different one every moment. The neutral fibre "migrates" twice through the cross-section of the beam during one period of vibration. It even leaves the beam during a certain part of the period. It will be quite clear that in this case the conditions (1 a) and (1 b, c) appear to be incompatible. Consequently a redefinition of the concept of pure bending is necessary.

   This definition may be based on either (1 b, c) dropping condition (1 a) or on (1 a) dropping (1 b, c). As pointed out above, the first possibility results in a vibration without a fixed position of the neutral fibre. This would not be called a pure bending by an experimental physicist. We call it a "vibration under pure bending moment"; it will be shown to be composed of a pure bending and a pure tensile vibration.

   The second alternative is chosen in defining pure bending by means of eq. (1 a). However, difficulties arise now in connection with the meaning of the concept of neutral fibre $x=-r$. No preferential position for this fibre exists as no value for r can be found, for which the longitudinal force F vanishes. (It is impossible to excite a pure bending vibration by means of a bending moment without a longitudinal force). Therefore the meaning of the neutral fibre has to be redefined.

The experimental physicist measuring the deflection and the elongation of the beam attaches a pointer to the free end of it at a fibre $x=-r$, say. The deflection and extension of the beam is then measured as the vertical and horizontal movement of the pointer, i. e. as the deflection and extension of the (arbitrarily chosen) fibre $x=-r$. This fibre will be called the neutral fibre. Pure bending of the beam will be defined as a state of strain where the neutral fibre does not undergo an extension, pure elongation as a state of strain where the neutral fibre does not undergo a deflection.

---

[1] A discussion of the principle of St. Venant may be found in N. I. Muskhelishvili, Some basic problems of the mathematical theory of elasticity. Noordhoff Ltd, Holland 1953, pp. 76 and 561.

[2] The position of the coordinate system may be found in Fig. 1. The z and x coordinates are directed parallel to the longitudinal fibres of the bar and the cross-section of the bar in the direction of bending respectively.

If defined in this way, superposed bending and tensile vibrations of the compound beam may be excited by the common action of a periodic bending moment and a periodic tensile force. However, a bending moment only does not suffice for a pure bending vibration and a tensile force only does not suffice for a pure tensile vibration. We may distinguish four basic experiments:

1. A pure tensile vibration excited by a tensile force and a bending moment.
2. A pure bending vibration excited by a bending moment and a tensile force.
3. A superposition of a bending vibration and a longitudinal vibration under a pure bending moment.
4. A superposition of a longitudinal vibration and a bending vibration under a pure tensile force.

Table I. Material constants of the two-layer beam

	Absolute Young's modulus	Damping	Storage modulus	Loss modulus	Thickness of layer	Poisson's ratio[5]
Material 1	E_1	$\tan\delta_1$	$E_1' = E_1 \cos\delta_1$	$E_1'' = E_1 \sin\delta_1$	d_1	ν
Material 2	E_2	$\tan\delta_2$	$E_2' = E_2 \cos\delta_2$	$E_2'' = E_2 \sin\delta_2$	d_2	ν
Ratio $\frac{\text{Material 2}}{\text{Material 1}}$		$b = \frac{\tan\delta_2}{\tan\delta_1}$	$a = E_2'/E_1'$	$ab = E_2''/E_1''$	$\xi = d_2/d_1$	—

The apparent stiffness against bending or tension and the energy dissipation in these four experiments will be discussed in dependence of the elastic constants and the thickness of the two layers.

These considerations may be applied to two problems of technical interest. The measurement of the viscoelastic constants of materials too soft to support their own weight may be established by glueing them to a thin layer of a stiff material. From the viscoelastic properties of the lamellated bar the properties of the soft material may be deduced, as proposed by van Oort[3].

A more important application is the antivibration damping of constructional parts in machines, ships or cars. The propagation of noise through the metal frame of those constructions is usually prevented by a cover of antivibration points or of an other highly damping material. The attenuation of transverse bending vibrations through the total system (metal + layer) will be governed by the aparent loss tangent of this system. Therefore optimum conditions are required in order to obtain high losses. This problem has been analyzed by Oberst[4].

The calculations made by van Oort and by Oberst may be classified as special cases of our problem 2, as mentioned above. Their calculations contain certain approximations which will be discussed in section 5.

2. Forced vibrations of a two-layer beam under the common action of a periodic bending moment and a periodic tensile force

Forced vibrations of a two-layer compound beam are considered. The beam has a length $2l$ and a width unity. It is composed of two different materials, the viscoelastic constants of which are summarized in Table I. Both materials are assumed to be joined rigidly together.

In the undeformed state the origin of the coordinate system is placed in the middle of the plane separating the materials with the x direction perpendicular to this plane; the z direction is taken parallel to the length of the beam (see Fig. 1). The fibres of material 1 extend from $x = -d_1$ to $x = 0$, those of material 2 from $x = 0$ to $x = +d_2$.

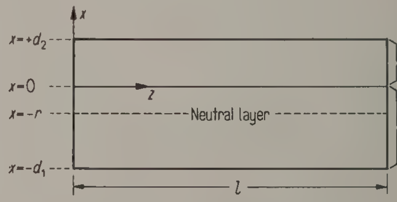

Fig. 1. Right half of the composite two-layer beam and position of the coordinate system.

The deflection and the elongation of the beam will be defined by means of the movement of a pointer attached to the free end of the beam at a fibre $x = -r$. The distance r between this fibre and the boundary between the layers will not be specified for the present. In special cases the value of r may either be given by the experimental arrangement or be chosen by the desire for simple mathematical expressions.

We shall try to solve the problem by means of the following system of displacements (u, v, w are the displacements in the x, y, z direction respectively):

---

[3] W. P. van Oort, Transactions of Instruments and Measurement Conference, Stockholm 1952.

[4] H. Oberst, Acustica 2 [1952], Beiheft 4, AB 181 – AB 194.

[5] Poisson's ratio is assumed to be independent of the frequency and to be equal for both materials.

$$\begin{aligned} u(x,y,z;t) &= -\tfrac{1}{2}\,\alpha[z^2+\nu(x+r)^2-\nu y^2]\sin\omega t- \\ &\quad -s\,\nu(x+r)\sin(\omega t-\eta), \qquad (2) \\ v(x,y,z;t) &= -\alpha\nu\,y(x+r)\sin\omega t- \\ &\quad -s\,\nu\,y\sin(\omega t-\eta), \\ w(x,y,z;t) &= \alpha\,z(x+r)\sin\omega t+s\,z\sin(\omega t-\eta). \end{aligned}$$

This system of displacements corresponds to the superposition of a pure bending with the amplitude α and the neutral fibre at $x=-r$, and an elongation in the longitudinal direction with the amplitude s. A phase lag η is assumed to exist between bending and elongation.

The system of strains corresponding to (2) is found as

$$\gamma_{xy}=\gamma_{yz}=\gamma_{zx}=0\,,\quad \varepsilon_{xx}=\varepsilon_{yy}=-\nu\,\varepsilon_{zz}\,, \qquad (3)$$

$$\begin{aligned} \varepsilon_{zz} &= \alpha(x+r)\sin\omega t+s\sin(\omega t-\eta)= \\ &= \alpha(x+r)\sin\omega t+s'\sin\omega t-s''\cos\omega t\,. \end{aligned}$$

The tensile strain, ε_{zz}, consists of a bending part, which varies linearly with the x coordinate[6], and an extensional part, independent of x. The total state of strain seems to be determined by four constants, viz. α, r, s and η. However, if the extension is separated in a component $s'=s\cos\eta$ in phase and a component $s''=s\sin\eta$ out of phase with the bending vibration, the state of strain is seen to be completely determined by three constants, viz. α, s'' and $\alpha r+s'$. Up to now the decomposition of (3) in a bending and an extension in phase with it is purely artificial.

However, the fourth constant, r, obtains an independent physical significance, if we consider the deflection and the elongation of the beam. The deflection of the beam is measured as the vertical displacement of the pointer, viz. the displacement of the fibre $x=-r$ in the negative x direction (4)

$$D=-u(x=-r\,,y=0\,,z=l;\,t)=\tfrac{1}{2}\,l^2\,\alpha\sin\omega t\,.$$

Similarly the elongation of the beam is measured as the displacement of the fibre $x=-r$ in the positive z direction. (5)

$$L=+w(x=-r\,,y=0\,,z=l;\,t)=l\,s\sin(\omega t-\eta)\,.$$

By the definitions (4) and (5) the meaning of r is fixed, $x=-r$ being the fibre at which elongation and deflection measurements are to be performed.

Next the stress distribution is calculated from (3) by means of the equations for linear viscoelastic behaviour[7]. The only stresses different from zero turn out to be the tensile stresses in the z direction. These show a component in phase with the strain proportional to E_1', and a component out of phase with the strain proportional to E_1''

$$\begin{aligned} &\sigma_{xy}=\sigma_{yz}=\sigma_{zx}=\sigma_{xx}=\sigma_{yy}=0\,, \qquad (6) \\ &\sigma_{zz}=\alpha(E_1'\sin\omega t+E_1''\cos\omega t)\,(x+r)+ \\ &\qquad +s[E_1'\sin(\omega t-\eta)+E_1''\cos(\omega t-\eta)] \end{aligned}$$

(for material 1).

For material 2 a corresponding formula is valid with all the lower indices changed correspondingly.

The stress system (6) satisfies the equilibrium conditions without inertia terms

$$\partial\sigma_{xz}/\partial x+\partial\sigma_{xy}/\partial y+\partial\sigma_{xz}/\partial z=0$$

and therefore constitutes a possible solution of the viscoelastic equations[8]. Further it may easily be seen that (6) obeys the right boundary conditions: All lateral faces of the beam are free from external forces, with the exception of the planes perpendicular to the z direction. On the cross-sections of the beam two types of resulting forces are found. The stresses are equivalent to a longitudinal tension

$$F=\int\limits_{\text{cross-section}}\sigma_{zz}\,\mathrm{d}x \qquad (7)$$

and a bending couple

$$M=\int\limits_{\text{cross-section}}(x+r)\,\sigma_{zz}\,\mathrm{d}x\,. \qquad (8)$$

Here we have chosen $x=-r$ as the fibre relative to which the bending moment is defined. This is in accordance with the selection of this fibre in the definitions (4) and (5).

If the integrations in (7) and (8) are performed, we get the tensile force and the bending moment each as a sum of four components:

A component proportional to s and in phase with the elongation,

a component proportional to s and out of phase with the elongation,

a component proportional to α and in phase with the deflection, a component proportional to α and out of phase with the deflection;

---

[6] This special form of the bending deformation is a consequence of the assumption of St. Venant (vanishing shear stresses). The equality of the strain gradient in both materials is a consequence of the continuity of the displacements at the plane $x=0$. (The materials are joined rigidly together.)

[7] These equations valid for linear viscoelastic isotropic materials under sinusoidal strain under the assumption of a frequency-independent Poisson's ratio ν may be found in H. A. Stuart, Die Physik der Hochpolymeren, Band IV, § 6 c.

[8] Neglecting the inertia terms in the dynamic equations means that our solution is restricted to forced nonresonance vibrations; however, we know from the theory of elasticity that the expressions for the stiffness obtained in this way, may also be used for the approximate description of resonance vibrations.

$$F = s R' \sin(\omega t - \eta) + s R'' \cos(\omega t - \eta) + \alpha m' \sin \omega t + \alpha m'' \cos \omega t , \qquad (9)$$

$$M = s m' \sin(\omega t - \eta) + s m'' \cos(\omega t - \eta) + \alpha B' \sin \omega t + \alpha B'' \cos \omega t . \qquad (10)$$

R' and R'' represent the tensile force due to elongation, B' and B'' represent the bending moment due to the deflection. m' and m'' are cross components which give the tensile force due to the deflection and the bending moment due to the elongation. All these characteristic quantities depend on the viscoelastic constants of both materials and on the thicknesses of both layers. m and B depend further on the choice of the fibre r where the elongation, the deflection and the bending moment are determined.

$$R' = E_1' d_1 + E_2' d_2 , \quad R'' = E_1'' d_1 + E_2'' d_2 , \qquad (11)$$

$$m' = r R' - \tfrac{1}{2} (E_1' d_1^2 - E_2' d_2^2) ,$$
$$m'' = r R'' - \tfrac{1}{2} (E_1'' d_1^2 - E_2'' d_2^2) , \qquad (12)$$

$$B' = \tfrac{1}{3} (E_1' d_1^3 + E_2' d_2^3) - r (E_1' d_1^2 - E_2' d_2^2) + r^2 R' ,$$
$$B'' = \tfrac{1}{3} (E_1'' d_1^3 + E_2'' d_2^3) - r (E_1'' d_1^2 - E_2'' d_2^2) + r^2 R'' . \qquad (13)$$

Finally we calculate the energy dissipation per period; the energy dissipated per unit of volume and per period of the vibration is equal to

$$w = \int_0^{2\pi/\omega} \sigma_{zz} \frac{\mathrm{d}\varepsilon_{zz}}{\mathrm{d}t} \mathrm{d}t .$$

By using (3) and (6) this leads to

$$w = \pi E_1'' [\alpha^2 (x+r)^2 + s^2 + 2 \alpha s (x+r) \cos \eta]$$

for material 1

and to a similar formula for material 2. The energy dissipation per period in a strip of the beam of unit length and unit width is obtained by integration over the cross-section

$$W = \int_{\text{cross-section}} w \, \mathrm{d}x = \pi (\alpha^2 B'' + s^2 R'' + 2 \alpha s m'' \cos \eta) . \qquad (14)$$

3. Discussion of a special case: Equal damping in both layers

The most simple conditions are obtained if the damping in both layers is the same, viz. $\tan \delta_1 = \tan \delta_2 = \tan \delta$. It follows immediately that

$$R''/R' = m''/m' = B''/B' = \tan \delta . \qquad (15)$$

However, we may still choose the position of the neutral fibre r. There is only one choice which results in $m' = 0$, namely

$$r = r_0 \equiv (E_1' d_1^2 - E_2' d_2^2) / (E_1' d_1 + E_2' d_2) . \qquad (16)$$

Because of the equality of $\tan \delta_1$ and $\tan \delta_2$ (eq. (15)) m'' vanishes together with m' and the tensile force and the bending moment do not show cross-terms

$$F = s R' \sin(\omega t - \eta) + s R'' \cos(\omega t - \eta) ,$$
$$M = \alpha B' \sin \omega t + \alpha B'' \cos \omega t . \qquad (17)$$

If this "natural" choice $r = r_0$ for the neutral fibre is used, pure bending may be excited by a bending moment only and pure elongation may be excited by a tensile force only. This is a fundamental property inherent to the special case $\tan \delta_1 = \tan \delta_2$.

If $\tan \delta_1 \neq \tan \delta_2$, as generally, there is no choice of r, by which tensile force and bending moment may be separated. Still we may cause m' to vanish by a proper assumption about r, but m'' will remain different from zero or vice versa. There is no longer a "natural" position for the neutral fibre and the choice of r becomes an arbitrary decision, either prescribed by the experimental conditions or by the desire for simple mathematical expressions[9].

In the following discussion we shall still use $r = r_0$ as the position of the neutral fibre. By this choice m' vanishes and m'' takes a simple form.

$$m' = 0 , \qquad (18)$$
$$m'' \equiv m = \frac{1}{2} \frac{(d_1 + d_2) E_1' d_1 E_2' d_2}{E_1' d_1 + E_2' d_2} (\tan \delta_2 - \tan \delta_1) .$$

4. Discussion of the four basic experiments

We return to the general case of unequal damping and discuss the four basic experiments, where successively the deflection, the elongation, the tensile force and the bending moment are assumed to vanish. Note that the definitions of the experiments sub 4.2. and 4.4. depend on the choice for the situation of the neutral fibre.

4. 1. Pure extensional vibration; $D = 0$

Assuming $\alpha = 0$ in the general equations and using (16) and (18), we get immediately the result: A pure extensional vibration without deflection,

$$L = l s \sin \omega t , \quad D = 0$$

may be excited by means of a periodic tensile force and a periodic bending moment of the same fre-

---

[9] The choice of r will generally be restricted by the requirement

$$\lim r \to r_0 \quad \text{for} \quad \tan \delta_2 / \tan \delta_1 .$$

But this restriction is not sufficient to determine the expression for r in the general case $\tan \delta_2 \neq \tan \delta_1$.

quency. The periodic tensile force precedes the extension by an angle Δ : (19)

$$F = s\,R' \sin \omega t + s\,R'' \cos \omega t = s\,R \sin (\omega t + \Delta) .$$

The storage and loss parts of the extensional stiffness are given by

$$R' = E_1'\, d_1 (1 + a\,\xi), \quad R'' = E_1''\, d_1 (1 + a\,b\,\xi), \quad (20)$$

where the abbreviations of Table I have been used. The absolute stiffness R and the phase lag Δ are determined as usually from the equations

$$R^2 = R'^2 + R''^2, \quad \tan \Delta = R''/R' .$$

Apart from the tensile force, a periodic bending moment is required, which precedes the extension by 90 degrees.

$$M = s\,m \sin (\omega t + \pi/2) . \qquad (21)$$

Its amplitude is given by eq. (18).

These formulae are illustrated by a special example: Consider a two layer beam of total thickness unity $(d_1 + d_2 = 1)$, which consists of a material with low damping and high modulus $(\tan \delta_1 = 0.1;$ $E_1 = 1)$, and of a material with high damping and low modulus $(\tan \delta_2 = 10;$ $E_2 = 0.1)$. This corresponds to the following ratios

$$E_2/E_1 = 0.1, \quad a = E_2'/E_1' = 0.01,$$

$$b = \tan \delta_2/\tan\delta_1 = 100, \quad a\,b = E_2''/E_1'' = 1.$$

The energy dissipation per unit of deformation, the loss modulus, is the same for both materials.

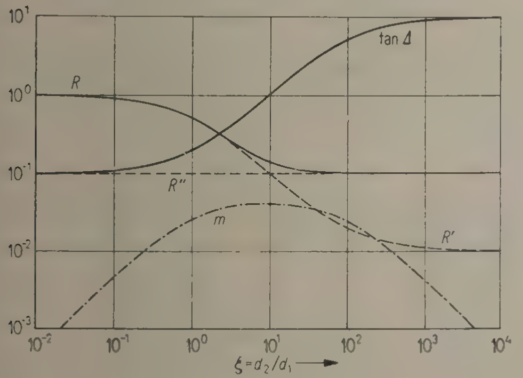

Fig. 2. The characteristic functions in pure tensile vibration for a two-layer beam according to formulae (19), (20) and (21): $E_1 = 1$; $\tan \delta_1 = 0.1$; $E_2 = 0.1$; $\tan \delta_2 = 10$ (R', R'' storage and loss part of the extensional stiffness, R ratio between the amplitudes of longitudinal force and extension, Δ phase lag between longitudinal force and extension, m ratio between the amplitudes of bending moment and extension).

Fig. 2 shows the quantities of formulae (19), (20) and (21) as a function of the thickness ratio $\xi = d_2/d_1$. With increasing relative thickness of the damping layer, the absolute stiffness R and its storage part R' decrease monotonously and the phase lag between elongation and tensile force increases monotonously. The energy dissipation per unit of elongation, R'', is independent of the thickness ratio as to be expected. The amplitude of the additional bending moment, m, shows a maximum at the thickness ratio $\xi = a^{-1/2} = 10$.

4.2. *Pure bending vibrations; $L = 0$*

The assumption $s = 0$ leads the following results: A pure bending vibration without extension

$$D = \tfrac{1}{2} l^2\, \alpha \sin \omega t , \quad L = 0$$

may be realised by means of a periodic bending moment and a periodic tensile force of the same frequency. The periodic bending moment precedes the deflection by an angle δ

$$M = \alpha\, B' \sin \omega t + \alpha\, B'' \cos \omega t = \alpha\, B \sin (\omega t + \delta) .$$

The storage and loss parts of the bending stiffness are given by

$$B' = \frac{E_1'\, d_1^3}{12}\, \frac{1 + 2\,a\,\xi\,(2 + 3\,\xi + 2\,\xi^2) + a^2\,\xi^4}{(1 + a\,\xi)} ,$$

$$B'' = \frac{E_1''\, d_1^3}{12}\, \frac{(1 + a\,\xi)\,(1 + 4\,a\,\xi + 3\,a\,\xi^2 + 3\,a\,b\,\xi^2 + 4\,a\,b\,\xi^3 + a^2\,b\,\xi^4) + 3\,a\,\xi\,(b - 1)\,(1 + \xi)\,(1 - a\,\xi^2)}{(1 + a\,\xi)^2} , \qquad (22)$$

$$B^2 = B'^2 + B''^2 , \quad \tan \delta = B''/B' . \qquad (23)$$

Apart from the bending moment, a periodic tensile force is required, which precedes the deflection by 90 degrees:

$$F = \alpha\, m \sin (\omega t + \pi/2) . \qquad (24)$$

The behaviour in pure bending is illustrated in Fig. 3. Again the stiffness is decreased and the phase lag between bending moment and deflection is increased by an increase of the relative thickness of the damping layer. However, this course is no longer monotonous as there is a relative maximum in $\tan \delta$ and a relative minimum in B at thickness ratios of about 10 and 1 respectively. At these thickness ratios a relative increase of the amount of the soft, damping material may lower the damping of the total system or raise its bending stiffness. It will be quite clear that the situation of these extreme values may be of importance for the design of practical systems. The energy dissipation per unit of deflection, B'' equals 0.1 for a beam of either material 1 or material 2. However, if both materials are joined rigidly together, the energy dissipation in bending may be up to three times as high.

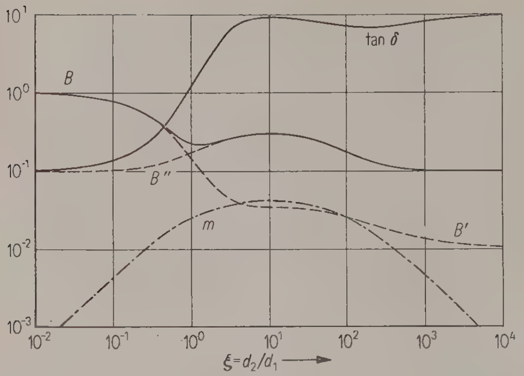

Fig. 3. The characteristic functions in pure bending vibration for a two-layer beam according to formulae (22), (23) and (24); the material constants are chosen as in Fig. 2 (B', B'' storage and loss part of the bending stiffness, B ratio between the amplitudes of bending moment and deflection, δ phase lag between bending moment and deflection, m ratio between the amplitudes of extensional force and deflection).

4.3. *Vibration under pure bending moment; $F=0$*

A vibration under pure bending moment is characterized by the condition $F=0$. This condition yields equations for $s\sin\eta$ and $s\cos\eta$

$$s\sin\eta = \alpha\, m\, R'/R^2\,, \qquad (25)$$
$$s\cos\eta = -\alpha\, m\, R''/R^2\,.$$

If the deflection is assumed to be a sinusoidal function of time,

$$D=\tfrac{1}{2}\, l^2\, \alpha \sin\omega t\,,$$

the longitudinal vibration is determined by means of (25) as follows

$$L = l\,\alpha\frac{m}{R}\sin\left(\omega t - \frac{\pi}{2} - \Delta\right). \qquad (26)$$

Inserting (25) into (10) yields the bending moment

$$M=\alpha\,\hat{B}'\sin\omega t + \alpha\,\hat{B}''\cos\omega t = \alpha\,\hat{B}\sin(\omega t+\hat{\delta}) =$$
$$=\alpha\, B\sin(\omega t+\delta)+\alpha\frac{m^2}{R}\sin(\omega t-\Delta)\,. \qquad (27)$$

The storage and loss parts of the flexural stiffness now become

$$\hat{B}' = B' + m^2 R'/R^2\,,$$
$$\hat{B}'' = B'' - m^2 R''/R^2\,, \qquad (28)$$
$$\hat{B}^2 = \hat{B}'^2 + \hat{B}''^2, \quad \tan\hat{\delta} = \hat{B}''/\hat{B}'\,. \qquad (29)$$

The result of a periodic bending moment will therefore be a vibration composed of a bending and an extension of the same frequency. The phase lag between bending and extension equals $\Delta+\pi/2$ and the ratio of their amplitudes equals m/R (determined by eq. (18) and (20)).

As may be seen from (14) and (25) the energy dissipation is given by $W=\pi\,\alpha^2\,\hat{B}''$. Eq. (28) constitutes a direct comparison between the flexural stiffness in pure bending and the flexural stiffness under pure bending moment. The storage part of the flexural stiffness is always larger in the case of bending under pure bending moment, whilst the loss part (and therefore the energy dissipation) as well as the loss tangent are always larger in pure bending.

The behaviour in vibration under a pure bending moment is illustrated in Fig. 4.

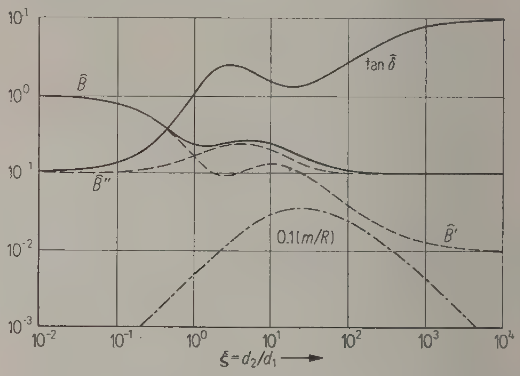

Fig. 4. The characteristic functions in vibration under pure bending moment for a two-layer beam according to formulae (26), (28) and (29); the material constants are chosen as in Fig. 2 ($\hat{B}', \hat{B}''$ storage and loss parts of the bending stiffness, $\hat{B}$ ratio between amplitudes of bending moment and deflection, $\hat{\delta}$ phase lag between bending moment and deflection, m/R ratio between the amplitudes of extension and deflection).

4.4. *Vibration under pure tensile force; $M=0$*

This case is characterized by the condition $M=0$. Inserting this into (10), we get two equations which yield

$$\alpha\sin\eta = -s\, m\, B'/B^2\,,$$
$$\alpha\cos\eta = -s\, m\, B''/B^2\,. \qquad (30)$$

If the extension is assumed to be a sinusoidal function of time

$$L = l\, s\sin\omega t$$

the deflection is obtained by means of (30) as

$$D=\tfrac{1}{2}\, l^2\frac{s\, m}{B}\sin\left(\omega t-\frac{\pi}{2}-\delta\right). \qquad (31)$$

The tensile force is found by inserting (20) into (9)

$$F = s\,\hat{F}'\sin\omega t + s\,\hat{F}''\cos\omega t = s\,\hat{F}\sin(\omega t+\hat{\Delta}) =$$
$$= s\, R\sin(\omega t+\Delta) + s\frac{m^2}{B}\sin(\omega t-\delta)\,. \qquad (32)$$

Table II. Description of the four basic experiments in terms of the characteristic quantities R, Δ, B, δ, m

	Pure tensile vibration	Pure bending vibration	Vibration under pure bending moment	Vibration under pure tensile force
$D/\frac{1}{2}l^2$	0	$\alpha \sin \omega t$	$\alpha \sin \omega t$	$s \frac{m}{B} \sin\left(\omega t - \delta - \frac{\pi}{2}\right)$
L/l	$s \sin \omega t$	0	$\alpha \frac{m}{R} \sin\left(\omega t - \Delta - \frac{\pi}{2}\right)$	$s \sin \omega t$
F	$s R \sin(\omega t + \Delta)$	$\alpha m \sin\left(\omega t + \frac{\pi}{2}\right)$	0	$s R \sin(\omega t + \Delta) + s \frac{m^2}{B} \sin(\omega t - \delta)$
M	$s m \sin(\omega t + \pi/2)$	$\alpha B \sin(\omega t + \delta)$	$\alpha B \sin(\omega t + \delta) + \alpha \frac{m^2}{R} \sin(\omega t - \Delta)$	0
W/π	$s^2 R''$	$\alpha^2 B''$	$\alpha^2 \left(B'' - \frac{m^2}{R^2} R''\right)$	$s^2 \left(R'' - \frac{m^2}{B^2} B''\right)$

The storage and loss parts of the extensional stiffness are

$$\begin{aligned} \hat{F}' &= F' + m^2 (B'/B^2), \\ \hat{F}'' &= F'' - m^2 B''/B^2, \end{aligned} \tag{33}$$

$$\hat{F}^2 = \hat{F}'^2 + \hat{F}''^2, \quad \tan \hat{\Delta} = \hat{F}''/\hat{F}'. \tag{34}$$

We conclude that a periodic tensile force causes a vibration composed of an extension and a bending of the same frequency. The phase lag between these vibrations equals $\delta + \pi/2$ and the ratio of their amplitudes equals m/B (determined by eq. (18) and (23)).

From eq. (33) we may compare the stiffness under pure tensile force and the stiffness in pure extension. The storage part is larger in the case of vibration under pure tensile force, whilst the loss part, the energy dissipation and the loss tangent are larger in pure extension.

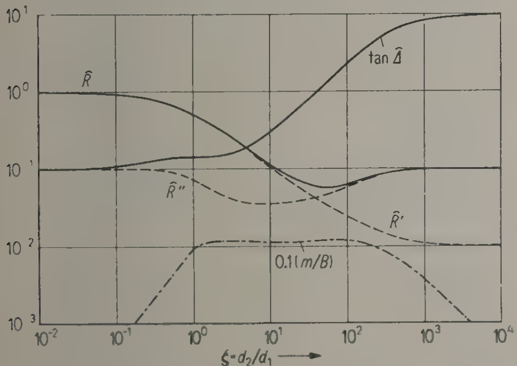

Fig. 5. The characteristic functions in vibration under pure tensile force for a two-layer beam according to formulae (31), (33) and (34); the material constants are chosen as in Fig. 2 ($\hat{R}'$, $\hat{R}''$ storage and loss part of the extensional stiffness, $\hat{R}$ ratio between the amplitudes of longitudinal force and extension, $\hat{\Delta}$ phase lag between longitudinal force and extension, m/B ratio between amplitudes of deflection and extension).

The course of the characteristic functions is shown in Fig. 5).

The results for the four basic experiments are compiled in Table II. Note that the expressions of column 3 and 4 may be obtained by a superposition of those of column 1 and 2.

5. Comparison with the results of other authors; Application to the problem of anti-vibration damping

As already mentioned in the introduction, the same problem has been treated earlier by van Oort and Oberst. Both authors did not realize the existence of cross components between bending and extension. Accordingly they did not distinguish between pure bending and vibration under pure bending moment. Both authors assumed the case of pure bending and calculated the corresponding bending moment without paying attention to the required tensile force. Therefore their treatments should conform to case 4.2. and the expressions (22) for the bending stiffness[10].

Van Oorth[11] calculated the absolute bending stiffness without taking into account the effect of damping. Accordingly he obtains an approximation

$$B \approx A_1 + A_2\,,$$

---

[10] Unfortunately they used their results partially for the description of the forced bending vibrations of a two layer cantilever beam. Such vibrations, however, will take place under conditions of zero longitudinal force rather than zero extension, and case 4.3 would be more appropriate for this problem.

[11] W. P. van Oort, Transactions of Instruments and Measurement Conference, Stockholm 1952, Appendix I, formula (11) and appendix II, formula (8).

where
$$A_1 = d_1\,E_1\left[\tfrac{1}{3}\,d_1^2 + r_0(r_0 - d_1)\right],$$
$$A_2 = d_2\,E_2\left[\tfrac{1}{3}\,d_2^2 + r_0(r_0 + d_2)\right].$$

As may be seen from eq. (13) the exact formulae in the same notation would read

$$\begin{aligned} B' &= A_1 \cos\delta_1 + A_2 \cos\delta_2\,, \\ B &= \sqrt{B'^2 + B''^2}\,, \qquad (22\,\mathrm{a}) \\ B'' &= A_1 \sin\delta_1 + A_2 \sin\delta_2\,. \end{aligned}$$

Van Oort's expression is therefore valid, as long as both loss ratios $\tan\delta_1$ and $\tan\delta_2$ may be neglected against unity.

For the calculation of the damping van Oort starts with a consideration of the energy dissipation. Consequently he obtains the exact formula in complete agreement with eq. (23):

$$\tan\delta = \frac{A_1 \sin\delta_1 + A_2 \sin\delta_2}{A_1 \cos\delta_1 + A_2 \cos\delta_2}\,. \qquad (23\,\mathrm{a})$$

The theory of Oberst[12] refers chiefly to the problem of antivibration damping, where the lamellated bar or plate consists of a constructional material [1] of high modulus and low damping and of a damping layer [2] of low modulus and high damping. This implies a high damping ratio and a small modulus ratio[13].

$$a = E_2'/E_1' \ll 1\,, \quad b = \tan\delta_2/\tan\delta_1 \gg 1\,. \qquad (35)$$

Under these conditions we may simplify formulae (22) considerably:

$$B' = \frac{E_1'\,d_1^3}{12}\,\frac{1 + 2\,a\,\xi\,(2 + 3\,\xi + 2\,\xi^2) + a^2\,\xi^4}{(1 + a\,\xi)}\,, \qquad (36)$$

$$B'' \approx \frac{E_1''\,d_1^3}{12}\,\frac{1 + a\,b\,\xi\,(3 + 6\,\xi + 4\,\xi^2 + 2\,a\,\xi^3 + a^2\,\xi^4)}{(1 + a\,\xi)^2}\,, \qquad (37)$$

$$\tan\delta \approx \qquad (38)$$
$$\approx \tan\delta_1\,\frac{1 + a\,b\,\xi\,(3 + 6\,\xi + 4\,\xi^2 + 2\,a\,\xi^3 + a^2\,\xi^4)}{(1 + a\,\xi)\,[1 + 2\,a\,\xi\,(2 + 3\,\xi + 2\,\xi^2) + a^2\,\xi^4]}\,.$$

The application of these formulae to the problem of antivibration damping is postponed to a separate treatment.

In his calculations Oberst assumed the damping of the constructional material to be zero, i. e. $\tan\delta_1 = 0$. This does not effect formula (36) which agrees exactly with the expression found by Oberst. However, instead of (38) he obtained the approximation (39)

$$\tan\delta \approx \tan\delta_2\,\frac{a\,\xi}{1 + a\,\xi}\,\frac{3 + 6\,\xi + 4\,\xi^2 + 2\,a\,\xi^3 + a^2\,\xi^4}{1 + 2\,a\,\xi\,(2 + 3\,\xi + 2\,\xi^2) + a^2\,\xi^4}\,,$$

This expression may be derived from (38) by neglecting in the numerator 1 against $3\,a\,b\,\xi$. Consequently eq. (39) for the damping is valid in cases where

$$3\,a\,b\,\xi \gg 1\,,$$

i. e. where the thickness of the damping layer is sufficiently high. It fails for thin damping layers.

Acknowledgement

The author is indebted to Prof. Dr. H. C. Brinkman for many stimulating discussions on this subject and his continuous interest in this work.

(Received 18th May, 1957.)

---

[12] H. Oberst, Acustica **2** [1952], Beiheft 4, AB 181 – AB 194; formulae (13) and (14).

[13] Note that these conditions do not claim anything about the order of magnitude of the product ab, which may be well comparable with unity in many cases.

MEASUREMENT OF SOUND TRANSMISSION THROUGH AN ORIFICE IN A DUCT WITH AN APPLICATION TO A RESONATOR

by W. K. R. Lippert

Division of Building Research, Commonwealth Scientific and Industrial Research Organization,
Melbourne, Australia

Summary

Magnitude and phase values of both the reflected and transmitted (plane) sound waves at an orifice in a brass plate terminated by a square input duct and a non-reflecting output duct were carefully measured at numerous frequencies and at an intensity level at which linearity is valid.

A resonator was formed by terminating portion of the output duct with a brass piston, and a formula for the reflection of sound from this resonator is derived and proved to be valid by experiments.

Sommaire

On a mesuré l'amplitude et la phase des ondes sonores planes incidente et réfléchie, au droit d'un orifice pratiqué dans une plaque de bronze séparant un tuyau d'amenée à section carrée d'un tuyau de départ non réfléchissant. Les mesures ont été faites avec soin, pour de nombreuses valeurs de la fréquence, et à des niveaux d'intensité où les phénomènes sont linéaires.

Le tuyau de sortie a été ensuite fermé par un piston de bronze, de manière à former un résonateur: on établit une formule donnant la réflexion du son par ce résonateur; la validité de cette formule est expérimentalement confirmée.

Zusammenfassung

Betrag und Phase der reflektierten und durchgelassenen (ebenen) Schallwellen an einem Loch in einer Messingplatte, die von einem quadratischen Eingangsrohr und einem nichtreflektierenden Ausgangsrohr abgeschlossen ist, sind bei vielen Frequenzen und im linearen Intensitätsbereich sorgfältig gemessen worden.

Durch Abschluß eines Teiles des Ausgangsrohres mit einem Messingkolben wird ein Resonator gebildet; eine Formel für die Schallreflexion von diesem Resonator wird hergeleitet und ihre Gültigkeit durch Messungen bestätigt.

1. Introduction

The classic theory of the propagation of sound waves through simple apertures in unlimited plane walls was presented by Rayleigh [1] when he developed a theory of acoustical (Helmholtz) resonators. His well-known result was that an end correction has to be added to the length of an orifice when the resonance frequency is computed from the volume and orifice dimensions of such resonators.

The more general problem of the complex impedance of an orifice has been treated theoretically by Crandall [2]. Efforts of other workers to verify experimentally the theoretical results obtained by Rayleigh and Crandall were unsuccessful, and there is still no general agreement as to the extent of the differences between theory and experimental results. A critical discussion of these earlier experiments can be found in the introduction to Bolt, Labate and Ingard's paper [3], which presents a precise experimental study of the acoustic reactance of small circular orifices in thin walls. These workers derived an empirical formula for the effective orifice radius provided that the intensities of the sound fields are such that linearity is valid, as will also be assumed throughout this paper.

The resistive component of an orifice impedance has been determined by Sivian [4] and there are more recent investigations on related subjects by Ingard [5], Ingerslev and Nielsen [6], Ferrero and Sacerdote [7] and others (see references in [3]).

The sound transmission through an orifice is a fundamental problem of considerable practical interest, e. g. in the design of acoustical resonators or perforated sound absorbers, and the results of the various workers suggest that further precision measurements are very desirable.

The purpose of this paper is to record the results obtained when applying an experimental technique, described by the author [8], to measure the propagation of sound through a circular orifice in a brass plate which is terminated on either side by a square input or output duct, the output duct being non-reflecting. Magnitude as well as phase values of the input and output sound fields have been measured carefully and used to derive characteristic quantities for specifying the discontinuity in the duct formed by the orifice. Interesting new conclusions are drawn and a simplified theory of certain types of resonators[1] in a duct is derived; this is shown by experiment to be valid in a wide frequency range.

2. Measuring technique

The method used successfully and with good accuracy by the present author in other discontinuities and filters in acoustical ducts [9], [10] has been applied to a duct discontinuity consisting of a circular orifice in a brass plate.

Fig. 1 shows the position and measurements of the orifice used in the experiments. The orifice is a circular opening of diameter 2.07 cm in a brass plate 0.635 cm thick. These particular measurements of the orifice were chosen because they were considered favourable for obtaining good experimental conditions and accuracy of final results. The brass plate is terminated at one side by the input duct and at the other side by the output duct, both of square cross-section 7.6 cm × 7.6 cm and with their axes perpendicular to the brass plate and coincident with the axis of the cylindrical orifice. The plate and the terminating duct ends with angle pieces have been carefully machined to provide a tight fit when bolted together. The duct walls made of brass 0.95 cm thick are rigid and free of unwanted vibrations and resonances, the input duct being 170 cm long and the output duct being 160 cm long, followed by the non-reflecting terminal 123 cm long. The non-reflecting terminal and its measured frequency characteristic of the reflection factor (about 2 to 4 per cent, in a wide frequency range) have been described in a previous paper [9].

A hole (0.6 cm diameter) is drilled through the lower part of the brass plate, and a brass tube 4.1 cm long is pressed into this hole. The inner diameter of the tube is such that the probe tube can slide in it easily. The probe tube (steel, 3.5 mm inner and 5 mm outer diameter) is about 300 cm long between microphone and probe tube orifice, and has an extension piece of methyl methacrylate (5 mm diameter) about 180 cm long. The function of this extension piece is to seal the passage tube when the sound field in the input is probed, and to guide the probe tube through the passage tube when the output sound field is explored. (In the latter case the extension piece can slide along the bottom of most of the length of the non-reflecting terminal.)

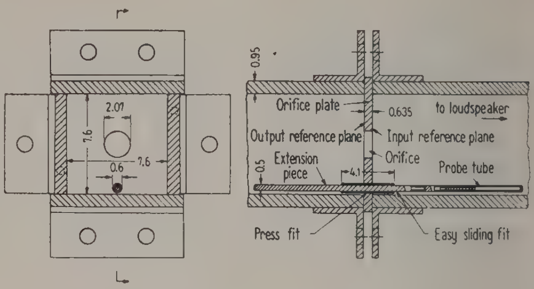

Fig. 1. Orifice plate terminated by the square input and output ducts showing position of orifice, input and output reference planes, the passage tube and probe tube with extension piece. (Measurements are in cm.)

A check was made to determine if any appreciable leakage of sound occurred through the passage tube, leading to a reduction in measuring accuracy. For this purpose the orifice in the brass plate was sealed by a well fitting cylindrical brass piece and the input and output sound fields were probed. The encouraging result was that in the frequency range from about 300 to 2000 c/s the magnitude of the transmitted sound wave was very small. The magnitude ratio of the transmitted sound wave in the non-reflecting ouput duct and of the incident sound wave in the input duct was 0.01 in most of the measured frequency range, with slightly higher ratios (up to 0.03) at the lowest and highest frequencies. These measurements showed also that the pattern of the standing wave in the input duct was regular, i. e. showing maxima and minima envelope curves that can be expected from sound attenuation in the duct [11]. This means that unwanted vibrations of the probe tube and similar disturbing effects are very small, so that it is possible to correct the measurements for attenuation effects in the input duct.

After the plugging disc had been removed from the orifice a number of tentative measurements of the characteristic reflection and transmission factors were made using the method described elsewhere [8]. These measurements were made at various frequencies in the range from 300 to 2000 c/s with the lowest sound intensity in the duct which was sufficient to ensure good experimental conditions. This level was specified by determining the current through the loudspeaker coil at each frequency. The measurements were then repeated by changing the coil current by factors 2, 4 and 10 corresponding to increases of 6, 12 and 20 dB. There were no changes of the measured characteristic factors at increases of 6 and 12 dB, and only slight changes at an increase of 20 dB. These results were taken as evidence that measurements at the lower intensities were free from non-linear effects.

---

[1] These resonators consist of an orifice plate terminated by a highly reflecting duct of which the length is greater than the cross-sectional dimensions.

3. The measured characteristic factors

In Fig. 2 the measured magnitude and phase values of the characteristic reflection factor[2] $R = A \exp(\mathrm{j}\,\alpha)$ and of the characteristic transmission factor

$$T = B \exp(\mathrm{j}\,\beta)$$

are plotted against $\theta/\pi = 2\,a/\lambda$, where λ is the wavelength in the input and output duct and $a = 7.6$ cm the width of the square duct cross-section. The input and output reference planes are the surfaces of the orifice plate facing the input and output ducts respectively, as shown in Fig. 1.

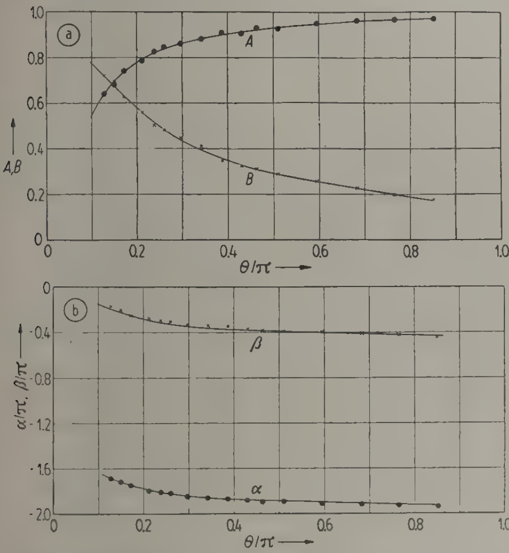

Fig. 2. (a) Measured magnitude values A(●) and B(×) and (b) phase values α(●) and β(×) of the characteristic reflection and transmission factors of the orifice plate of Fig. 1 plotted against θ/π.

Several independent sets of measurements of the reflection and transmission factors at various frequencies were made by the method previously described [8], and the results of one set are illustrated in Fig. 2 as smooth curves of A, B, α and β plotted against θ/π. The room temperature during the measurements was 15 °C ± 2°.

From Fig. 2 a it can be seen that $A^2 + B^2$ is close to unity $(0.93 - 0.97)$, indicating that the orifice is nearly loss-free. In earlier investigations on symmetrical and nearly loss-free discontinuities it was shown that $\alpha - \beta = \pm\pi/2$ [9], [12], [13]. In the present case is will be noted from Fig. 2 b that the measured difference between the phase values of the characteristic factors is also very closely equal to $\pi/2$. In fact, the following equation is fulfilled with good accuracy:

$$\beta = \alpha - (\pi/2)\,. \qquad (1)$$

4. The reflection and transmission factors for completely reflecting termination (resonators)

Two interesting problems arise, viz. (i) how can measured values of A, B, α and β be used to find an analogous impedance circuit for the orifice, and (ii) how can the sound reflection and transmission be described in cases of other than non-reflecting termination? A special case of the latter problem will be considered first.

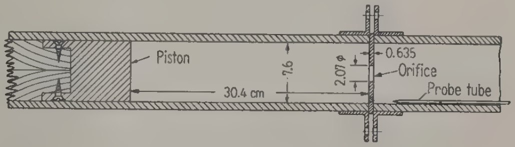

Fig. 3. Cross-section of the resonator with the orifice plate, portion of output duct and terminating piston.

The output duct behind the orifice plate was terminated by a well fitting brass piston at a distance $l_0 = 30.4$ cm from the output reference plane as shown in Fig. 3, the whole device representing a resonator. The probe tube with extension piece (Fig. 1) was replaced by a shorter one, the passage tube was removed and the hole was plugged by a cylindrical brass disc and the sound field in the input duct was probed at numerous frequencies. From the pattern of the standing waves in the input duct the reflection factor $R_{\mathrm{M}} = A_{\mathrm{M}} \exp(\mathrm{j}\,\alpha_{\mathrm{M}})$ was determined in the usual way [8], [10]. In Fig. 4 the measured values of A_{M} and α_{M} are plotted against θ/π showing three successive resonances after the principal resonance which is below the measured frequency range. It has been shown previously [10] that these measured frequency characteristics can be computed if the values of the characteristic factors of the orifice plate are known.

The distance $l_0 = 30.4$ cm being great compared with the width of the duct to ensure a plane output wave at the piston, the characteristic reflection and transmission factors

$$R = A \exp(\mathrm{j}\,\alpha) \quad \text{and} \quad T = B \exp(\mathrm{j}\,\beta)$$

of a symmetrical discontinuity determine the modified reflection and transmission factors

$$R_{\mathrm{M}} = A_{\mathrm{M}} \exp(\mathrm{j}\,\alpha_{\mathrm{M}}) \quad \text{and} \quad T_{\mathrm{M}} = B_{\mathrm{M}} \exp(\mathrm{j}\,\beta_{\mathrm{M}}),$$

as has been derived in the earlier paper [10]:

---

[2] The characteristic reflection factor is by definition the complex ratio of the sound pressure amplitudes of the reflected and incident waves at the input plane. The characteristic transmission factor is the complex ratio of the sound pressure amplitude of the transmitted wave at the output plane and of the incident wave at the input plane, when the discontinuity is terminated by a non-reflecting duct [8].

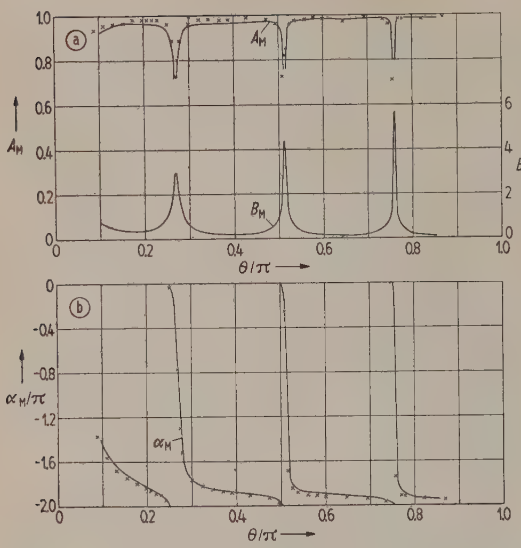

Fig. 4. (a) Measured magnitude values A_M (×) and computed values of A_M and B_M (———) plotted against θ/π, (b) measured (×) and computed (———) phase values α_M for the resonator of Fig. 3 plotted against θ/π.

$$R_M = R + \frac{\varrho T^2 \exp(-\mathrm{j}\, 4\pi l_0/\lambda)}{1-\varrho R \exp(-\mathrm{j}\, 4\pi l_0/\lambda)}, \tag{2}$$

$$T_M = \frac{T}{1-\varrho R \exp(-\mathrm{j}\, 4\pi l_0/\lambda)}, \tag{3}$$

where ϱ is the reflection factor at the reflection reference plane (piston). In the special case considered above where $\varrho = 1$ and $\beta = \alpha - (\pi/2)$, eq. (2) yields:

$$A_M = \sqrt{A^2 + B^2 \frac{B^2 + 2A^2 - 2A\cos(\alpha - 4\pi l_0/\lambda)}{1 + A^2 - 2A\cos(\alpha - 4\pi l_0/\lambda)}}$$

and (4)

$$\alpha_M = \alpha - \arctan \frac{\sin(\alpha - 4\pi l_0/\lambda)}{\frac{A}{A^2+B^2} - \cos(\alpha - 4\pi l_0/\lambda)} + \arctan \frac{\sin(\alpha - 4\pi l_0/\lambda)}{\frac{1}{A} - \cos(\alpha - 4\pi l_0/\lambda)} \tag{5}$$

and eq. (3) yields:

$$B_M = \frac{B}{\sqrt{1 + A^2 - 2A\cos(\alpha - 4\pi l_0/\lambda)}} \tag{6}$$

and

$$\beta_M = \alpha - \frac{\pi}{2} + \arctan \frac{\sin(\alpha - 4\pi l_0/\lambda)}{\frac{1}{A} - \cos(\alpha - 4\pi l_0/\lambda)}. \tag{7}$$

With eqs. (4) and (5) and the values of A, B and α from the measured curves of Fig. 2 (taking $l_0 = 30.4$ cm) A_M and α_M have been computed and plotted against θ/π in Fig. 4. These computed curves for A_M and especially for α_M agree very well with the measurements, thus justifying the procedure adopted above. Figure 4 indicates that eqs. (4) and (5) are also valid in the lower frequency range, e. g. at the principal resonance, which in the particular example can be found by extrapolation to occur at $\theta/\pi \approx 0.07$ which is below the measured frequency range. The validity of eqs. (4) and (5) being established by the measurements suggests that the related eqs. (6) and (7) are valid with a similar degree of accuracy. These equations are therefore useful for finding the sound pressure amplitude within the resonator at some distance from the orifice plate. For the case illustrated in Fig. 3 the values of B_M (which is the ratio of the magnitude of the plane sound pressure wave at the output reference plane propagated along the axis of the resonator and in the direction of the piston to that of the incident plane wave in the input duct) have been computed with eq. (6) and plotted against θ/π (Fig. 4a). There are resonances of B_M and the sound pressure amplitude close to the brass piston being $2\,B_M$ (because of pressure duplication at a hard surface) it can be seen that at the three resonances the pressure amplitude at the piston is from 6 to 11 times greater than the amplitude of the incident wave.

5. Electrical circuit analogy for an orifice impedance in a duct

The other problem mentioned at the beginning of the preceding section, viz., how to find an analogous impedance circuit for the orifice, will now be discussed. Using A, B and α with $\beta = \alpha - (\pi/2)$ for specifying the orifice discontinuity, it has been shown elsewhere [8], [10] that the symmetrical discontinuity consisting of the orifice plate between the input and output reference planes can be represented by an analogous four-terminal electrical circuit, e. g. by the lattice type circuit of Fig. 5 between transmission lines. The impedances of the two lattice arms are Z_1 and Z_2 and the characteristic impedance of the transmission lines is Z_0. In the analogous acoustical case the characteristic impedance of the input and output duct is

$$Z_0 = \varrho_0\, c/a^2, \tag{8}$$

where ϱ_0 density of medium (air), c velocity of sound, a width of square duct.

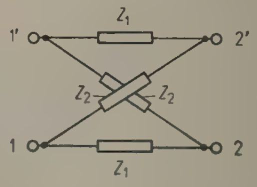

Fig. 5. Lattice type circuit (analogous to the orifice plate of Fig. 1) with the impedances Z_1 and Z_2 of the two arms.

It has also been shown previously [8] that the impedance ratios

$$Z_1/Z_0 = z_1 = z_{1R} + \mathrm{j}\, z_{1J}\,, \quad Z_2/Z_0 = z_2 = z_{2R} + \mathrm{j}\, z_{2J} \tag{9}$$

are simply related to the characteristic factors R and T of a discontinuity

$$z_1 = \frac{1+(R-T)}{1-(R-T)}\,, \quad z_2 = \frac{1+(R+T)}{1-(R+T)}\,. \tag{10}$$

These formulae yield in the present case with $\beta = \alpha - (\pi/2)$ (11)

$$z_1 = z_{1R} + \mathrm{j}\, z_{1J} = \frac{1 - A^2 - B^2 + \mathrm{j}\, 2(A \sin\alpha + B\cos\alpha)}{1 + A^2 + B^2 - 2(A\cos\alpha - B\sin\alpha)}\,,$$

$$z_2 = z_{2R} + \mathrm{j}\, z_{2J} = \frac{1 - A^2 - B^2 + \mathrm{j}\, 2(A \sin\alpha - B\cos\alpha)}{1 + A^2 + B^2 - 2(A\cos\alpha + B\sin\alpha)}\,.$$

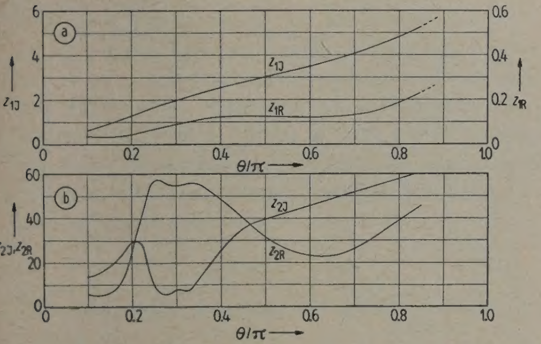

Fig. 6. (a) and (b) Real and imaginary components of the impedance ratios $z_1 = Z_1/Z_0 = z_{1R} + \mathrm{j}\, z_{1J}$ and $z_2 = Z_2/Z_0 = z_{2R} + \mathrm{j}\, z_{2J}$ of the lattice type circuit of Fig. 5. (Z_0 is the characteristic impedance of input and output ducts.)

With these formulae the real (z_{1R}, z_{2R}) and imaginary (z_{1J}, z_{2J}) components of the impedance ratios have been computed using A, B and α (Fig. 2). They are plotted against θ/π in Fig. 6. It can be seen that z_1 has a positive imaginary component z_{1J} and a relatively small real component z_{1R}, i. e. $z_{1R} \approx \frac{1}{20} z_{1J}$. The impedance ratio z_2 has also positive imaginary (z_{2J}) and real (z_{2R}) components but the magnitude of z_2 is great compared with unity and is about 20 times larger than that of z_1. This means that in the lattice type circuit the two impedances Z_2 can be omitted as a first approximation and Z_1 can be simplified by $Z_1 \approx \mathrm{j}\, z_{1J}\, Z_0$. Fig. 6 shows that z_{1J} is roughly proportional to θ/π. As θ/π is proportional to the (circular) frequency $\omega = c\,\theta/a$, the value of z_{1J} is also proportional to ω so that the analogous impedance of the orifice is approximately a mass reactance ($\mathrm{j}\omega M$) with

$$M = \frac{2\, z_{1J}\, Z_0}{\omega} = \frac{2\, z_{1J}\, \varrho_0}{\theta\, a} \tag{12}$$

From this formula and the data in Fig. 6 an averaged mass value $M_{\mathrm{av.}} = 0.64 \times 10^{-3}\ \mathrm{g \cdot cm^{-4}}$ has been found, taking $\varrho_0 = 0.00123\ \mathrm{g \cdot cm^{-3}}$ (air density at 15 °C and 760 mm Hg [14]). A calculated value $M_{\mathrm{comp.}} = 0.68 \times 10^{-3}\ \mathrm{g \cdot cm^{-4}}$ is obtained by applying the formulae derived by Bolt, Labate and Ingard [3]. The difference between these two results is only 6 per cent and they comparse well as far as the averaged mass reactance of Z_1 is concerned. (The value of M from the classic theory is in this particular case $M_{\mathrm{class.}} = 0.87 \times 10^{-3}\ \mathrm{g \cdot cm^{-4}}$ which is about 36 per cent too high.)

6. Discussion

The impedance of an orifice discontinuity in a duct is usually represented by an analogous series impedance between transmission lines. In this case it is assumed that the reflected and transmitted waves are inter-dependent ($R + T = 1$ see eq. (10) for $z_2 = \infty$) so that only one set has to be measured, for instance the standing wave in the input duct, and the series impedance can then be specified in terms of A and α.

The experimental method adopted here has been extended to measuring the transmitted (plane) waves in the output duct as well. If the inter-dependence mentioned above is not taken for granted *a priori*, an evaluation of these measurements requires the series impedance ($2\,Z_1$) to be replaced by a four-terminal circuit which can be regarded as a lattice type circuit with two arm impedances Z_1 and Z_2 or with the corresponding impedance ratios z_1 and z_2.

Z_1 and Z_2 of the lattice type circuit analogous to the orifice discontinuity were specified in terms of A, B, α (and $\beta = \alpha - (\pi/2)$), yielding the satisfactory result the measured orifice discontinuity is, as usually, very nearly equivalent to a series impedance ($2\,Z_1$) as $|Z_2| \gg |Z_1|$ and $|Z_2| \gg Z_0$.

The experimental method adopted here is considered to be advantageous from several reasons. Firstly, measurements of both the reflected and transmitted waves can be evaluated, paying due consideration to each set of measurements which may improve the accuracy. Secondly, *a priori* assumptions about an inter-dependence between input and output measurements do not have to be postulated, and this may be very useful in extreme cases, e. g. when the orifice plate is very thick. Finally, z_{1R} and z_{2R} must both be positive. This is a sensitive test of the reliability of experimental results.

To improve the accuracy of the measurements, smoothed curves representing measurements at many frequencies have to be used. There are two possibilities, either to smooth the curves for the characteristic factors or those for the various components of the impedance ratios. As the curves in Fig. 6 appear to be more complex than those in Fig. 2 it was considered preferable to smooth the curves for the characteristic factors as long as the accuracy of the single measurement cannot be improved further. It may be mentioned here that an accuracy greater than that achieved in the present investigation would most likely reveal that equation (1) has to be modified slightly.

In the preceding section it was shown that the measured values of z_{1J} in Fig. 6a agree well with theory. It is interesting to make a similar comparison for the values of z_{1R}, an accurate measurement of which is far more difficult. Applying SIVIAN's formula (eq. (4) in [4]) to the orifice discontinuity measured above would yield values of $z_{1R} \approx 0.042 \sqrt{\theta/\pi}$, but the actual values of z_{1R} in Fig. 6a are several times greater and not directly proportional to $\sqrt{\theta/\pi}$. Satisfactory checks have been made concerning nonlinear effects and the substantial difference cannot be explained solely by inaccuracies in the present measurements, (e. g. by disturbances caused by the probe tube) or by the particular analogy chosen (the lattice type circuit). (It can be shown that the values of z_{1R} determined from A and α of Fig. 2 for an analogous circuit like that of Fig. 5 with the two arm impedances omitted are still of the same order as those shown in Fig. 6 a.) The close agreement between computed and measured curves in Fig. 4 is further evidence that the values of A, B and α, and thus the derived values of z_{1R}, will not be very inaccurate, unless there are hidden systematic errors.

There are maxima and minima of z_{1R} in Fig. 6 a and it seems possible that these may be explained by INGARD's method [5]. Unfortunately the diagrams given in his paper (Fig. 24) cannot be used to find z_{1R} of the orifice discontinuity under discussion.

All measurements reported in the present paper have been deliberately restricted to a frequency range at which only the principal mode or plane waves can be propagated along the duct and higher order modes are confined to the vicinity of the orifice plate. This makes it possible to measure plane (reflected and transmitted) waves in the duct only and to specify the orifice discontinuity by the corresponding characteristic factors. The actual sound fields close to the orifice plate are in general rather complex because of the superposition of the higher order modes [5] and have not been investigated in detail by the method adopted here. This is not necessary in many practical cases in which the overall effect of these higher order modes on the magnitude and phase values of the reflected and transmitted waves is all that matters. An example of this was provided by measurements of the reflection factor of the resonator of which the reflecting terminating duct was long enough ($l_0 = 4\,a$) to ensure that at all frequencies practically nothing but plane waves were reflected at the piston.

The derivation of the resonator formulae (eqs. (4) to (7)) illustrates the usefulness of the proposed method, and it is of practical interest to note that the complex general theory in such cases can be greatly simplified.

7. Conclusions

It is shown in a practical example that magnitude and phase values of both the reflected and transmitted plane waves at an orifice discontinuity in a duct can be measured accurately and at such low intensity level that linearity is valid.

The reflection and transmission of plane waves at certain resonators in a duct – consisting of the orifice plate terminated by a sufficiently long duct portion and a hard piston – can be conveniently represented by the characteristic factors.

An analogy for the impedance of an orifice discontinuity in a duct is set up in form of a lattice-type circuit, the various impedances of which are computed and discussed for the particular example.

(Received February 13th, 1957.)

References

[1] RAYLEIGH, Lord, Theory of sound. Macmillan, London 1897.
[2] CRANDALL, I. B., Theory of vibrating systems and sound. D. Van Nostrand Co., New York 1926.
[3] BOLT, R. H., LABATE, S. and INGARD, U., The acoustic reactance of small circular orifices. J. acoust. Soc. Amer. **21** [1949], 94 – 97.
[4] SIVIAN, L. J., Acoustic impedance of small orifices. J. acoust. Soc. Amer. **7** [1935], 94 – 101.
[5] INGARD, U., On the radiation of sound into a circular tube, with an application to resonators. J. acoust. Soc. Amer. **20** [1948], 665 – 682.
[6] INGERSLEV, F. and NIELSEN, A. K., On the transmission of sound through small apertures and narrow slits. Ingen. Vidensk. Skr. **5** [1944], 1 – 62.
[7] FERRERO, M. A. and SACERDOTE, G. G., Acoustic impedance measurement using a resonance method. Acustica **4** [1954], 359 – 364.
[8] LIPPERT, W. K. R., A method of measuring discontinuity effects in ducts. Acustica **4** [1954], 307 – 312.
[9] LIPPERT, W. K. R., The measurement of sound reflection and transmission at right-angled bends in rectangular tubes. Acustica **4** [1954], 313 – 319.
[10] LIPPERT, W. K. R., A new method of computing acoustical filters. Acustica **4** [1954], 479 – 488.
[11] LIPPERT, W. K. R., The practical representation of standings waves in an acoustic impedance tube. Acustica **3** [1953], 153 – 160.
[12] LIPPERT, W. K. R., Wave transmission around bends of different angles in rectangular ducts. Acustica **5** [1955], 274 – 278.
[13] LIPPERT, W. K. R., Sound propagation in ducts with side-branches. Acustica **7** [1957], 137 – 145.
[14] BERANEK, L. L., Acoustic measurements. J. Wiley & Sons, New York 1949.

LETTERS TO THE EDITORS

SIMPLE CALIBRATION OF SMALL VIBRATION PICK-UPS

In the frequency range 8 to 800 c/s the calibration of vibration pick-ups is rather simple as is well known. For example there are available electrodynamic vibrators for which the current-force constant can be determined accurately. When the total mass of vibrator and pick-up and moreover the exciting current are known the resulting acceleration can be calculated. In practice this method is very useful for instance when measurements must be carried out in the field: before starting the measurements the complete apparatus consisting for example of pick-up, cathode follower, amplifier, filters and decibel-meter may be checked. Some of the many types of vibration pick-ups are known to have a constant sensitivity over a wide frequency band. A check at one or two low frequencies is then sufficient for many applications. Nevertheless an accurate check at higher frequencies is sometimes necessary, the more so when measurements must be carried out in a frequency range where resonance of the pick-up may occur. In any case there is a need for simple reliable calibration methods for the range 0.8 to 16 kc/s; there are already a few. It seems, however, worthwhile to describe a new method that has been in use for some time in our laboratory. Essentially the pick-up to be calibrated is compared with an accurately calibrated condenser microphone. The absolute calibration of this microphone does not meet with difficulties whatsoever. On top of a vertical travelling-wave tube (length 2 m, inner diameter 4.6 cm, with ρc-termination) a vibrating table (copper disk, thickness 1 cm, diameter 6 cm) is mounted. An electrodynamic vibrator excites this table vertically. Between the table and the upper tube flange is a small rubber ring of, say, four millimeters thickness (same inner diameter as tube) so as to enable the table to vibrate without appreciably exciting the tube wall. It will be clear that a travelling wave in air is sent down the tube.

About half way down the tube the microphone (membrane mounted flush with tube wall) measures the sound pressure of this wave. On the table the pick-up is mounted preferably outside the tube. In this way the pick-up may be calibrated directly in dB velocity (a better designation might be "rapidity") level rel. $4.6 \cdot 10^{-8}$ m/s (for: $p = \rho c v$, and in air 46 nm/s corresponds to 20 μN/m^2).

Above 4.3 kc/s hydrogen instead of air must be used. This is to prevent the higher modes of sound propagation, that might be excited by an unsymmetrically vibrating table, to travel down the tube. If the pick-up is sufficiently insensitive to tangential or rotational vibrations the calibration is not affected by not exactly vertical vibrations of the table. Up to 16 kc/s small vibration pick-ups may easily be calibrated in this way, the accuracy being estimated as better than ±1.5 dB Comparison in the common (overlapping) frequency range 200 to 800 c/s) of this method and of the "electrodynamic" calibration shows differences not greater than 0.5 dB. The measured sound pressure in the tube is always slightly higher than would be expected at first sight. This is due to the extra "pumping effect" of the small rubber ring between the table and the flange. Correction for this effect is very simple as rubber is essentially incompressible. It is thought that the method lends itself very well for automatic calibration of vibration pick-ups.

Acknowledgment

The author wishes to thank Mr. J. C. Tukker of this laboratory for his careful measurements.

(Received November 28th, 1957.)

J. H. Janssen
Technical Physics Department
T.N.O. and T.H.
Delft, Netherlands

ULTRASONIC ABSORPTION IN BONES

The absorption of ultrasonic waves in bones has been investigated by Hüter, mainly as to its frequency dependence [1]. We have measured further the temperature change of the absorption coefficient. The experiment has been performed by using the pulse method, the sample (bones of horses) being placed between the transmitting and receiving probes in a water bath. The main results are as follows.

1. Variation of absorption in different specimens

The density varied markedly with the position of the bones, $\rho \approx 1.5 \ldots 2$, even when they are cut out from the same specimen, subsequently the absorption coefficients showed a similar wide variation. Fig. 1 shows the transmission loss (dB) vs. thickness of the bones at three frequencies 1.43 Mc/s, 2.86 Mc/s and 4.5 Mc/s. In this figure, the three absorption curves cut the ordinate at a common point A, and the intercept 0A ($= 5$ dB) represents the reflection loss. This value of 5 dB is in accord with the value calculated from the value of the density ($\rho = 1.9$) and the velocity ($V = 3700$ m/s), the latter being obtained from the angle of total reflection for the longitudinal wave. The average absorption coefficients of 80 dB/cm at 4.5 Mc/s, 40 . . . 50 dB/cm at 2.86 Mc/s and 22 dB/cm at 1.43 Mc/s are obtained from this figure. This result indicates that the absorption coefficient of the ultrasonic waves in tissues is proportional to the frequency in agreement with the data by Hüter. Measurements were performed also at 0.7 Mc/s and the linear dependency of absorption on frequency seems to be valid also in the frequency range below 1 Mc/s. The accuracy of the measurement in this range, however, is not satisfactory, because of the disturbance by multiple reflection and interference phenomena in samples becoming conspicuous with the decrease of absorption.

2. The temperature dependence of the absorption coefficient

Fig. 2 shows the temperature dependence of ultrasonic absorption in bones at 4.5 Mc/s, 2.86 Mc/s and

1.43 Mc/s respectively, the thickness of the bones being indicated in the figure. These values include the reflection loss, so the true values of the transmission loss in the sample are about 5 dB lower. These measurements indicate that the temperature dependence of ultrasonic absorption is nearly the same in the frequency range of our experiment, the absorption increasing about 25% when the temperature changes from 0° to 60° C, though the temperature coefficient at 4.5 Mc/s is somewhat lower than those at lower frequencies.

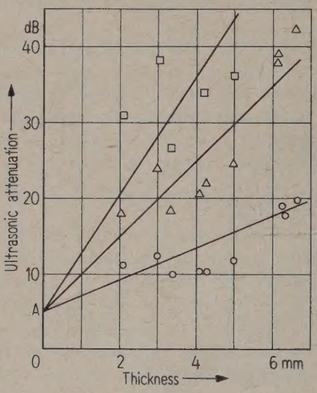

Fig. 1. Ultrasonic attenuation vs. thickness in bones at various frequencies; □ 4.5 Mc/s, △ 2.86 Mc/s, ○ 1.43 Mc/s.

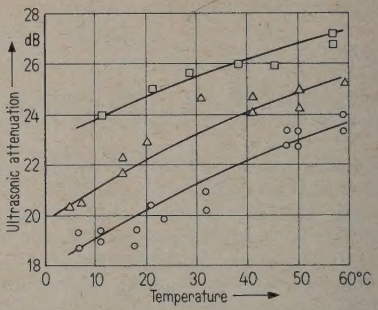

Fig. 2. Temperature dependence of ultrasonic attenuation in bones at various frequencies; □ 4.5 Mc/s (thickness 3.3 mm), △ 2.86 Mc/s (thickness 4.9 mm), ○ 1.43 Mc/s (thickness 6.7 mm).

3. Conclusion

As indicated above, the absorption of ultrasonic waves in bones is proportional to the frequency and the increase with temperature rise is only small, as compared with various artificial high polymers. These facts permit us to conclude that the mechanism of absorption in bones has not to do with the inter- or intramolecular relaxation processes, but may be accounted for by a hysteresis type loss.

(Received February 15th, 1958.)

T. Kishimoto
Kobayasi Institute of
Physical Research
Kokubunzi, Tokyo, Japan

Reference

[1] Hüter, Th. F., Naturwiss. **39** [1952], 21.

Buchbesprechung

J. Matauschek, Einführung in die Ultraschalltechnik. VEB Verlag Technik, Berlin 1957, Din A 5, 536 Seiten, 349 Bilder, 22 Tafeln, Ganzleinen DM 36,—.

Kaum ein anderes Gebiet der Technik ist in seiner schnellen Entwicklung von so viel Erwartungen begleitet gewesen wie die Ultraschalltechnik. Nicht ohne Grund sah man in den hochfrequenten Ultraschallschwingungen ein ideales Mittel, die Struktur der Materie zu beobachten und zu beeinflussen, d. h. einerseits Meß- und Beobachtungsmethoden und andererseits Bearbeitungsverfahren zu gewinnen. Viele zu hoch gespannte Hoffnungen wurden enttäuscht, daneben wurde aber eine Fülle von Anwendungen des Ultraschalls in den verschiedenen Gebieten der Technik verwirklicht. Zu diesen gehören: Ortungsverfahren in Schiffahrt und Fischerei, Materialfehler-Suche in der Fertigungstechnik, Dickenmessung in der Walztechnik, Materialbearbeitung harter Werkstoffe, Emulgierung und Molekülabbau in der chemischen Industrie, Therapie in der Medizin.

Der Verfasser des neu erschienenen Buches hat sich in verdienstvoller Weise die Aufgabe gestellt, eine systematische Darstellung des Gesamtgebietes zu geben. Ausgehend von den physikalischen Grundlagen: den Eigenschaften der Schwingungen und Wellen kleiner Amplitude (Kap. 2) und der Wellen endlicher Amplitude (3) behandelt er die technischen Probleme: die mechanische Ultraschallerzeugung (4), die elektromechanisch-aktiven Stoffe (5) und allgemein die Ultraschallsender (6) und -empfänger (7) sowie die Meßtechnik und die Abbildungsverfahren (8). Den letzten Teil des Buches bilden die Anwendungen des Ultraschalls in Ortungs-, Meß- und Untersuchungsverfahren (9) und zur Materialveränderung in Metallurgie, Fertigung, Nahrungsmittelindustrie, Textilindustrie, Chemie, Pharmazie und Medizin.

Auf allen diesen Gebieten werden die wesentlichen Dinge dargestellt und praktische Kenntnisse vermittelt; es wird aber vermieden, zu weit ins Einzelne zu gehen. Daß dadurch an einigen Stellen spezielle Wünsche offen bleiben müssen, ist verständlich und zum Teil auch auf die schnelle Entwicklung zurückzuführen. Besonders klar dargestellt ist die Systematik der Schallwandler.

Im ganzen gesehen, wurde die gestellte Aufgabe in sehr befriedigender Weise erfüllt. Dazu tragen auch die vielen Diagramme und Tafeln sowie die Berechnungsbeispiele bei. Besonders verdienstvoll ist die konsequente Durchführung des VAms-Maßsystems. Das Buch kann allen auf dem Gebiet der Ultraschalltechnik arbeitenden Ingenieuren, Technikern, Physikern und den Wissenschaftlern aus den angrenzenden Gebieten, aber auch den Studierenden sehr empfohlen werden.

K. Tamm.